Quantum detection at millimeter wavelengths

John R. Tucker

*Department of Electrical Engineering and Coordinated Science Laboratory, University of Illinois
at Urbana-Champaign, Urbana, Illinois 61801*

Marc J. Feldman*

NASA/Goddard Space Flight Center, Institute for Space Studies, 2880 Broadway, New York, New York 10025

Photon-assisted tunneling of electrons through an insulating barrier may be used to detect long-wavelength radiation with a sensitivity approaching the limit imposed by the Heisenberg uncertainty principle. A new generation of ultra-low-noise millimeter-wave receivers, currently being developed for astronomical observation, utilizes the extremely sharp nonlinearity produced by single-electron quasiparticle tunneling between two superconductors in a superconductor-insulator-superconductor (SIS) tunnel junction. At millimeter wavelengths, the quantum energy $\hbar\omega/e$ may be larger than the voltage width for onset of quasiparticle tunneling in a SIS junction; and under these conditions the absorption of a single photon can cause one additional electron to tunnel through the barrier. Several newly discovered quantum effects become possible in this regime, including power amplification of an incoming signal during the process of frequency down-conversion in a heterodyne receiver. The experimental development of SIS millimeter-wave receivers is reviewed, along with the quantum theory of mixing which predicts their performance.

CONTENTS

*Also at Columbia University. Present address: Electrical Engineering Department, University of Virginia, Charlottesville, VA 22901.

I. INTRODUCTION

Quantum detection of electromagnetic radiation is a familiar concept in the visible and near-infrared portions of the spectrum. The devices used as detectors in this region—photomultipliers, photoconductors, and photodiodes—are all conceptually based on the photoelectric effect. An individual electron is ejected off the surface of a metal, or out of a bound state in a semiconductor, through the absorption of a single quantum whose energy $\hbar\omega$ is sufficient to create a free carrier. These carriers are then amplified and counted to yield a measure of the incident flux. Each such device possesses a long-wavelength cutoff, beyond which an incident photon will no longer have sufficient energy to create a carrier.

At much lower frequencies in the microwave and millimeter-wave portions of the spectrum, quantum detection has until recently been possible only within narrow bandwidths centered on the resonant frequencies of a few molecular maser amplifiers. By contrast, the standard detection technique over most of this region employs nonlinear resistive elements, usually Schottky barrier diodes, as classical rectifiers and heterodyne mixers. Applied radiation induces oscillatory potentials across the diode, and these potentials combine via the nonlinearity to generate an output signal at difference frequencies suitable for electronic processing. The performance of nonlinear resistive devices as detectors and mixers is typically mea-

sured in terms of the conversion of power between frequencies, rather than the conversion of quanta to carriers. This characterization is fundamentally classical, and employs language and concepts far removed from those used to describe the high-frequency quantum detectors.

Recent research on nonlinear effects in photon-assisted tunneling has provided a link between classical and quantum behavior in a new class of resistive mixers; and this understanding has opened the way to quantum-limited detection at millimeter wavelengths. The primary requirement is a tunnel junction whose dc I-V characteristic is extremely nonlinear. An extraordinary nonlinearity is created by the gap in available energies for single-electron quasiparticles on both sides of a superconductor-insulator-superconductor (SIS) tunnel barrier. In these SIS junctions, a very sharp onset of normal tunneling current is observed beyond a dc threshold voltage equal to the superconductor energy gap. This abrupt nonlinearity in the single-particle tunneling, as distinct from the Josephson pair tunneling, is then used for resistive mixing. When the quantum energy $\hbar\omega/e$ at the incident frequency exceeds the voltage width of the threshold for onset of quasiparticle tunneling, a SIS junction ceases to behave classically and instead responds to individual quanta through the mechanism of photon-assisted tunneling.

Several newly discovered quantum effects occur in nonlinear quasiparticle tunnel junctions at high frequencies that are forbidden in the low-frequency classical regime. These phenomena arise from coherent modulation of the relative phases of the quantum-mechanical wave functions for electrons on opposite sides of the barrier in the presence of an applied potential. At frequencies sufficiently low that $\hbar\omega/e$ is smaller than the voltage scale of the nonlinearity, the net result is simply a classical modulation of the dc I-V curve. At higher frequencies, however, the coherent phase modulation produces new effects which depend upon the magnitude $\hbar\omega$ of the quantum energy. The most important of these is known as conversion gain, and it allows the incident signal power in a heterodyne mixer to be amplified during the process of frequency down-conversion. This internal amplification reduces the importance of output amplifiers in determining the overall system noise temperature, and makes quantum-limited detection a practical possibility at very long wavelengths.

Heterodyne receivers which utilize SIS quasiparticle tunnel junctions as the mixing element have recently demonstrated sensitivities approaching the quantum limit at frequencies between 36 and 115 GHz. There now appears to be no major obstacle to detection at the level of a single quantum across the entire microwave and millimeter-wave portion of the spectrum. This emerging capability to detect ultra-low-level signals at these frequencies is expected to have a profound impact on future progress in radio astronomy, and eventually on spectroscopy, space communications, and many other branches of science and engineering.

The function of a heterodyne receiver is to mix a weak incoming signal at frequency ω_S with a large-amplitude local oscillator (LO) at ω_{LO}, in order to produce an intermediate-frequency (IF) output at $\omega_{IF} = |\omega_S - \omega_{LO}|$ suitable for electronic processing. Phase information carried by the incoming signal is preserved in the mixing process, and noise is greatly suppressed by filtering the output to retain only a relatively narrow bandwidth centered on ω_{IF}. The key component of a heterodyne receiver is the nonlinear mixing element. The performance of the mixer is characterized by (1) its conversion efficiency (gain or loss) in transforming signal power to the output frequency, (2) the response time (instantaneous bandwidth) of the mixing element in its embedding network, and (3) the mixer noise temperature T_M, defined as the noise power kT_M per unit bandwidth added to the signal in the process of frequency down-conversion. There is a fundamental limit to the noise temperature $T_M \gtrsim \hbar\omega/k$ imposed by the Heisenberg uncertainty principle on any simultaneous measurement of the amplitude and phase of the electromagnetic field. This may be appreciated by noting that a bandwidth $\Delta\nu$ represents an effective measurement time $(\Delta\nu)^{-1}$, so that the detection of a single quantum within this interval corresponds to an incoming signal power $h\nu\Delta\nu$. The minimum uncertainty of any coherent measurement must be of this order, and in fact the true "quantum-noise"-limited mixer temperature is $T_M = h\nu/2k$. A quantum-limited heterodyne receiver can thus detect the presence of a stream of photons with an arrival rate approximately equal to its inverse bandwidth. In typical receivers this would correspond to a signal of $\sim 10^9$ photons per sec.

Realization of mixer noise temperatures approaching the quantum limit does not, of itself, imply a capability to detect at the level of individual quanta in the millimeter-wave region. The output signal from the mixer must be amplified before it can be processed, and present state-of-the-art IF amplifiers suitable for this purpose have noise temperatures in the 10-K range. This amplifier noise must be multiplied by the mixer conversion loss in evaluating the overall input noise temperature T_R of the entire receiver. Since the quantum energy is $h\nu/k \approx 5$ K for $\nu = 100$ GHz or $\lambda = 3$ mm, for example, even very modest amounts of conversion loss can result in an IF amplifier component of receiver noise temperature far in excess of the quantum limit at millimeter wavelengths. An ideal quantum-noise-limited receiver in this region must therefore be based upon a heterodyne mixer with (1) a mixer noise temperature $T_M \approx \hbar\omega/k$ near the fundamental limit, (2) a modest amount of conversion gain in order to suppress the IF amplifier noise contribution to the overall receiver temperature, and (3) a large instantaneous bandwidth (fast response time), potentially on the order of 1 GHz or larger.

Under appropriate conditions in the quantum regime, SIS quasiparticle mixers have demonstrated all of these properties required in order to construct millimeter-wave receivers that approach the fundamental limits of performance.

The rapid progress in developing SIS quasiparticle

mixers is the result of an unusual community of interest, which includes recent advances in widely separated disciplines, based upon (1) new techniques for fabricating high-quality superconducting tunnel junctions, (2) millimeter-wave receiver technology created for Schottky diode mixers, and (3) the interest and expertise of the radio astronomy community in engineering new ultra-low-noise millimeter-wave receivers. The SIS diodes used in these receivers are made possible by substantial previous investments in research to produce high-quality small-area superconducting tunnel junctions. Much of this effort, particularly at IBM, has been aimed at the reliable fabrication of large numbers of junctions for Josephson-effect logic circuits. Pb-alloy junctions with accurately controlled current densities can now be routinely produced down to submicrometer dimensions. Methods have also been devised to minimize degradation due to electrical shock and thermal cycling. Progress in developing the new millimeter-wave quantum receivers, which do not utilize the Josephson effect, has thus been greatly advanced by the extensive fabrication technology developed in order to produce small-area superconducting tunnel junctions with high current densities.

Millimeter-wave astronomy has grown rapidly since the discovery of the cosmic background radiation in 1965 into a broad exploration of the interstellar medium. An essential component of this progress has been the development of increasingly sophisticated techniques for engineering low-noise receivers. A new generation of millimeter-wave telescopes is currently under construction, and the new SIS quantum receivers are expected to enhance their capabilities greatly. The present expertise in millimeter-wave engineering is being directly translated into the development of these ultra-low-noise quantum receivers, since the only essential change is the substitution of a superconducting tunnel junction in place of a cryogenically cooled Schottky diode. Tunnel junction mixers have been utilized for astronomical observations almost from their inception, and a recently constructed $\lambda = 2.6$ mm wave receiver designed to observe the 115-GHz rotational emission from interstellar CO has achieved an overall receiver noise temperature $T_R \approx 70$ K, only a factor of 10 above the nominal quantum limit $\hbar\omega/k \approx 6$ K at this frequency (Pan et al., 1983a,1983b). The SIS mixer in this system was not designed to operate in the conversion gain regime, so that only a small fraction $T_M \approx 15$ K of the noise is due to the mixer itself, with the majority coming from the intermediate-frequency amplifiers. Nevertheless, this 115-GHz receiver represents a factor of 2–3 improvement in noise temperature over the previous state-of-the-art cooled Schottky diode systems. Future designs which utilize the conversion gain effect are expected to produce dramatically lowered receiver temperatures in the range $T_R \approx 20$ K at 115 GHz. Mixer noise temperatures $T_M \approx 9$ K approaching the quantum limit have already been achieved in the presence of large conversion gain $L^{-1} \gtrsim +4$ dB at 36 GHz (McGrath et al., 1981). It now appears likely that tunnel junction mixers will reduce receiver temperatures by at least a factor of 7–10 over most

of the millimeter-wave region within the next few years. When they are used as radiometers for astronomical observation, the integration time required to discriminate a given difference in sky temperature depends upon the square of the receiver noise temperature. Therefore the advent of this new generation of quantum mixers is expected to improve the potential for millimeter-wave astronomy by factors of 50–100, and perhaps more. Although full utilization of this potential will eventually require radio telescopes deployed in space, in order to escape thermal radiation from the Earth's atmosphere, this increased capability to observe at millimeter wavelengths should eventually produce major advances in exploring the structure of the Universe.

The physical phenomenon that provides the basis for this work is the photon-assisted tunneling of single-electron quasiparticles across a SIS tunnel barrier. This effect was discovered experimentally by Dayem and Martin (1962), and their results are reproduced in Fig. 1(a). Microwave radiation of frequency $\nu = 38$ GHz applied to the junction was found to induce structure onto the dc I-V curve, with current steps appearing at voltage displacements corresponding to integral multiples of $h\nu/e \approx 0.16$ mV above and below the sharp onset of single-electron tunneling at a dc voltage $V_0 = (\Delta_1 + \Delta_2)/e \approx 0.9$ mV. The essential features of this effect were soon explained theoretically by Tien and Gordon (1963), and can be understood in terms of the simplified energy-band diagram shown in Fig. 1(b). The superconductors on both sides of the tunnel barrier are in their ground states at $T = 0$, and there is an energy gap 2Δ for each electrode required in order to break up a Cooper pair to produce two single-particle excitations. The energies of the available quasiparticle excitations are given according to the BCS theory (Bardeen et al., 1957) by

$$E_k = (\varepsilon_k^2 + \Delta^2)^{1/2}, \tag{1.1}$$

where ε_k is the normal-state quasiparticle energy measured from the Fermi level. The density of states for single-particle excitations in the superconductor therefore becomes

$$D(E)dE \approx N(0)\frac{d\varepsilon_k}{dE_k}dE$$

$$= N(0)\frac{E}{(E^2 - \Delta^2)^{1/2}}dE, \tag{1.2}$$

where $N(0)$ represents the density of states at the Fermi level in the normal metal above the superconducting transition. The divergence in this density of states near the gap edge for both superconductors is illustrated in Fig. 1(b). The onset of single-particle tunneling then takes place at a dc voltage $eV_0 = \Delta_1 + \Delta_2$, where there is sufficient energy to allow the tunneling electron to enter an available quasiparticle state above the gap on the right in Fig. 1(b) and leave an unpaired electron quasiparticle behind on the left. The steep increase of the single-particle tunneling current seen in Fig. 1(a) at the sum of the gap voltages arises from crossing of the divergences in
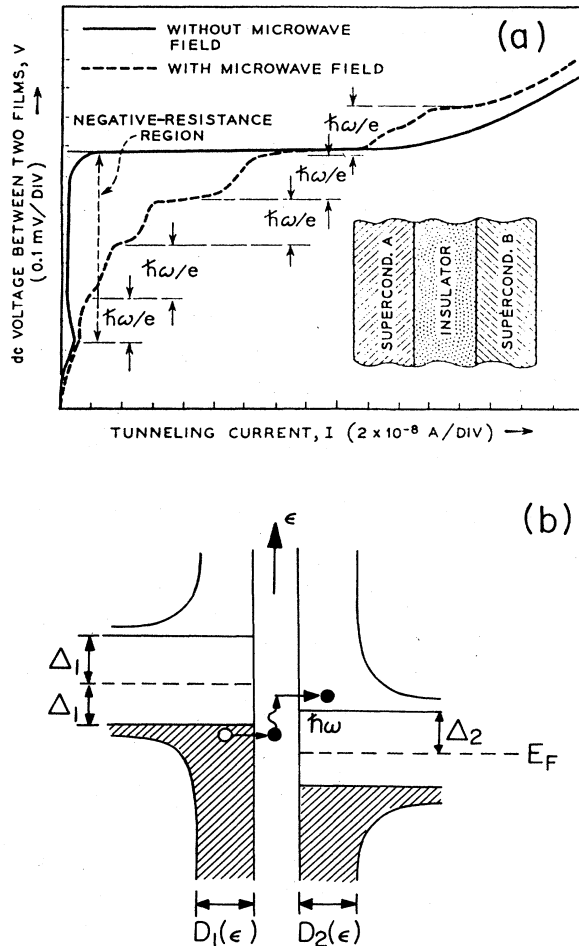
FIG. 1. (a) Photon-assisted tunneling steps (dashed curve) induced onto the dc I-V characteristic (solid curve) of a Al-Al$_2$O$_3$-In tunnel junction by applied microwave radiation at 38 GHz with $\hbar\omega/e = 0.16$ mV (Tien and Gordon, 1963), and (b) densities of states vs energy for quasiparticle excitations in superconductors on opposite sides of a tunnel barrier.

the densities of states, and in an ideal junction this would produce an infinitely sharp discontinuity.

The step structure is induced by the process illustrated in Fig. 1(b). In the presence of a microwave field, the absorption of n quanta inside the barrier can provide enough energy to open this channel for quasiparticle tunneling when $eV_0 > \Delta_1 + \Delta_2 - n\hbar\omega$. The current steps below the dc onset in Fig. 1(a) then represent the threshold voltages for which the absorption of at least $n = 1, 2, 3, \ldots$, microwave photons is required for single-electron tunneling. The representation in terms of a semiconductorlike band picture shown in Fig. 1(b) neglects the mixture of "electron" and "hole" properties involved in constructing quasiparticle wave functions near the gap edge in a superconductor. The "coherence factors," which in general enter linear response functions because of this admixture, were shown to cancel out for single-particle tunneling between two superconductors by

Cohen, Falicov, and Phillips (1962). Their pioneering work developed the Hamiltonian formulation of tunneling theory, based on a concept introduced by Bardeen (1961); and their results confirmed Giaever's (1960a,1960b) original interpretation of a direct observation of the energy gap in his tunneling experiments, using total quasiparticle densities of states and energy-band diagrams similar to those shown here. The simplified band picture in Fig. 1(b) thus ignores important physical properties of the quasiparticle excitations in a superconductor, but those properties do not enter in determining the total single-particle tunneling current.

Two important observations can be made with regard to the results illustrated in Fig. 1. First, the step structure induced onto the dc I-V curve by applied microwave radiation reflects the extremely abrupt onset of quasiparticle tunneling at the sum of the gap voltages for the two superconductors. This rise is perfectly sharp for an idealized SIS junction, but in a real diode it will be spread over a finite voltage range by a variety of physical mechanisms. The existence of the induced photon steps in Fig. 1(a) will therefore be evident only for frequencies sufficiently high that $\hbar\omega/e$ is large compared to the voltage width of the dc nonlinearity. At lower frequencies, an applied ac potential will smoothly average the dc I-V curve, and the response will be essentially classical. New phenomena predicted by the quantum mixer theory can therefore be observed only in this high-frequency quantum regime. The second important observation is that the process of photon-assisted tunneling illustrated in Fig. 1(b) is capable of generating one additional carrier flowing across the junction for each microwave photon absorbed inside the barrier. Such a device thus has the capability, at least in principle, to detect individual quanta at very long wavelengths.

In addition to the single-particle current, a tunnel junction between two superconductors can also support the tunneling of Cooper pairs (Josephson, 1962). This pair tunneling results in a dc supercurrent through the junction up to a maximum critical value $I_c = \pi\Delta/2eR_n$ for identical BCS superconductors at low temperatures, where R_n is the normal-state resistance. With a finite dc voltage bias applied to the junction, the pair current oscillates at the Josephson frequency $\nu_J = 2eV_0/h = 484$ GHz/mV. The junction shown in Fig. 1(a) has sufficient capacitance to short-circuit these high-frequency oscillations on the millivolt scale shown here. This capacitive shunting of the ac Josephson current allows the diode to operate on the nonlinear quasiparticle portion of its I-V characteristic; and in fact the existence of Josephson pair tunneling was unknown at the time of the Dayem and Martin (1962) experiments. Josephson's enormously important discovery focused the attention of the physics community on the many strange and beautiful pair tunneling phenomena that now bear his name. Much work in the ensuing years was, in fact, devoted to attempts at constructing low-noise millimeter-wave receivers utilizing the ac Josephson effect. The Josephson heterodyne mixer experiments, however, used point-contact junctions in or-

der to avoid capacitive shunting of the pair current. These junctions are nonhysteretic, and their quasiparticle current is generally linear. The basic problem with Josephson point-contact mixers is that noise originating at a large number of harmonics of the signal frequency is mixed into the IF output. Even though the nonlinear reactance due to the ac Josephson effect could produce conversion gain, the mixer noise temperatures were found to have a practical lower bound $T_M > 40\hbar\omega/k$, far in excess of the quantum limit (Claassen and Richards, 1978), and so provided no significant advantage over the more conventional Schottky diode receivers.

More than ten years elapsed between the Dayem and Martin (1962) experiments and the invention of the super-Schottky diode by McColl, Millea, and Silver (1973). This device consists of a Schottky barrier between a degenerate semiconductor and a superconducting metal contact. Extremely heavy doping in the semiconductor produces a depletion layer sufficiently thin that tunneling of electrons near the Fermi surface, rather than thermionic emission over the barrier, dominates the diode's conduction at low temperatures. Below the superconductor's transition temperature, the opening of the energy gap for quasiparticle excitations produces an exponentially nonlinear dc tunneling current $I_{dc} \propto \exp(eV_0/kT)$ for bias voltages $kT < eV_0 < \Delta$ below the gap. At operating temperatures $T \approx 1$ K, this extraordinary nonlinearity was utilized to construct direct detectors and heterodyne mixers at 9 GHz with record sensitivities (Vernon et al., 1977; McColl et al., 1977). Even though they surpassed all previous microwave receivers, the performance of super-Schottky mixers was essentially classical at the frequencies employed, since their dc I-V nonlinearity was considerably less sharp than that of the SIS diode shown in Fig. 1(a). The anticipated extension of the super-Schottky operating frequency toward 100 GHz, however, stimulated an inquiry by Tucker (1975) and Tucker and Millea (1978,1979) into the potential relationship between photon-assisted tunneling and detector performance. An extension of the Tien-Gordon analysis clearly indicated that tunnel junctions should respond to individual quanta when $\hbar\omega/e$ is larger than the voltage width of the dc nonlinearity. A full quantum generalization of classical microwave mixer theory was subsequently developed (Tucker, 1979) in order to predict the high-frequency behavior of nonlinear single-particle tunnel junctions as heterodyne mixers, and it was demonstrated that mixer noise temperatures could be reduced toward the fundamental limit $T_M \sim \hbar\omega/k$ in the high-frequency quantum regime. Super-Schottky mixers were eventually operated at 31 GHz (McColl et al., 1979), still as classical devices, but their operating frequencies could not be successfully extended into the projected quantum region near 100 GHz (Dickman et al., 1981) because of parasitic losses due to increased spreading resistance in the semiconductor as the diameter of the diodes was reduced. Nevertheless, the extraordinary detection and mixing properties demonstrated by the super-Schottky diode, together with the predictions of the quantum mixer theory, stimulated progress along a

more technically feasible direction.

The concept of utilizing the nonlinear quasiparticle I-V characteristic available in a SIS junction for detection and mixing originated independently, and roughly simultaneously, in several laboratories. By the mid-1970s, work on high-current-density superconducting tunnel junctions had progressed to the point where small-area SIS devices could be fabricated having characteristic frequencies $(R_n C)^{-1}$ in the microwave region and impedance levels $R_n \sim 100$ Ω suitable for detector applications. The first published description of work in progress on SIS mixers appeared in an article by Richards (1978).

In the spring of 1979, three groups reported initial heterodyne mixing experiments using the quasiparticle nonlinearity of SIS tunnel junctions. The results of Richards, Shen, Harris, and Lloyd (1979) at 36 GHz, shown in Fig. 2, gave clear evidence of photon-assisted tunneling on the output mixing signal and a noise temperature $T_M \lesssim 7$ K $\approx 4\hbar\omega/k$ strikingly close to the quantum limit. Dolan, Phillips, and Woody (1979) directly observed the photon steps induced onto the dc I-V curve by their 115-GHz local oscillator and placed an upper bound $T_M < 100$ K on the mixer noise temperature. Rudner and Claeson (1979) demonstrated the use of a 40-element series array of tunnel junctions operating as a heterodyne mixer in the classical regime at 9 GHz, with a low noise temperature $T_M \approx 10$–40 K. The observation of photon-assisted tunneling effects in heterodyne mixing at the
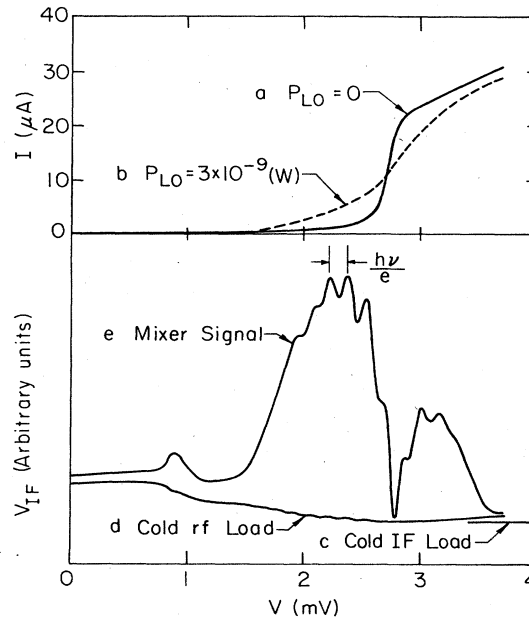
FIG. 2. dc I-V curves of a Pb-alloy junction SIS mixer at 1.5 K a, without and b, with applied LO power at 36 GHz. Curves c and d represent the output of the IF amplifier obtained with matched 1.5-K loads placed at the output and input ports of the mixer, respectively, and are used to deduce noise temperature. Curve e is the IF output with a calibrated 36-GHz signal applied at the input, and is used to determine conversion efficiency (Richards et al., 1979).

higher frequencies greatly stimulated interest in comparing experimental results with the quantum theory. The nonclassical response of SIS junctions to individual quanta in low-level direct detection was soon confirmed by Richards, Shen, Harris, and Lloyd (1980) at 36 GHz, and subsequently by Hartfuss and Gundlach (1981a) at 70 GHz, in agreement with theoretical predictions.

A computer simulation based on the quantum mixer theory was developed in order to characterize the heterodyne mixing properties of a SIS tunnel junction, and this model produced several extraordinary predictions (Tucker, 1980). It showed that these devices should not only be capable of quantum-limited mixer noise temperatures, but that conversion gain would also be possible in the quantum regime. In addition, the low-frequency output impedance [the dynamic resistance on the steps in Fig. 1(a)] was predicted to become infinite and then negative under appropriate conditions. The available small-signal conversion gain in this case approaches infinitely large values as the output impedance increases, and remains infinite in the negative-resistance region.

The first observation of conversion efficiencies slightly in excess of the classical limit was made only a few weeks after its prediction in SIS mixer experiments at 36 GHz by Shen, Richards, Harris, and Lloyd (1980). Similar results were soon achieved at 73 GHz by Rudner, Feldman, Kollberg, and Claeson (1981a,1981b), using a six-element series array. This latter work demonstrated the potential advantages of series arrays in terms of dynamic range and relaxation of fabrication constraints at high frequencies, and the quantum mixer theory was shown to provide a detailed interpretation of their data. Meanwhile, high-current-density single-junction SIS receivers were developed and tested in astronomical observations at 115 GHz by Phillips, Woody, Dolan, Miller, and Linke (1981) and in collaboration with Sollner (Dolan et al., 1981). Negative resistance and infinite available conversion gain were confirmed in experiments at 115 GHz by Kerr, Pan, Feldman, and Davidson (1981). Negative resistance and a net conversion efficiency greater than unity were reported by Smith, McGrath, Richards, van Kempen, Prober, and Santhanam (1981) at 36 GHz; and in collaboration with Batchelor (McGrath et al., 1981) they obtained a large conversion gain $L^{-1} \gtrsim 4$ dB together with a mixer noise temperature $T_M \approx 9$ K $< 5\hbar\omega/k$ near the quantum limit.

Research in this field has recently taken several new directions. Greatly improved experimental measurements of noise temperature are now being implemented in order to evaluate the performance of mixers operating near the quantum limit. The properties of series arrays, and in particular the question of whether these devices show any excess noise over their single-junction counterparts, is an area of intensive investigation. The possibility of submillimeter quasiparticle mixers is being addressed, using either SIS junctions or superconductor—insulator—normal metal (SIN) junctions. SIN junctions are less nonlinear, but are free from the adverse effects of Josephson pair tunneling.

It is already clear that these new receivers will have a major impact on the science and technology of ultra-low-noise detection across the millimeter-wave and microwave region. It also appears that the concepts upon which this work is based may be successfully extended toward both higher and lower frequencies, and perhaps to the description of radically different types of tunneling phenomena as well (Bardeen, 1980). Here we shall attempt to present a review of this subject which can serve as both an introduction to the field and a summary of progress thus far.

II. BACKGROUND

The development of photon-assisted quasiparticle tunneling as a means of detection has, to a great extent, been motivated by the need for low-noise millimeter-wave receivers in astronomical observations. The experimental successes to date have been made possible by the recent sophisticated development of Josephson junctions intended for digital applications. In this section, these two topics are briefly reviewed, along with previous efforts to utilize the Josephson pair tunneling for mixing and detection.

A. Millimeter-wave receivers

The most immediate practical application of SIS mixers is in millimeter-wave astronomy. This field has advanced rapidly in the last decade and has revolutionized our understanding of the colder components of the Universe. For instance, millimeter-wavelength observations have resulted in the discovery of giant molecular clouds, the most massive objects known in our galaxy. An intricate organic chemistry in the interstellar medium has been revealed. The detection of massive and energetic molecular outflows from young stellar objects, generally collimated into pairs of oppositely directed jets, suggests a total revision of our concepts of early stellar evolution. This cursory list could be extended for pages. In the near future, important new results are likely in studies of the 3-K microwave background, the evolution of galaxies, the interstellar medium, star formation, stellar chromospheres, and the planetary system.

In light of this rapid progress, a number of new millimeter-wave observatories are under construction or are being planned. For example, the NSF Subcommittee on Millimeter- and Submillimeter-Wavelength Astronomy has strongly recommended the design of a large aperture-synthesis array of many millimeter-wave antennas (Barrett et al., 1983). The potential of all of these new facilities will be greatly enhanced by utilizing SIS receivers.

It is universally acknowledged that a rapid increase in receiver sensitivity has been one of the major factors driving millimeter astronomy research. Yet the present receivers leave considerable room for further improvement. At millimeter and submillimeter wavelengths, more so than in any other spectral region, astronomy systems are still receiver limited: the receiver's noise contribution is larger than the other contributions (telescope losses, the

atmosphere, and the celestial background). Ideally, millimeter-wave receiver noise temperatures would be considerably less than 100 K for ground-based observatories, and 10 K for space telescopes. Over most of the millimeter- to submillimeter-wave spectral region this criterion is far from being met, so that any further improvement in receiver sensitivity will yield immediate rewards for the observer.

Almost all spectral line millimeter-wavelength observations use heterodyne receivers. A rough prototype of a heterodyne receiver is shown in Fig. 3. The input signal radiation at frequency ω_S from the telescope is coupled into the mixer through a feed horn or some equivalent structure. The mixer combines the signal with local oscillator radiation at frequency ω_{LO} to produce a beat at the intermediate frequency $\omega_{IF} = |\omega_S - \omega_{LO}|$. The IF output is then amplified, perhaps mixed down to a still lower frequency, and fed to some sort of spectrometer to reproduce and display the spectrum of the input signal.

Note that in heterodyne detection the primary amplification is achieved in the *second* major component of the receiver. Thus both the IF amplifier and the mixer must have low noise. An alternative to this somewhat hybrid technique is, of course, to use an amplifier as the first stage of a receiver, with sufficiently high gain that the subsequent signal-processing stages can add little noise. But with present technology, the high-gain amplifiers having the lowest noise temperatures, less than 10 K, are cooled GaAs FET (field-effect transistor) devices (Weinreb *et al.*, 1982) operating in the frequency range 1–5 GHz. Heterodyning takes advantage of these amplifiers. The job of the mixer is to reproduce the signal at the appropriate IF, with as little loss and as little added noise as possible. This is evident in the equation for the total receiver noise temperature,

$$T_R = T_M + LT_{IF} . \qquad (2.1)$$

Here T_M is the noise due to the mixer itself referred to its input, T_{IF} is the noise temperature of the IF amplifier referred to *its* input, and L is the conversion loss of the mixer. The definition of a "noise temperature" is discussed in Sec. VI.E. We use this term to represent a noise *power*, expressed as a temperature by equating it to $kT\Delta\nu$.

An important complication arises from the heterodyne technique. Most mixers operate in the double-sideband (DSB) mode; that is, since ω_{IF} is relative small, most mixers will convert incoming radiation both at $\omega_{LO} + \omega_{IF}$

FIG. 3. Block diagram representing a heterodyne receiver.

and at $\omega_{LO} - \omega_{IF}$ to the same output frequency ω_{IF}. If the performance of a receiver is measured using broadband thermal input signals, which have equal power in both sidebands, the inferred noise temperature is called $T_R(\text{DSB})$, and this value is commonly quoted. Likewise, DSB values of T_M and L may be defined. For spectral line observations, however, the narrow-band signal appears in only one sideband, whereas noise is contributed from both, unless some arrangement is made to remove the unwanted "image" sideband frequency. The appropriate figure of merit for a spectroscopic receiver is thus the single-sideband (SSB) value of T_R, which is twice $T_R(\text{DSB})$ if the mixer responds equally to both sidebands. On the other hand, a receiver may be designed to operate in the intrinsically single-sideband mode, accepting input radiation in one sideband only. In this case measurements of the performance give $T_R(\text{SSB})$ and $L(\text{SSB})$ directly. Equation (2.1) is correct if either SSB or DSB values are used consistently. In this paper, SSB noise temperatures will be quoted throughout, except where explicitly noted.

Numerous variations of Fig. 3 are possible. The local oscillator may accompany the signal through the input horn. The local oscillator may be at one-half of the usual frequency: subharmonic pumping. Various image-rejection schemes may be used. Note that any real receiver will have some loss between its input and the mixer and between the mixer and the IF amplifier, and this will always modify Eq. (2.1) to increase T_R.

T_R measures the sensitivity of a receiver. A receiver will give a signal-to-noise ratio of unity in an integration time Δt for a signal channel of bandwidth $\Delta\nu$ if the equivalent temperature of the signal is (on the order of) $T_R/\sqrt{\Delta\nu\Delta t}$ (see, for example, Tiuri, 1966). Thus reducing T_R allows the observer to cut his integration time by the *square* of the improvement. Alternatively with the same integration time, weaker signals become observable. Figure 4 shows a plot of the best reported receiver noise temperatures for a number of different mixer types, as a function of frequency. Also shown is the approximate lower limit for a receiver's noise temperature $T_R \sim \hbar\omega/k$. It is seen that no millimeter-wave receiver has as yet come within an order of magnitude of this "quantum limit."

Most millimeter-wave astronomy observations have used Schottky diode heterodyne receivers, recently reviewed by Schneider (1982). The last ten years have seen a remarkable improvement in their performance: the SSB T_R for these receivers at 115 GHz has been reduced from ~2000 K to less than 150 K at present. A large increase in sensitivity came with the development of Schottky diodes that show a marked reduction in intrinsic noise when cooled to cryogenic temperatures. Schottky diode technology is now relatively mature, and there appears to be little prospect of a further dramatic improvement in performance, at least in the (30–120)-GHz range. At frequencies above 300 GHz, the InSb bolometer mixer receiver has achieved the lowest noise temperatures (Phillips and Woody, 1982). However, this receiver is unsuitable for many purposes, because its instantaneous bandwidth is only ~1 MHz, limited by the hot-electron recombination
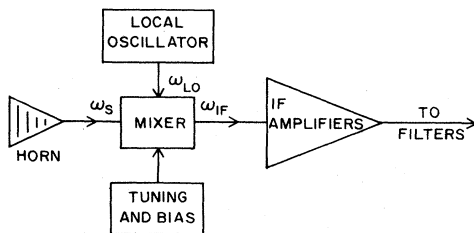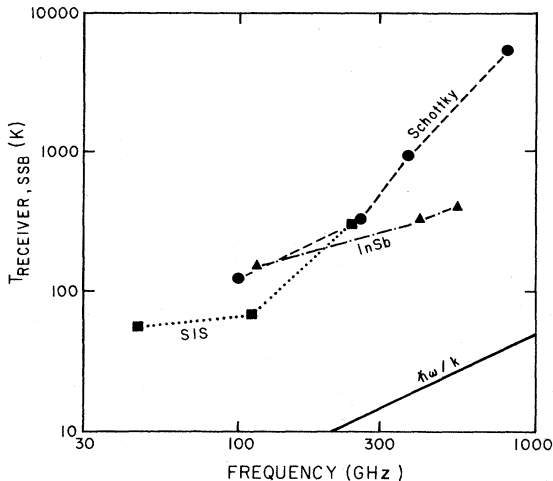
FIG. 4. Lowest reported single-sideband noise temperatures T_R for complete receiver systems in the millimeter and submillimeter-wave regions: ●, Schottky receiver results (Predmore et al., 1984; Erickson, 1984; Röser and Wattenbach, 1984); ▲, InSb receiver results (Phillips and Woody, 1982; Wilson, 1983); ■, SIS receiver results (Pan et al., 1983b; and Sutton, 1983).

FIG. 5. Typical Schottky diode mixer mounting configuration used at long millimeter wavelengths.

time. Below about 50 GHz, maser amplifier receivers have provided extremely low noise temperatures. Unfortunately, these solid-state masers are extremely difficult to fabricate, require large amounts of pump power, and are cumbersome to operate; and the extension of this technology to higher frequencies is problematic. Superconductor-based receiving elements, discussed in the next section, have been used only sporadically for radio astronomy, generally for purposes of demonstration, until the recent development of SIS mixers.

All of these receivers require an input system to couple the signal radiation into the detecting element, with as little loss as possible. The input system may also perform the functions of filtering, diplexing (combining the LO and signal waves), switching, and calibration. Much work has gone into developing Schottky diode mixer coupling systems, and most if not all of this technology is directly adaptable to SIS mixers. Therefore we shall discuss this topic in some detail.

In the long-millimeter-wavelength region, low-noise Schottky mixer mounts have become somewhat standardized, as sketched in Fig. 5. The diode is mounted along the broad wall of a waveguide, and the contact wire, which serves as an antenna to couple the microwave radiation into the diode, is connected to the opposing broad wall. The current path for the IF and dc must be filtered to prevent rf radiation from escaping the waveguide. The waveguide is generally of reduced height, usually one-quarter of the standard, to give an impedance transformation (to about 100 Ω at the diode) and to suppress an out-of-band resonance inherent in this type of mount. A sliding backshort and perhaps a second tuning element are
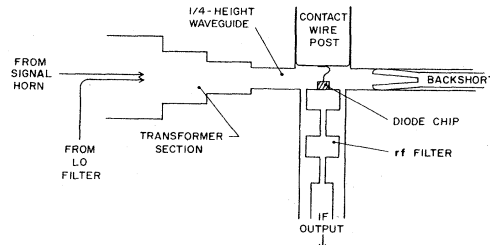
used to optimize the coupling of radiation into the diode. The signal radiation is introduced into the waveguide through a feed horn, and the LO generally enters through a directional filter. As we shall see, this receiver design has been adapted for use in most SIS experiments, with only minor variations.

At higher frequencies, in the submillimeter region, waveguide-mounted receivers are much less successful, for two reasons. Most importantly, the machining dimensions required to scale waveguide components accurately to higher frequency become very difficult or impossible to fulfill. But even with exact scaling, the surface loss per wavelength of the waveguide increases as the square root of the frequency, and this loss compounds every design problem. Therefore submillimeter-wavelength receivers have instead used a variety of quasioptical coupling systems, recently reviewed by Archer (1984), each with its own advantages and drawbacks. Among them are the planar slot-line antenna (Thungren et al., 1982), in which the diode is suspended across a slot line which opens out into a planar antenna, the cavity-backed slot radiator (Kerr et al., 1977), in which the diode is mounted across two parallel slots in a substrate, and the corner cube reflector (Krautle et al., 1977), in which the diode is mounted near the vertex of a three-wall metallic corner. These techniques are still rudimentary, and great opportunity remains for new, clever, coupling schemes. Filtering and diplexing of the incident submillimeter radiation is generally accomplished by a dual-beam (e.g., Martin-Puplett) or multibeam (e.g., Fabry-Perot) interferometer.

In the short-millimeter-wave region some combination of waveguide and quasioptical techniques is generally used. For instance, the diode may be mounted in an oversized waveguide and the radiation applied through an interferometer which serves as a diplexer and an image-rejection filter. The variations are legion. Waveguide techniques are being used at ever higher frequency (Erickson, 1983), and it remains to be seen how far this technology can be successfully extended.

One marked advantage of a waveguide mount is that sliding short circuits and other tuning elements can provide a wide in situ tuning range. In most quasioptical coupling schemes it is difficult to include adjustable tuning elements. In this circumstance it is especially important that the mixer embedding circuitry be well characterized and appropriate. But complex impedance measurements are extremely difficult at millimeter wavelengths.

Instead, the complex embedding impedance seen by a diode in a mixer circuit can be determined using a low-frequency network analyzer on a scale model of the mixer. One example of this technique is given by Held and Kerr (1978). To analyze an (80—120)-GHz Schottky mixer, a 65× scale model was constructed of the entire mixer mount, but not including the Schottky diode itself. The diode was replaced by the tip of a small coaxial cable. The other end of the cable was connected to a network analyzer, which then measured the complex impedances seen by the Schottky diode at the various relevant frequencies, as a function of the position of the tuning backshort. This same technique was successfully adapted to analyze a SIS mixer (Feldman et al., 1983), as is described in Sec. V.B. Scale modeling is valuable in actually designing the mixer circuitry as well; elements of the scale model can be adjusted while monitoring to achieve the requisite impedance range. One potential problem with scale models is that skin effect loss does not scale directly with frequency, so care must be taken when this is important.

The SIS junction performs the same function as the Schottky diode, so it is only natural that the first SIS mixers used straightforward modifications of existing Schottky mixer mount designs. But there are significant differences between the two types of diode. Most important in this context is that the most sensitive Schottky diode is a three-dimensional point-contact device, and Schottky mixers have been designed around this geometry. The SIS junction is a planar, thin-film structure, which is potentially much more versatile. SIS mixers could be built using integrated-circuit techniques to combine coupling structures, tuning circuits, and even IF signal-processing circuits on the same substrate as the SIS junction. To date, little advantage has been taken of this possibility. Another difference is that SIS mixers require much less LO power than Schottky mixers. Schottky design constraints due to inadequate LO power, important at higher frequencies, can be avoided. In time, one may expect that mixer structures more appropriate for SIS junctions will be developed.

The various coupling and tuning structures that have been used in experimental SIS mixers are discussed in Sec. V.A. In addition, Irwin et al. (1985) have demonstrated an 88-GHz SIS direct detector, which is integrated with a planar vee-type antenna. Two suggestions have appeared for electrically adjustable tuning elements for SIS mixers. Whiteley (1982) notes that a pumped SIS junction that is inductively terminated at its IF port presents an inductive reactance at its rf port; this can serve as a tuning element for a second SIS junction, the mixer junction. Irwin et al. (1981) propose using the kinetic inductance of a Josephson junction for tuning a SIS mixer. These techniques have not yet been tried.

B. Superconductor tunnel junctions

The phenomenon of superconductivity was originally discovered early in this century by Kamerlingh Onnes

(1911). After a rich experimental and theoretical history, the understanding of superconductivity reached a major milestone with the BCS theory (Bardeen, Cooper, and Schrieffer, 1957). In brief, this theory states that the electron-phonon interaction results in a weak attraction between electrons, which, in certain materials and at low enough temperatures, is sufficient to cause the electrons to form bound pairs. Although a single electron is a fermion, an electron pair is a boson, and all of the electron pairs in the metal are condensed into the same state, the superconducting ground state, whose collective degrees of freedom are described by a single quantum-mechanical wave function. A single-particle excitation above this ground state requires a minimum threshold energy Δ (the "energy gap"), and consists of a quasiparticle with both "electron"- and "hole"-type properties.

Cohen, Falicov, and Phillips (1962) formulated a Hamiltonian theory describing quasiparticle tunneling through a potential barrier between two bulk superconductors; and their formalism provides the starting point for the quantum mixer theory described in Sec. IV.A. Very shortly thereafter, Josephson (1962) made the remarkable prediction that superconducting pairs could also tunnel through a potential barrier, and deduced the consequences of this "Josephson tunneling," using the same Hamiltonian model. The lossless pair tunneling current was found to depend upon the difference between the phases of the condensate wave functions for the superconductors on either side of the barrier as

$$I = I_J \sin\varphi , \qquad (2.2)$$

where φ is the phase difference and I_J is the critical current, the maximum zero-voltage current which can be passed, dependent upon the specific physical structure. When a finite potential drop V occurs across the barrier, the phase difference varies in time as

$$\frac{d\varphi}{dt} = \frac{2eV}{\hbar} . \qquad (2.3)$$

In the presence of a time-independent voltage V_0, Eq. (2.3) can be integrated and substituted into Eq. (2.2) to predict an alternating current which flows across the barrier at frequency

$$\nu_J = 2eV_0/h . \qquad (2.4)$$

This Josephson frequency, $\nu_J = 484$ GHz/mV, is in the appropriate range to encourage attempts to use pair tunneling for the detection of microwave and millimeter-wave radiation. In spite of a great deal of effort spent in exploring various detection modes, Josephson detectors for a variety of reasons have never been fully competitive with conventional detectors. Even so, there is still strong reason to believe that practical Josephson-effect radiation detectors may yet be developed. In addition, the Josephson-effect detection work is important in the context of this paper, since it set the stage for the eventual development of SIS mixers, which rely on quasiparticle tunneling.

In this section we shall briefly review a few of the various types of Josephson junctions and some of the high-frequency experimental work using these devices. In other areas, Josephson junctions have come into widespread practical use only in the SQUID (superconducting quantum interference device), which is the most sensitive magnetic field sensor, and to establish the standard of voltage, which is now defined through a frequency measurement by Eq. (2.4). In addition, a great deal of effort has gone into the development of digital circuit elements which rely upon Josephson junctions, with the long-range hope of building a Josephson-based computer. An offshoot of this work is the development of junctions, discussed below, that are quite well suited to the requirements of SIS mixers.

All of the topics mentioned in this section are discussed at much greater length in Barone and Paternò (1982) and the references therein. An excellent general introduction to the subject of superconductivity may be found in Tinkham (1975).

1. Types of junctions

Any Josephson junction consists of two bulk superconductors which are "weakly" connected, so that a pair current can pass between them but only by tunneling through the weak barrier. The archetypical Josephson junction is the superconductor-insulator-superconductor (SIS) sandwich, illustrated in the inset of Fig. 1(a). The insulator is most often the oxide of the base superconductor electrode, leading to the term "oxide-barrier junction." In an insulator-barrier junction the quasiparticle current, as well as the pair current, must tunnel through the barrier, which leads to a quasiparticle-branch I-V characteristic of the type seen in Fig. 1(a). The junction may be biased on its supercurrent branch or on its quasiparticle branch. The physical geometry of this junction is that of a parallel plate capacitor with a very narrow dielectric gap. This considerable capacitance and the attendant hysteresis can mask certain Josephson-related effects, and so much of the earlier experimental work aimed at high-frequency applications used other types of Josephson junctions. At the present time, however, experimental interest is largely focused on insulator-barrier junctions because of their many advantages: they are very stable, operate at a moderate current density, and lend themselves to photolithography and modern integrated-circuit fabrication techniques.

There are many other types of Josephson junctions; the major criterion is that Eq. (2.2) apply on a microscopic scale. For our purposes we need mention only a few. Perhaps at the furthest extreme from the insulator-barrier junction is the Josephson microbridge (Anderson and Dayem, 1964). The weak connection in a microbridge is a very narrow and short constriction, generally only a few tenths of a micrometer in dimension, in what would otherwise be a single superconducting region. Very roughly, the "size" of a superconductor's electron pair wave func-

tion is the coherence length ξ, and if the maximum dimension of the constriction is less than ξ, then pairs cannot inhabit the constriction region and must in some sense tunnel through it. The quasiparticles, on the other hand, pass through the microbridge by direct conduction. An advantage of the microbridge is that it can be rather faithfully represented in many cases by a very simple model, the resistively shunted junction (RSJ) model, in which the junction's linear resistance to the quasiparticle current is in parallel with the supercurrent given by Eqs. (2.2) and (2.3), with negligible capacitance. This model gives a nonhysteretic dc I-V curve, illustrated as the solid line in Fig. 6. The pair current oscillations described by Eq. (2.3) are not in this case shunted through a parallel capacitance, as in the insulator-barrier junction, and this introduces a complicated time-dependent behavior onto the finite voltage portions of the dc I-V characteristic in Fig. 6 that must be accurately modeled in analyzing any Josephson-effect device. Perhaps the strongest objection to microbridges has been that under reasonable operating conditions the current densities in the bridge region can become large enough to create a nonequilibrium quasiparticle distribution, an undesirable effect in some ways similar to heating.

Most high-frequency experiments have used the "point-contact" junction, which consists of a very fine superconducting point pressed onto a flat superconductor. Depending upon the nature of the point and upon the pressure, the point contact's physical and electrical characteristics can span the range from oxide-barrier junction to microbridge. The point-contact structure assures a reasonably low capacitance and an adequate sink for nonequilibrium quasiparticles. The adjustment of the point-contact pressure is extremely critical, and although this provides considerable versatility, the mechanical in-

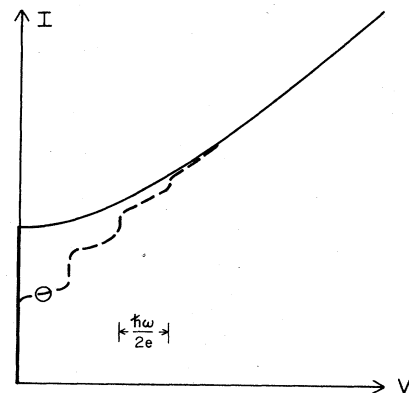FIG. 6. dc I-V curves calculated for an ideal Josephson element shunted only by a linear resistance. Without microwave radiation (solid curve) the maximum zero-voltage supercurrent is I_J. When microwave radiation at frequency ω is applied (dashed curve) the dc supercurrent is depressed and Josephson steps appear at integral multiples of $\hbar\omega/2e$. The optimum bias point for a Josephson-effect mixer is circled.

stability of these devices has been a serious problem, much more so than for the pointed structures used for high-sensitivity Schottky mixers, where the point is used to contact the junction rather than to form it.

The subject of this paper is nonlinear quasiparticle tunneling, as opposed to Josephson pair tunneling. The SIS junctions used in quasiparticle mixers are, indeed, Josephson junctions, even though the name "SIS junction" was coined to maintain this distinction. By happy circumstance, the best Josephson junctions for digital computer elements are also the best SIS junctions for quasiparticle mixing. This is in part because the digital requirement of rapid response time, i.e., relatively low capacitance, is also a requirement for good high-frequency performance. A great deal of developmental research has been directed towards designing Josephson junctions for digital circuits, and the availability of these junctions has been essential to the realization of practical SIS mixers.

Most experimental SIS mixers, reviewed in Sec. V.A, are based on Pb-alloy junctions. Lead is a favorable material because it is relatively easy to work with and has a relatively high superconducting transition temperature, $T_c = 7.2$ K. A high T_c is important for two reasons. The quasiparticle current is most nonlinear at low temperatures, "low" meaning $\lesssim T_c/2$, and it is convenient experimentally to work at $T \gtrsim 2$ K or preferably at $T = 4.2$ K, the boiling point of helium at atmospheric pressure. Also, the "gap frequency" $\omega_g = 2\Delta/\hbar$ is in some sense the characteristic frequency for SIS mixing, and it appears advantageous to operate at a frequency $\omega \ll \omega_g$. For physical temperatures $T \lesssim T_c/2$, $2\Delta \cong 3.5kT_c$ in a BCS superconductor (Tinkham, 1975). Thus lead, or better a substance with a higher transition temperature, is required for SIS mixers to operate in the mid-millimeter- to submillimeter-wavelength region.

Unfortunately, pure lead films have a disqualifying property. Upon thermal cycling from liquid-helium temperatures to room temperature, lead films form stress-induced hillocks, which puncture the thin oxide barriers of SIS junctions. To circumvent this problem, and others less serious, researchers at IBM have developed a type of Pb-alloy junction consisting of a base electrode of $Pb_{0.84}In_{0.12}Au_{0.04}$ and a counterelectrode of $Pb_{0.71}Bi_{0.29}$ (compositions in weight fraction), and a procedure for reproducibly fabricating these junctions (Huang et al., 1980); and they have thoroughly characterized these junctions. The IBM junctions are in all ways at least "almost" suitable for use in a Josephson computer requiring millions of junctions, and so they are clearly overdesigned from the standpoint of SIS mixers. Most SIS mixers have used the IBM-type junctions or a variant thereof.

The standard IBM junctions are (2.5 μm)^2 in area, formed by a photoresist-stencil liftoff technique. With a specific capacitance of 4.2 μF/cm^2 (Magerlein, 1981), these junctions have $\omega RC = 3.3$ at 100 GHz and $R = 50$ Ω. For many purposes, especially at higher frequencies or with a higher-dielectric-constant insulator, smaller junctions are required, and two very clever techniques have been developed to make these small-area junctions reli-

ably. The first is the photoresist overhang technique (Dolan, 1977), for which a thin finger of photoresist is suspended above a substrate. The junction base electrode and counterelectrode are deposited at different oblique angles, so that the overlap region, which is under the photoresist finger, constitutes the junction. A suspended photoresist segment and its resulting SIS junction are shown in Fig. 7. The second technique (Kleinsasser and Buhrman, 1980) is to form an "edge" junction on the (sloped) edge of the base electrode thin film, so that one junction dimension, corresponding to the film thickness, is very small and quite precisely controlled.

Eventually it will be desirable for SIS mixers to use junctions of all-refractory materials, for their indestructibility. The Nb-based mixers described in Sec. V.A.6 are a step in this direction, even though their counterelectrodes are Pb alloy. Unfortunately, the native oxide of Nb has
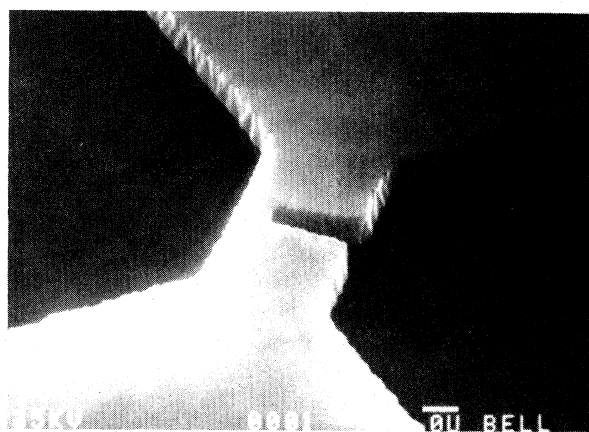
(a)
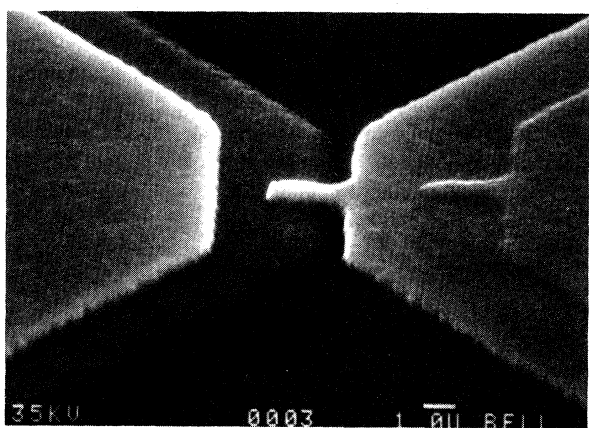
(b)

FIG. 7. Scanning electron microscope photographs of (a) a suspended photoresist bridge structure, and (b) a small-area SIS junction fabricated by angle evaporation past this photoresist bridge (Phillips et al., 1981).

poor tunneling properties (discussed by Halbritter, 1985), and so Nb-based junctions benefit from using a deposited insulating barrier. Some such junctions (e.g., Kroger et al., 1983) appear suitable for SIS mixers. The transition temperature of niobium, $T_c = 9.3$ K, is the highest of any metallic element, but is only marginally better than that of lead. Good quality SIS junctions made of high-T_c materials, for instance NbN, whose $T_c = 16$ K, may soon be available.

In this section we have only glanced at the body of Josephson-junction fabrication literature, which is very extensive and still rapidly growing, much to the benefit of SIS quasiparticle mixers.

2. High-frequency results

When a SIS tunnel junction is irradiated with microwave radiation of frequency ω, as was seen in Fig. 1(a), photon-assisted tunneling steps are induced onto the quasiparticle branch of its dc I-V characteristic, arrayed about the energy-gap voltage with step separation $\delta V = \hbar\omega/e$. In addition to this, any Josephson junction that is irradiated will show constant-current steps on its I-V characteristic at integer multiples of the voltage $V_J = \hbar\omega/2e$. This can be seen by integrating the time-dependent voltage $V(t) = V_0 + v\cos\omega t$ in Eq. (2.3), substituting the result into Eq. (2.2), and expanding. These "Josephson steps" are illustrated by the dashed curve of Fig. 6 for the resistively shunted junction (RSJ) model. The factor of 2 in the step spacing in these two effects reflects the difference between pair and single-particle tunneling.

Only recently have these steps been seen in SIS junctions irradiated with submillimeter radiation. Danchi et al. (1982) studied the Josephson steps in small-area SIS junctions under 604-GHz radiation. The results were close to, but could not distinguish between, the full Werthamer (1966) theory (see Sec. IV.A) and the simpler resistively shunted model. The same group also investigated the photon-assisted tunneling steps under the same conditions (Habbal et al., 1983) in both SIS and SIN junctions and found excellent agreement with the Tien-Gordon (1963) theory (see Sec. III.A). Morita et al. (1983) measured the response of very small Nb-SnO$_x$-Sn tunnel junctions to radiation at frequencies as high as 1.4 THz, which is 2.7 times larger than their gap frequency, and found very distinct Josephson steps and photon-assisted tunneling steps. These important experiments hold open the possibility that superconductor tunnel junctions can be useful detection elements, for quasiparticle mixers or for Josephson-effect devices, at these very high frequencies.

Many possible modes for using the Josephson effect in sensitive high-frequency detection have been explored, both theoretically and experimentally. Although in many cases the initial results are encouraging, the Josephson-effect devices were never fully competitive with conventional detectors. At present, this work has largely abated

in favor of SIS mixers. In this section we shall briefly review a few of the Josephson-effect detection modes that appeared most promising, with emphasis on the major problems encountered. This work formed the historical background for the emergence of quasiparticle mixers.

We feel that it is premature to dismiss the possibility of practical Josephson-effect high-frequency detectors. Although the earlier experiments were quite varied, they had certain common elements. As we shall see, most of these experiments were adversely affected by the extreme nonlinearity of the Josephson effect. They focused almost entirely on point-contact junctions (except at frequencies below 35 GHz) and suffered from the problems inherent with these junctions. SIS junctions were considered unsuitable because of their large capacitance and because their I-V curves are hysteretic. But the very-small-area SIS junctions available today may make competitive Josephson-effect detectors possible, in particular for submillimeter wavelengths. The Josephson nonlinearity will be less extreme for high frequencies, both because of the moderate junction capacitance and because the minimum response time is on the order of the inverse gap frequency. And at high enough frequency the junction's response should be nonhysteretic. This possibility is completely unexplored.

a. Josephson-effect mixer

The Josephson mixer generally uses a point-contact junction with LO power at frequency ω applied sufficient to depress the dc critical current to half of its full value, and is biased with a constant dc current at the point circled in Fig. 6. A small signal at ω_S sees a real impedance and produces an output at frequency $|\omega - \omega_S|$ due to modulation of the magnitude of the pair current by the combined ac potential. The Josephson-effect mixer can have conversion gain (Taur et al., 1974). A variety of experimental and theoretical results find that the best noise temperature of this mixer is on the order of 40 times the larger of either the physical temperature or $\hbar\omega/2k$ (Claassen and Richards, 1978), most of this noise being attributed to the down-conversion of many high-frequency noise components by the strong Josephson nonlinearity. Note, however, that this figure has been surpassed (Taur and Kerr, 1978). Josephson point-contact harmonic mixers are used, without regard to noise temperature, to determine accurately the frequency of far-infrared laser lines (see, for example, Blaney, 1978).

b. Externally pumped parametric amplifier

Examination of Eqs. (2.2) and (2.3) shows that an unbiased Josephson junction behaves like a nonlinear inductor with a small-signal inductance $L_J = \hbar/2eI_J$. If the unbiased junction is "pumped" by radiation at frequency ω, and signal radiation at ω_S is applied, the signal is parametrically amplified in reflection and "idler" radiation at ω_I is also generated (Feldman et al., 1975). The

symmetry of the junction to physical inversion implies that the nonlinear inductance depends only upon even powers of the current, so $\omega_I = 2\omega - \omega_S$ and the amplifier is generally operated with $\omega_S \approx \omega_I \approx \omega$, the "doubly degenerate" mode. If the junction is dc current biased, the symmetry is broken and the parametric amplifier is operated in the singly degenerate mode, $\omega_S \approx \omega_I \approx \omega/2$ (see, for example, Soerensen et al., 1980). Much of the experimental work on these parametric amplifiers has used small SIS Josephson junctions, but at relatively low frequencies below ~ 35 GHz. The major problem encountered has been a "noise rise" with the peculiar property that the input noise temperature rises in direct proportion to the amplifier's gain, rather than being independent of the gain as in all other linear amplifiers. The origin of this noise rise is disputed (Feldman and Levinsen, 1981), but it seems clear that the Josephson nonlinearity that produces the gain must also in some way produce the noise.

c. Internally pumped parametric amplifier

This device takes advantage of the Josephson oscillation in a dc-voltage-biased junction to provide a pump, at the Josephson frequency of Eq. (2.4), for parametric amplification. An extensive analysis by Vystavkin et al. (1977) gives a relatively high noise temperature, due to very-low-frequency noise on the dc bias voltage appearing as phase noise at the pump frequency, and to high-frequency noise down-converted by the strong Josephson nonlinearity. Nevertheless, Kuzmin et al. (1979) conclude that this mode is the most promising in the short submillimeter band. Recently Calander et al. (1982), the first to use SIS Josephson junctions in this mode, achieved a noise temperature of less than 30 K at a signal frequency of 10 GHz. They succeeded in shorting out the very-low-frequency noise by means of an inductive shunt, whereas the high-frequency noise was suppressed by the junction capacitance.

III. SIMPLIFIED MODELS

A full quantum theory of mixing due to photon-assisted tunneling of single-electron quasiparticles is described in Sec. IV. The formal complexity inherent in such an analysis is considerable, however, and tends to obscure the important physical results. Fortunately, most of the significant new effects that arise from the quantum response of nonlinear tunnel junctions at high frequencies can be appreciated on the basis of two simplified models. Section III.A discusses the case where the applied high-frequency radiation is weak and the junction acts as a direct detector. Section III.B treats the case where the applied radiation is strong and the junction acts as a heterodyne mixer, responding to small changes in the amplitude of the incoming radiation.

A. Direct detection of millimeter-wave quanta

The quantum response of a nonlinear tunnel junction at high frequencies may be illustrated by an extension of the

original Tien-Gordon (1963) picture of photon-assisted tunneling (Tucker, 1975; Tucker and Millea, 1978,1979). Suppose that one side of the junction is grounded, and consider the Schrödinger wave function representing a single-electron quasiparticle eigenstate on the opposite side of the tunnel barrier. The presence of a high-frequency ac signal may be represented by a time-dependent voltage applied across the junction in addition to the dc bias:

$$V(t) = V_0 + V_\omega \cos\omega t \ . \tag{3.1}$$

This applied voltage will be assumed to modulate adiabatically the potential energy for each quasiparticle level on the ungrounded side of the barrier. (This assumption is expected to be valid below the plasma frequencies of the two electrodes, typically well into the ultraviolet.) The time dependence of the wave function for every one-electron state in the ungrounded electrode will therefore be modified according to

$$\psi_i(x,t) = \psi_i(x)\exp\left[-\frac{i}{\hbar}\int^t dt'[E_i + eV(t')]\right]$$

$$= \psi_i(x)\exp[-i(E_i + eV_0)t/\hbar]$$

$$\times \sum_{n=-\infty}^{\infty} J_n(eV_\omega/\hbar\omega)e^{-in\omega t} \ , \tag{3.2}$$

where E_i is the unperturbed energy of the Bloch state. The adiabatic modulation of the Fermi sea on this side of the junction can thus be viewed in terms of a probability amplitude $J_n(eV_\omega/\hbar\omega)$ for each quasiparticle level to be displaced in energy by $n\hbar\omega$. This interpretation of Eq. (3.2) is illustrated schematically in Fig. 8. Since all one-electron states are modulated together, these (virtual) displacements in energy are equivalent to dc voltages $(V_0 + n\hbar\omega/e)$ applied across the junction with a probability $J_n^2(eV_\omega/\hbar\omega)$ that depends upon the ac signal amplitude. The resulting dc tunneling current will, therefore, be given by the expression

$$I_0(V_0, V_\omega) = \sum_{n=-\infty}^{\infty} J_n^2(eV_\omega/\hbar\omega)I_{dc}(V_0 + n\hbar\omega/e) \ , \tag{3.3}$$
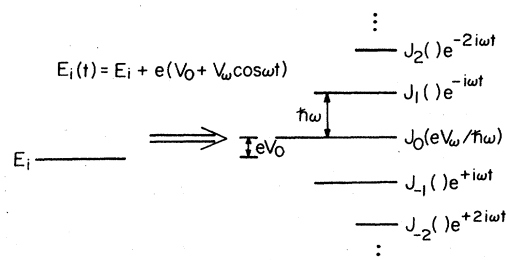

FIG. 8. Virtual energy levels generated according to Eq. (3.2) by adiabatic modulation of the energy $E_i(t)$ for each quasiparticle state within the ungrounded electrode of a tunnel junction in the presence of a microwave field.

where $I_{dc}(V_0)$ represents the unmodulated dc I-V characteristic.

This result of Tien and Gordon (1963) for the dc tunneling current in the presence of an ac potential may be seen to account for the behavior observed in Fig. 1(a) in a particularly simple way. The effect of the applied microwave field is to superpose contributions from the unmodulated I-V characteristic, displaced in voltage by integral multiples of the quantum energy $\hbar\omega/e$. The abrupt rises in current on the steps in Fig. 1(a) are caused by reflections of the sharp onset of dc quasiparticle tunneling at the gap voltage $V_g \equiv (\Delta_1 + \Delta_2)/e$; and the magnitude of the nth photon-assisted tunneling step is determined,

through $J_n^2(eV_\omega/\hbar\omega)$, by the amplitude of the microwave potential actually impressed across the barrier. Under appropriate experimental conditions, an analysis of this step structure may be utilized to infer V_ω as a function of V_0 in order to deduce the high-frequency source impedance seen by the junction.

In this section we shall consider the nonlinear tunnel junction as a direct detector for small incoming signals. The rectified component of the tunneling current may be obtained by expanding the Bessel functions in Eq. (3.3) and retaining only the lowest-order terms in the ac potential V_ω. Using $J_0(x) \sim 1 - x^2/4$, $J_{\pm n}(x) \sim (\pm x/2)^n/n!$, this gives

$$\Delta I_{dc}(V_0) = \frac{1}{4} V_\omega^2 \left[\frac{I_{dc}(V_0 + \hbar\omega/e) - 2I_{dc}(V_0) + I_{dc}(V_0 - \hbar\omega/e)}{(\hbar\omega/e)^2} \right] . \tag{3.4}$$

The quantity in large parentheses is a finite second difference of the unmodulated I-V characteristic that reflects the emission or absorption of a single quantum during the tunneling. All higher-order processes $n = 2, 3, \ldots$, contributing to the dc current may be neglected in the limit of small ac amplitude. This second difference form is seen to reduce to the second derivative of the dc I-V curve, reproducing the standard classical result for the rectification, when the photon energy $\hbar\omega/e$ is smaller than the voltage scale of the dc nonlinearity.

The dissipative, in-phase, component of the junction current induced at the applied ac frequency will be derived in Sec. IV.C:

$$I_\omega(V_0, V_\omega) = \sum_{n=-\infty}^{\infty} J_n(eV_\omega/\hbar\omega)[J_{n+1}(eV_\omega/\hbar\omega) + J_{n-1}(eV_\omega/\hbar\omega)]I_{dc}(V_0 + n\hbar\omega/e) . \tag{3.5}$$

This result may be appreciated by noting that the phase difference between adjacent virtual levels in Fig. 8 is $e^{\pm i\omega t}$. The tunneling amplitude for transitions between the modulated state shown in Fig. 8 and any unmodulated eigenstate across the barrier will contain quantum interference terms proportional to $J_n(eV_\omega/\hbar\omega)e^{-in\omega t}$ arising from these virtual levels. When the tunneling amplitude is squared to obtain the current, there will be terms proportional to $J_n J_{n\pm 1}e^{\pm i\omega t}$ due to this quantum interference that generate a current component at the applied ac frequency. In the limit of small ac amplitude, expanding the Bessel series in Eq. (3.5) yields

$$I_\omega = V_\omega \left[\frac{I_{dc}(V_0 + \hbar\omega/e) - I_{dc}(V_0 - \hbar\omega/e)}{2(\hbar\omega/e)} \right] . \tag{3.6}$$

Here the classical conductance dI_{dc}/dV_0 is replaced by the corresponding first difference involving single-photon absorption or emission for weak incoming signals. The expressions in Eqs. (3.4) and (3.6) thus constitute simple and intuitively appealing quantum generalizations of the classical analysis to account for the effects of photon-assisted tunneling.

The current responsivity of a direct detector is defined as the induced change in dc current per unit ac signal power absorbed by the detecting element. Combining Eqs. (3.4) and (3.6) yields

$$R_i = \Delta I_{dc} / \frac{1}{2} V_\omega I_\omega$$

$$= \frac{e}{\hbar\omega} \left[\frac{I_{dc}(V_0 + \hbar\omega/e) - 2I_{dc}(V_0) + I_{dc}(V_0 - \hbar\omega/e)}{I_{dc}(V_0 + \hbar\omega/e) - I_{dc}(V_0 - \hbar\omega/e)} \right]$$

$$\rightarrow \frac{1}{2} \frac{d^2 I_{dc}/dV_0^2}{dI_{dc}/dV_0}, \quad \text{classical limit}$$

$$\rightarrow \frac{e}{\hbar\omega}, \quad \text{quantum limit} . \tag{3.7}$$

The standard classical expression for rectification is recovered when the dc I-V characteristic changes slowly on the quantum voltage scale $\hbar\omega/e$. This classical result would imply that a direct detector could be made arbitrarily sensitive by increasing the curvature $d^2 I_{dc}/dV_0^2$ of the dc nonlinearity. Photon-assisted tunneling theory, however, demonstrates that there is a fundamental limit $R_i = e/\hbar\omega$ to the current responsivity for any single-particle tunnel junction. The quantum limit corresponds to the tunneling of one additional electron across the barrier for each signal photon absorbed. The general expression obtained in Eq. (3.7) characterizes direct detection for any single-particle tunnel junction, and describes a continuous transition between classical behavior and quantum response as the photon energy becomes comparable to the voltage scale of the dc I-V nonlinearity.

Quantum-limited responsivity can be achieved in practice for an SIS junction biased immediately below the energy-gap voltage $V_g = (\Delta_1 + \Delta_2)/e$, in the range

$V_g - \hbar\omega/e < V_0 < V_g$ [see Fig. 1(a)]. This region is called the "first photon step," with other photon steps defined accordingly. Over this region, the value of $I_{dc}(V_0 + \hbar\omega/e)$ will be much larger than either $I_{dc}(V_0)$ or $I_{dc}(V_0 - \hbar\omega/e)$, and the quantity in large parentheses in Eq. (3.7) approaches unity. It is clear that quantum-limited responsivity will be attained, irrespective of the detailed shape of the dc I-V curve, so long as $I_{dc}(V_0 + \hbar\omega/e) \gg I_{dc}(V_0), I_{dc}(V_0 - \hbar\omega/e)$, and that this can occur only when the photon energy $\hbar\omega/e$ is larger than the voltage scale of the quasiparticle current onset at the gap voltage.

The sensitivity of a nonlinear tunnel junction as a direct detector is limited by noise due to the bias current. For dc voltages $eV_0 \gtrsim 2kT$ larger than thermal energies, the mean-square noise current is given by the usual shot-noise expression,

$$\langle I_n^2 \rangle = 2eI_{dc}(V_0)B , \tag{3.8}$$

where B represents the output bandwidth. The noise-equivalent power (NEP) is defined as the incident power required to give an output signal equal in magnitude to the average output noise. For a nonlinear tunnel junction, Eqs. (3.7) and (3.8) may be combined to yield an estimate:

$$\begin{aligned} \text{NEP} &= \frac{\langle I_n^2 \rangle^{1/2}}{\eta R_i} \\ &= \frac{\sqrt{2}\hbar\omega B}{\eta} \left[\frac{I_{dc}(V_0)}{eB} \right]^{1/2} , \quad \text{quantum limit .} \end{aligned} \tag{3.9}$$

Here η is a factor characterizing the efficiency for impedance-matching incoming signal power into the diode. The quantum limit for NEP shown here has a simple physical interpretation. The quantity $N = I_{dc}(V_0)/eB$ is the average number of electrons tunneling through the barrier due to the dc bias voltage during a resolution time $\sim 1/B$ determined by the output bandwidth. Since these individual events are statistically uncorrelated, the mean fluctuation in the number of electrons tunneling during this interval is $\sqrt{N}$. The quantum-limited value for NEP in Eq. (3.9) therefore represents the absorption of $\sim\sqrt{N}$ photons per resolution time, in order to generate a signal current equal in magnitude to the average noise. Equation (3.9) is, in fact, identical to the corresponding result for a photomultiplier, a photodiode, or a photoconductor. For these more familiar quantum detectors, the dc bias current in the above expression would be replaced by either the dark current or by generation-recombination currents in determining the noise-equivalent power (see, for example, Yariv, 1976). The general form of Eq. (3.9) is characteristic of all types of direct quantum detectors in which the dominant source of noise is not due to the signal itself.

The first experimental demonstration of direct detection in the quantum regime was reported by Richards et al. (1980), using a Pb(In,Au) alloy SIS junction at 36 GHz. Their results for current responsivity as a function of dc bias are reproduced in Fig. 9, along with the mea-
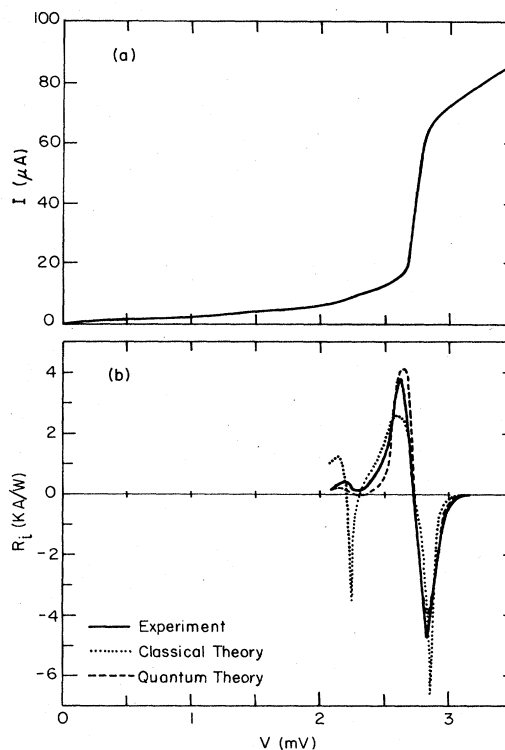

FIG. 9. (a) dc I-V characteristic of a ~ 4-μm^2 Pb(In,Au) alloy SIS tunnel junction at 1.4 K, and (b) measured and calculated current responsivity for direct detection, as a function of dc bias voltage (Richards et al., 1980).

sured dc I-V characteristic. The dashed curve illustrates the quantum theory prediction obtained by inserting measured values for the dc tunneling current into the finite difference form of Eq. (3.7), and the dotted curve is the classical result calculated from the first and second derivatives. Although the differences between the classical and quantum predictions are not generally large in this case, the photon-assisted tunneling theory provides a significantly better overall fit to the experimental data. One characteristic feature of the quantum theory is that it will average out small anomalies in $d^2 I_{dc}/dV_0^2$ which are narrow compared with $\hbar\omega/e = 0.15$ mV. The classical analysis thus predicts a sharp negative peak in the current responsivity near $V_0 = 2.25$ mV which is not present in the quantum prediction, and is not observed. The peak value for the current responsivity $R_i \approx 3500$ A/W obtained in this experiment is within a factor of 2 of the quantum limit $e/\hbar\omega = 6700$ A/W at 36 GHz. The optimum NEP $\approx 2.6 \times 10^{-16}$ W/Hz$^{1/2}$ achieved using this junction is also in very good agreement with predictions based on Eq. (3.9), and represented the lowest value ever reported for a direct microwave detector at the time. It should be noted, however, that the noise power was evaluated within a bandwidth about 50 MHz in this experiment. At the much lower frequencies suitable for mechanical chopping, $1/f$ noise may increase the total NEP of a radiometer.

Hartfuss and Gundlach (1981a) subsequently measured the direct response of Pb-alloy junctions to 70-GHz radiation. Their best result was an NEP of 1.7×10^{-15} W/Hz$^{1/2}$ at a chopping frequency of 400 Hz, along with a responsivity of $0.46 e / \hbar \omega$. They mention that their direct detector was saturated by an input power of 10^{-9} W. Habbal *et al.* (1983) investigated the submillimeter response of superconductor–insulator–normal metal (SIN) junctions, using very small Sn-SnO-Pb junctions at a physical temperature of 4.2 K. Though not able to measure the signal power, they experimentally inferred a responsivity of $0.4 e / \hbar \omega$ under 604-GHz radiation, in good agreement with the theory of this section. Note that the signal frequency in this experiment is approximately twice the gap frequency $\Delta / h \sim 310$ GHz for these SIN junctions.

The dc bias current for a SIS direct detector can be made much smaller than the "leakage" current observed below the gap voltage in Fig. 9, and this will yield much lower values of NEP. For a theoretically ideal SIS junction, the dc quasiparticle current vanishes in this region at absolute zero. Thus in principle, though not in practice, it would be possible to reduce the bias current sufficiently that the average number of electrons tunneling during a resolution time of the detector, $N = I_{dc}(V_0)/eB$, becomes less than unity. Under these conditions, the noise generated by the signal itself could no longer be neglected in estimating the noise-equivalent power. The rectified current $\Delta I_{dc} = \eta R_i P_s$ proportional to the incoming signal power should therefore be added to the bias current $I_{dc}(V_0)$ in Eq. (3.8) for the shot noise. When $I_{dc}(V_0)/eB < 1$, the limiting form of Eq. (3.9) in the quantum regime then yields an NEP $\approx \hbar \omega B$ for good impedance matching that approaches the level of single-photon detection. By analogy with other photon detectors—a noisy photomultiplier, for example—it might be expected that this limit could be approached in practice by utilizing heterodyne techniques to suppress the background noise due to the dc bias current. The full quantum mixer theory predicts this result, and experimental measurements of noise temperature for SIS heterodyne mixers are observed to be within small factors of the nominal quantum limit $\hbar \omega / k$.

B. A simplified heterodyne mixer model

The full quantum theory of mixing described in Sec. IV is so complex as to obscure the most important physical results. In particular, it can be difficult to trace the origin of the differences between the quantum mixer theory and the standard classical analysis. Therefore, for maximum clarity, we present in this section the simplest mixer analysis which still faithfully describes the relationship of the mixing element to its environment. This discussion is a condensed version of the phenomenological theory of mixing, which can be found in more general form in Torrey and Whitmer (1948).

The phenomenological theory of mixing treats the case

of very low intermediate frequency. The IF is so low that the mixing element sees the same high-frequency rf circuit at the signal, image, and LO frequencies; and therefore the incoming signal can be treated as a small differential change in the applied LO waveform. For simplicity we shall also assume that the mixing element sees the same circuit at both IF and dc, so that the generated IF amplitudes can be considered as small differential changes in the dc current and voltage. The equivalent circuits seen by the mixing element, both at rf and at low frequency, are shown in Fig. 10. The local oscillator is represented as a current I_{LO} with source conductance G_S. The dc bias is applied by an ideal voltage source in series with the output load conductance G_L. Two further implicit assumptions have been made in presenting Fig. 10: that no harmonic voltages appear at the rf terminals of the mixing element, and that the equivalent embedding circuits are purely resistive.

So far, this model is very closely approximated by the most common experimental mixer configuration. For example, SIS junctions usually have a relatively large geometrical capacitance, which effectively shorts out any harmonic currents. This capacitance can (and should) be tuned out at the LO frequency so that the rf equivalent circuit is purely resistive. If this tuning is not critical, then for the relatively low IF generally used, the signal, image, and LO frequency embedding circuits will in fact be identical. Although the IF and dc embedding circuits generally do *not* coincide experimentally, this makes no difference in the analysis of the mixer. Nevertheless, it should be emphasized that this model will not provide an accurate description of mixers designed to operate in the single-sideband mode or with a large IF.

A more serious departure from the reality of the quantum mixer will occur when we assume, below, that the currents and voltages across the mixing element are in phase. It will be seen in Sec. IV that the complete quantum response of a tunnel junction generates nonlinear reactive components, which cannot, in principle, be completely tuned out. Nevertheless, it has been argued that these "quantum reactances" do not have a significant effect on the optimum performance of a properly tuned mixer (Feldman, 1982), and therefore this model should provide a reasonable guide to understanding many of the new phenomena that are observed in tunnel junction mixers.

One final simplification is necessary to avoid much of the complicated mathematics of Torrey and Whitmer's
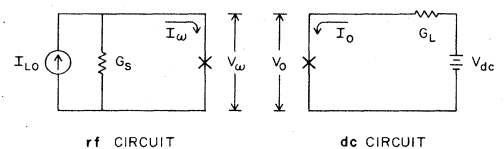

FIG. 10. Equivalent circuits for the simplified heterodyne mixer model at the rf and at low frequencies.

(1948) treatment. We shall choose our "signal" to produce a pure amplitude modulation of the applied LO waveform. With our previous assumptions, this will mean that all rf quantities are in phase. In general, an arbitrary signal results in a combination of amplitude and phase modulation of the LO. Any general calculation, such as Torrey and Whitmer's, must treat the LO frequency ω, the signal frequency ω_S, and the image frequency $2\omega - \omega_S$ as separate and distinct. By choosing to consider only amplitude modulation of the LO, we are in effect assuming that the "signal" consists of input radiation at both the signal and image frequencies, of the same amplitude and coherently phased with respect to the LO, such that there is no resulting phase modulation. Thus all of our signal and IF current and voltage amplitudes will be twice as large as in a more standard treatment. This radiation could, for example, be derived from a sinusoidally varying attenuator in the LO input line. Our justification for choosing this very uncommon special case is the simplicity it provides while yielding precisely the same results (see Sec. IV.F) as a more general analysis.

Within the assumptions of this model, the physical description of the processes taking place inside the mixing element is contained entirely in the expressions for the rf and dc components of the current generated by the combined applied potential:

$$V(t) = V_0 + V_\omega \cos\omega t . \tag{3.10}$$

Here V_0 and V_ω are the dc bias voltage and the amplitude of the local oscillator waveform, respectively, appearing across the mixing element. V_0 and V_ω will be treated as independent variables. The current components will be treated as dependent variables, functionally represented by

$$I_0 = I_0(V_0, V_\omega)$$

$$I_\omega = I_\omega(V_0, V_\omega) , \tag{3.11}$$

whose specific forms will be specified below for both classical and quantum mixers. The following definitions for the various differential conductances will prove useful:

$$G_{00} = \frac{\partial I_0}{\partial V_0}, \quad G_{0\omega} = \frac{\partial I_0}{\partial V_\omega} ,$$

$$G_{\omega 0} = \frac{\partial I_\omega}{\partial V_0}, \quad G_{\omega\omega} = \frac{\partial I_\omega}{\partial V_\omega} . \tag{3.12}$$

(Only monotonically increasing unpumped I-V curves will be considered: $dI_0/dV_0 \geq 0$ everywhere for $V_\omega = 0$. Then it can be shown that $G_{00}, G_{\omega\omega} \geq 0$ under arbitrary conditions.) The properties of the mixer will be formally worked out in terms of these conductances. The *only* difference between classical mixer theory and quantum mixer theory in this model lies in the specific forms taken by the current components in Eq. (3.11). In the end, however, it will be seen that the predictions of this model will be fundamentally altered in the quantum regime.

The mixer analysis begins with a differential expansion of small changes in the junction currents:

$$dI_0 = \frac{\partial I_0}{\partial V_0}dV_0 + \frac{\partial I_0}{\partial V_\omega}dV_\omega = G_{00}dV_0 + G_{0\omega}dV_\omega , \tag{3.13}$$

$$dI_\omega = \frac{\partial I_\omega}{\partial V_0}dV_0 + \frac{\partial I_\omega}{\partial V_\omega}dV_\omega = G_{\omega 0}dV_0 + G_{\omega\omega}dV_\omega . \tag{3.14}$$

The rf circuit equation, by examination of Fig. 10, is $I_{\rm LO} = G_S V_\omega + I_\omega$. A small differential change in $I_{\rm LO}$ is thus given by

$$dI_{\rm LO} = (G_S + G_{\omega\omega})dV_\omega + G_{\omega 0}dV_0 . \tag{3.15}$$

In the absence of such a change in the applied LO power, $dI_{\rm LO} = 0$, and this relation yields

$$\left.\frac{dV_\omega}{dV_0}\right|_{P_{\rm LO}} = -\frac{G_{\omega 0}}{G_S + G_{\omega\omega}} . \tag{3.16}$$

An increase in the dc bias voltage thus results in a reduction in the amplitude of the LO voltage across the element, since $G_{\omega 0}$ is generally positive. This may be understood as a result of holding the available rf power constant, while altering the reflection coefficient at the LO frequency. The differential dc conductivity is found by inserting Eq. (3.16) into Eq. (3.13):

$$G_L^0 \equiv \left.\frac{dI_0}{dV_0}\right|_{P_{\rm LO}} = G_{00} - \frac{G_{0\omega}G_{\omega 0}}{G_S + G_{\omega\omega}} . \tag{3.17}$$

It is important to note that G_L^0, the slope of the pumped dc I-V characteristic, will remain positive for any value of source impedance, provided that the following inequality is satisfied:

$$(G_{00}G_{\omega\omega} - G_{0\omega}G_{\omega 0}) > 0 . \tag{3.18}$$

We shall show that this condition is always satisfied for a classical resistive mixer. In the quantum regime, however, the expressions for the conductance components are altered by the quantum nature of photon-assisted tunneling. Under suitable experimental conditions, the inequality of Eq. (3.18) can be violated for a quasiparticle tunnel junction; and this can lead to induced negative-resistance regions on the measured dc I-V curve, and thus the possibility of theoretically infinite conversion gain.

The conversion efficiency of a mixer is both measured and calculated with the dc voltage source held constant, $dV_{\rm dc} = 0$. Therefore we must determine the relationship between V_0 and V_ω under this condition. The dc circuit equation from Fig. 10 is $V_{\rm dc} = G_L^{-1}I_0 + V_0$. Differentiating this and using Eq. (3.13), we find that

$$\left.\frac{dV_0}{dV_\omega}\right|_{V_{\rm dc}} = -\frac{G_{0\omega}}{G_L + G_{00}} . \tag{3.19}$$

As discussed previously, we consider the signal to be a small amplitude modulation of the LO. Thus, with $V_{\rm dc}$ held constant,

$$I_{\text{sig}} = dI_{\text{LO}} \mid_{V_{\text{dc}}} = \left[G_S + G_{\omega\omega} - \frac{G_{0\omega}G_{\omega 0}}{G_L + G_{00}} \right] dV_\omega \; ,$$

$$(3.20)$$

where we have used Eqs. (3.15) and (3.19). The effect of this signal along with the LO is to produce a small modulation of the dc current I_0; this modulation is seen to be the IF current amplitude,

$$L^{-1}(V_{\text{dc}}, P_{\text{LO}}, G_S, G_L) \equiv \frac{I_{\text{IF}}^2/2G_L}{I_{\text{sig}}^2/8G_S}$$

$$= 4G_S G_L \left[\frac{G_{0\omega}}{(G_{00}+G_L)(G_{\omega\omega}+G_S) - G_{0\omega}G_{\omega 0}} \right]^2$$

$$= \frac{G_S G_{0\omega}^2}{(G_{\omega\omega}+G_S)^2} \frac{4G_L}{(G_L + G_L^0)^2} \; .$$

$$(3.22)$$

The small-signal properties of the mixer may be most clearly represented by the Norton equivalent circuits shown in Fig. 11. The IF output of the mixer is characterized by a current generator I_{IF}^0 in parallel with the output conductance G_L^0 given by Eq. (3.17), which is also the differential dc conductivity in this low IF limit. The magnitude of this equivalent current generator may be found by combining Eqs. (3.19) and (3.20) to obtain an expression for $dV_0 = I_{\text{IF}}^0(G_L + G_L^0)^{-1}$, with the result

$$I_{\text{IF}}^0 = -I_{\text{sig}} \frac{G_{0\omega}}{G_{\omega\omega}+G_S} \; .$$

$$(3.23)$$

Note that neither I_{IF}^0 nor G_L^0 depends upon the load conductance G_L. Therefore it is clear from Fig. 11, as it is from Eq. (3.22), that the maximum *available* conversion efficiency will be obtained for a matched load, $G_L = |G_L^0|$.

In the signal frequency circuit of Fig. 11, the mixing element is represented by its small-signal conductance

$$G_S^0 \equiv \frac{dI_\omega}{dV_\omega} \bigg|_{V_{\text{dc}}} = G_{\omega\omega} - \frac{G_{0\omega}G_{\omega 0}}{G_{00}+G_L} \; ,$$

$$(3.24)$$

where we have used Eqs. (3.14) and (3.19). The fraction of the signal power reflected off the mixing element and
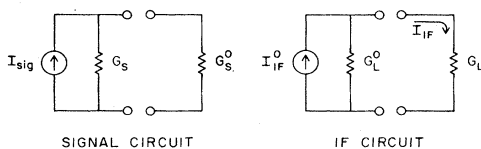

SIGNAL CIRCUIT　　　IF CIRCUIT

FIG. 11. Linearized equivalent circuits for the simplified heterodyne mixer model at both the signal frequency input and at the IF output.

$$I_{\text{IF}} = dI_{0} \mid_{V_{\text{dc}}} = \frac{G_L G_{0\omega}}{G_L + G_{00}} dV_\omega \; ,$$

$$(3.21)$$

where we have used Eqs. (3.13) and (3.19). The conversion efficiency (conversion gain, inverse conversion loss) of the mixer is defined as the ratio of the IF power delivered into the load resistance to the total available incoming rf signal power. Using the results obtained in Eqs. (3.20), (3.21), and then (3.17), this ratio may be written in the form

returned to the signal source is seen to be given in terms of this conductance by the standard formula

$$\frac{P_{\text{sig}}(\text{reflected})}{P_{\text{sig}}(\text{incident})} = \left| \frac{G_S - G_S^0}{G_S + G_S^0} \right|^2 \; .$$

$$(3.25)$$

The functional structure of the mixer equations will be more clearly displayed by defining the following dimensionless parameters:

$$L_0 \equiv \frac{G_{\omega 0}}{G_{0\omega}}, \quad \eta \equiv \frac{G_{0\omega}G_{\omega 0}}{G_{00}G_{\omega\omega}} \; ,$$

$$g_S \equiv \frac{G_S}{G_{\omega\omega}}, \quad g_L \equiv \frac{G_L}{G_{00}} \; .$$

$$(3.26)$$

The conversion efficiency may then be rewritten

$$L^{-1}(V_{\text{dc}}, P_{\text{LO}}, G_S, G_L) = L_0^{-1} \frac{\eta g_S}{(1+g_S)^2} \frac{4g_L}{(g_L + g_L^0)^2} \; ,$$

$$(3.27)$$

where the output conductance Eq. (3.17) is normalized as

$$g_L^0 \equiv \frac{G_L^0}{G_{00}} = 1 - \frac{\eta}{1+g_S} \; .$$

$$(3.28)$$

The maximum available conversion efficiency, that for $g_L = |g_L^0|$, is

$$L_{\text{avail}}^{-1}(V_{\text{dc}}, P_{\text{LO}}, G_S) = L_0^{-1} \frac{\eta g_S}{(1+g_S)(1+g_S-\eta)}$$

$$\text{for } g_L^0 > 0 \; , \quad (3.29)$$

but is infinite if g_L^0 is negative. This last equation emphasizes the fact that the conversion properties of the mixer depend critically upon the strength of the non-

linearity through the parameter η.

Thus far, we have defined general expressions for many of the important properties of this simplified heterodyne mixer model in terms of the conductances defined in Eq. (3.12), without any reference to the specific properties of the mixing element itself. We shall now examine the form that these conductances take in both the classical and quantum theories. The results will illustrate how the physics of the mixing process dramatically determines the mixer's overall properties.

For a classical nonlinear resistor, the current carriers respond to the driving voltage with no time delay, and so $I(t)$ is an instantaneous function of $V(t)$, whose form must be the unpumped dc I-V curve:

$$I(t)=I_{\mathrm{dc}}(V_0+V_\omega\cos\omega t) . \qquad (3.30)$$

The Fourier components of this current required for Eq. (3.11) are given by

$$I_0(V_0,V_\omega)=\frac{1}{\pi}\int_0^\pi d(\omega t)I_{\mathrm{dc}}(V_0+V_\omega\cos\omega t) ,$$

$$I_\omega(V_0,V_\omega)=\frac{2}{\pi}\int_0^\pi d(\omega t)\cos\omega t I_{\mathrm{dc}}(V_0+V_\omega\cos\omega t) , \qquad (3.31)$$

and explicit expressions for the conductances defined in Eq. (3.12), for this classical mixer, are therefore

$$G_{00}=\frac{1}{\pi}\int_0^\pi d(\omega t)\frac{\partial I_{\mathrm{dc}}(V_0+V_\omega\cos\omega t)}{\partial V_0} ,$$

$$G_{\omega\omega}=\frac{2}{\pi}\int_0^\pi d(\omega t)\cos^2(\omega t)\frac{\partial I_{\mathrm{dc}}(V_0+V_\omega\cos\omega t)}{\partial V_0} , \qquad (3.32)$$

$$G_{\omega 0}=2G_{0\omega}=\frac{2}{\pi}\int_0^\pi d(\omega t)\cos(\omega t)\frac{\partial I_{\mathrm{dc}}(V_0+V_\omega\cos\omega t)}{\partial V_0} .$$

From the form of these expressions we immediately see that the parameter L_0 is identically equal to 2, and also that the inequality of Eq. (3.18) is always satisfied for the classical resistive mixer:

$$(G_{00}G_{\omega\omega}-G_{0\omega}G_{\omega 0})=\frac{1}{\pi^2}\int_0^\pi d\varphi_1\int_0^\pi d\varphi_2\frac{\partial I_{\mathrm{dc}}(V_0+V_\omega\cos\varphi_1)}{\partial V_0}\frac{\partial I_{\mathrm{dc}}(V_0+V_\omega\cos\varphi_2)}{\partial V_0}(\cos\varphi_1-\cos\varphi_2)^2\geq 0 . \qquad (3.33)$$

Therefore $\eta\leq 1$. This implies that the output conductance G_L^0 of the classical mixer at the IF will always be positive, according to Eq. (3.28), and so regions of negative differential resistance can never be induced onto the dc I-V curve by the LO drive. Since $\eta\leq 1$, Eqs. (3.27)–(3.29) imply that the classical mixer has a maximum theoretical conversion efficiency $L^{-1}=0.5\eta/(1+\sqrt{1-\eta})^2$, which is reached for source and load conductances given by $g_S=g_L=\sqrt{1-\eta}$. If it is possible to approach the limit $\eta\to 1$, then the maximum conversion efficiency is $L^{-1}=0.5$.

Some classical mixers can approach the limit $\eta\to 1$ in principle. In a well-designed Schottky diode mixer, for example, modulation of the exponential nonlinearity $I_{\mathrm{dc}}(V_0)\propto\exp(eV_0/kT)$ leads to an expression (McColl, 1977) for the parameter η in terms of the modified Bessel functions I_0,I_1,I_2:

$$\eta=\frac{2I_1^2(eV_\omega/kT)}{I_0(eV_\omega/kT)[I_0(eV_\omega/kT)+I_2(eV_\omega/kT)]}$$

$$\approx 1-\frac{1}{2(eV_\omega/kT)^2} \quad\text{for } eV_\omega\gg kT , \qquad (3.34)$$

so that η approaches unity asymptotically in the limit of local oscillator amplitudes V_ω large compared to the voltage scale kT/e of the dc nonlinearity. Thus Schottky mixers are expected to be able to approach $L^{-1}=0.5$, and in fact they do typically achieve conversion losses $L\approx 4$ to 6 dB, within a factor of 2 of this limiting value.

The absolute limitation on the conversion efficiency of classical resistive mixers is more general than the restricted nature of our model might imply. A more complete calculation (Torrey and Whitmer, 1948) verifies our conclusion that the double-sideband mixer is limited to $L^{-1}=0.5$, and also finds that the single-sideband mixer is theoretically limited to $L^{-1}=1.0$. A classical mixer cannot have conversion gain. The simplicity of this result has given it the appearance of a general physical law. This is not the case. We have seen that the prohibition of conversion gain arises solely from the assumption of instantaneous response, as embodied in Eq. (3.30). At high enough frequency, in the quantum regime, the mixing element's response cannot be perfectly instantaneous, and
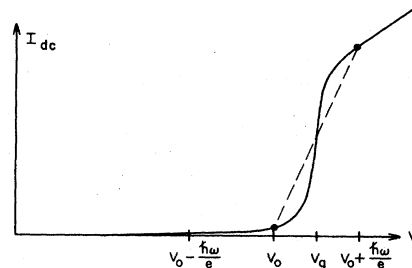

FIG. 12. dc I-V characteristic for a SIS tunnel junction, indicating a bias voltage V_0 in the center of the first photon step below the gap voltage V_g. The slope of the dashed line represents the left side of Eq. (3.37) for $n=0$.

Eq. (3.30) must be discarded. The correct form for the total time-dependent current due to the process of photon-assisted tunneling will be derived in Sec. IV. But we already have in hand the equations necessary to show that the performance of a tunnel junction mixer operating in the quantum regime will be radically altered.

For the simplified mixer model described in this section, the only results of the photon-assisted tunneling theory that are required are Eqs. (3.3) and (3.5) for the dc current and the ac component induced at the applied frequency, and these are reproduced here for convenience:

$$I_0(V_0, V_\omega) = \sum_{n=-\infty}^{\infty} J_n^2(eV_\omega/\hbar\omega) I_{\mathrm{dc}}(V_0 + n\hbar\omega/e) ,$$

$$\begin{aligned}
I_\omega(V_0, V_\omega) = \sum_{n=-\infty}^{\infty} J_n(eV_\omega/\hbar\omega) [J_{n+1}(eV_\omega/\hbar\omega) \\
+ J_{n-1}(eV_\omega/\hbar\omega)] \\
\times I_{\mathrm{dc}}(V_0 + n\hbar\omega/e) .
\end{aligned} \tag{3.35}$$

Differentiating these expressions yields the following results for the small-signal conductances defined in Eq. (3.12):

$$G_{00} = \sum_{n=-\infty}^{\infty} J_n^2(eV_\omega/\hbar\omega) \frac{dI_{\mathrm{dc}}(V_0 + n\hbar\omega/e)}{dV_0} ,$$

$$G_{\omega 0} = \sum_{n=-\infty}^{\infty} J_n(eV_\omega/\hbar\omega)[J_{n+1}(eV_\omega/\hbar\omega) + J_{n-1}(eV_\omega/\hbar\omega)] \frac{dI_{\mathrm{dc}}(V_0 + n\hbar\omega/e)}{dV_0} ,$$

$$\tag{3.36}$$

$$G_{0\omega} = \frac{e}{\hbar\omega} \sum_{n=-\infty}^{\infty} J_n(eV_\omega/\hbar\omega)J_{n+1}(eV_\omega/\hbar\omega)\{I_{\mathrm{dc}}[V_0 + (n+1)\hbar\omega/e] - I_{\mathrm{dc}}(V_0 + n\hbar\omega/e)\} ,$$

$$G_{\omega\omega} = \frac{e}{2\hbar\omega} \sum_{n=-\infty}^{\infty} [J_n^2(eV_\omega/\hbar\omega) + J_{n-1}(eV_\omega/\hbar\omega)J_{n+1}(eV_\omega/\hbar\omega)]\{I_{\mathrm{dc}}[V_0 + (n+1)\hbar\omega/e] - I_{\mathrm{dc}}[V_0 + (n-1)\hbar\omega/e]\} .$$

It may be shown that these Bessel series expressions explicitly reduce to the classical limit of Eq. (3.32) if the photon energy $\hbar\omega/e$ is small compared to the voltage scale of the dc nonlinearity at all values of dc bias (Tucker, 1979). In the high-frequency quantum regime, however, these quantities can behave very differently. As an example of the changes brought about by the finite energy $\hbar\omega/e$ of the rf quantum, let us examine the quantity $L_0^{-1} = G_{0\omega}/G_{\omega 0}$. Comparing the above series expressions, it may be seen that $2G_{0\omega}$ can be larger than $G_{\omega 0}$ if

$$\frac{I_{\mathrm{dc}}[V_0 + (n+1)\hbar\omega/e] - I_{\mathrm{dc}}(V_0 + n\hbar\omega/e)}{\hbar\omega/e} > \frac{1}{2}\left[\frac{dI_{\mathrm{dc}}[V_0 + (n+1)\hbar\omega/e]}{dV_0} + \frac{dI_{\mathrm{dc}}(V_0 + n\hbar\omega/e)}{dV_0}\right] \tag{3.37}$$

for the values of n which contribute significantly to the Bessel series. Figure 12 illustrates a SIS junction dc-biased in the region of the first photon step below the gap voltage. In this example the frequency is high enough that the photon energy $\hbar\omega/e$ is larger than the voltage width of the current onset at $V_g = (\Delta_1 + \Delta_2)/e$. Under these conditions, the term on the left in Eq. (3.37) for $n = 0$, which corresponds to the slope of the dotted line in Fig. 12, is large, while the terms on the right, the derivatives at both "photon points" V_0 and $(V_0 + \hbar\omega/e)$, are much smaller. At this bias point the $n = 0$ term will, in fact, dominate the Bessel sum for $G_{0\omega}$; and this quantity will be large compared to $G_{\omega 0}$ because the quantum response "steps over" the region where dI_{dc}/dV_0 is large. For a SIS junction operated at a high enough frequency, therefore, the quantity $L_0^{-1} = G_{0\omega}/G_{\omega 0}$ is no longer identically equal to 0.5, as it is in the classical limit, but can become much larger than unity. On this basis, it might be expected that the conversion efficiency expression in Eq. (3.27) could lead to net conversion gain, and this is indeed the case.

The most spectacular change that results from the physics of photon-assisted tunneling, however, is associat-

ed with the fact that under these same conditions it is possible to have values of the mixing parameter η which exceed unity. That this can happen is certainly not obvious by inspection of the series expressions in Eq. (3.36), and this possibility was initially discovered quite by accident in the course of computer simulations (Tucker, 1980). The implications of this effect are, nevertheless, very profound. The most direct and striking consequence is that the low-frequency output impedance of the pumped diode can become negative. This may be appreciated by examining Eq. (3.28), which shows that G_L^0 will be negative for $\eta > 1$ provided the source impedance is sufficiently large.

The dc I-V curves for a Sn SIS junction with an extremely sharp current rise at the gap voltage are reproduced in Fig. 13 (McGrath et al., 1981), for increasing values of applied local oscillator power at 36 GHz. Negative resistance is seen to be induced onto the first photon step below the gap voltage in these experiments, for certain values of LO power. Moreover, the output impedance is extremely large on the first photon step, so that $G_L^0 \approx 0$, over almost the entire range of applied local oscillator power shown here. An examination of Eqs.
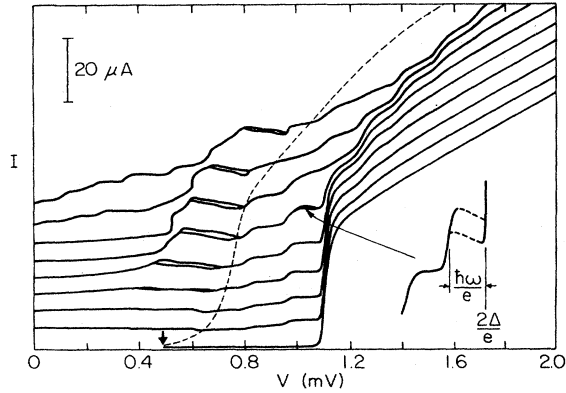
FIG. 13. dc I-V curves for a ~ 10-μm^2 Sn SIS junction at 1.5 K. The lowest curve is the unmodulated characteristic, and higher curves are for applied LO powers at 36 GHz increasing upward in 2-dB increments starting with 0.2 nW. To the left of the dashed line these curves are sensitive to magnetic field, indicating that Josephson pair tunneling is important. The inset shows a region of induced negative resistance (McGrath et al., 1981).

(3.27) and (3.28) indicates that, when G_L^0 is very small, the conversion efficiency becomes

$$L^{-1} \approx L_0^{-1} \frac{4g_S}{1+g_S} \frac{1}{g_L} \quad \text{for } g_L^0 \approx 0 . \tag{3.38}$$

The remarkable conclusion is that, under these conditions, the conversion efficiency will go up linearly with the load impedance. The mixer thus acts as a constant-current source at the IF when $G_L^0 \approx 0$ (this is also clear from Fig. 11), and the available output power will scale with the dynamic resistance $R_D = (G_L^0)^{-1}$. This important aspect of SIS mixer performance was first appreciated by McGrath et al. (1981), and results of their mixing experiments performed on Sn junctions similar to the one shown in Fig. 13 are illustrated in Figs. 14 and 15. The linear increase of conversion efficiency with the dynamic resistance R_D at the operating bias point is dramatically illustrated, along with the realization of considerable net conversion gain. From Eqs. (3.28) and (3.38), it is apparent that values of source impedance corresponding to g_S somewhat less than unity are consistent with achieving large or negative output impedance, but that extremely large rf impedances $g_S \ll 1$ would severely degrade the conversion efficiency. While the best value of G_S relative to the normal impedance R_N of the junction will involve detailed design considerations, the rough criterion that the optimum $g_S \lesssim 1$ is found to be about the same as for classical mixers. The quantum response of quasiparticle mixers will not, therefore, make qualitative changes in the rf matching conditions required for efficient performance. On the low-frequency side, however, the optimization of SIS mixers will require the utilization of impedance-transform techniques to present an effective IF load resis-
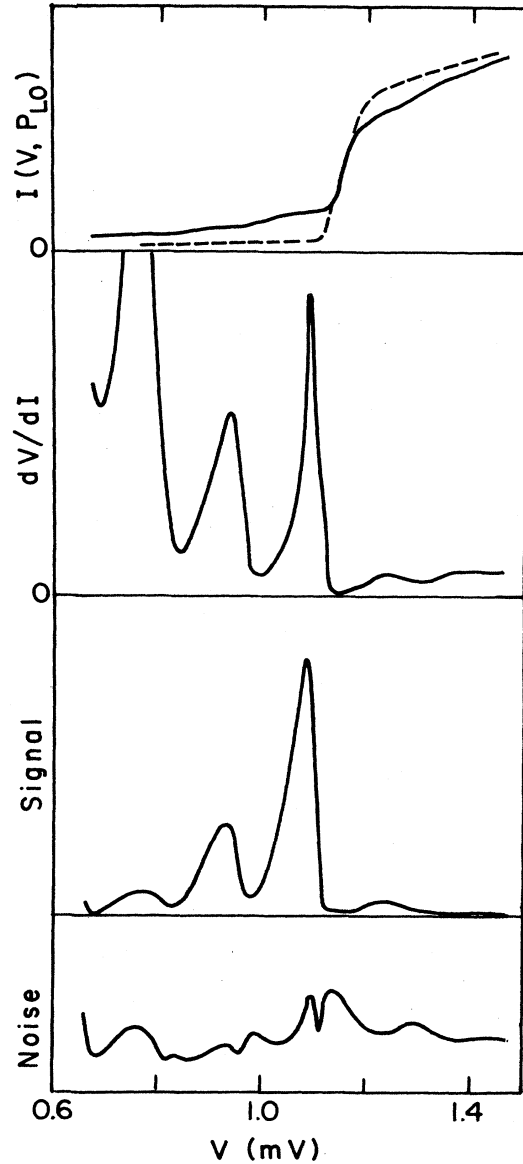

FIG. 14. Performance curves for a 36-GHz mixer using a Sn SIS junction similar to that of Fig. 13, with tuning optimized for maximum conversion efficiency. The signal and noise curves are measured at the IF amplifier output, and yield a maximum conversion gain $+ 4.3 \pm 1.0$ dB with a mixer noise temperature 9 ± 6 K (McGrath et al., 1981).

tance to the diode considerably larger than values typical for a classical resistive mixer.

The available conversion gain becomes infinite when the output impedance goes negative, and this effect was first observed by Kerr et al. (1981) in experiments at 115 GHz on 14-junction Pb-alloy arrays as illustrated in Fig. 16. A detailed consideration of performance for such arrays is presented in Sec. VI.B. For N junctions in series, the voltage scale will be expanded by a factor of N. The step interval is therefore given by $N\hbar\omega/e$, and this feature is apparent in Fig. 16. The dc bias circuit in this case had
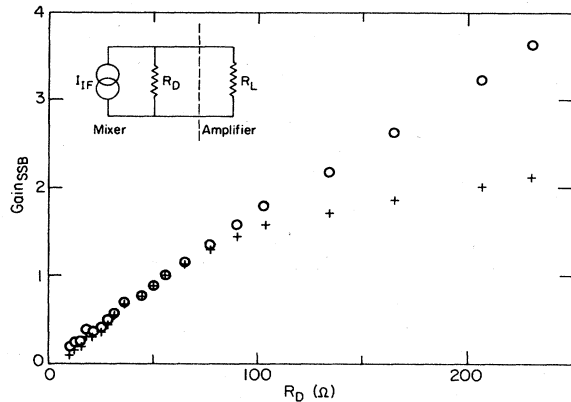
FIG. 15. Conversion gain of a 36-GHz mixer using a Sn SIS junction similar to that of Figs. 13 and 14, measured for various values of dc bias on the first photon peak below the gap voltage and plotted as a function of the dynamic resistance R_D. The measured gain values (crosses) saturate for large R_D due to IF impedance mismatch. The available gain (circles), however, which is corrected for IF mismatch, is nearly proportional to R_D, as expected from the inset equivalent circuit (McGrath et al., 1981).

a relatively low internal impedance, and this allowed for stable mixer operation in the negative-resistance region. Note that the converted output signal varies smoothly through this region, though the *available* power is infinite, consistent with the nonsingular form of Eq. (3.38). The experimentally realized conversion efficiency was found to be a net loss of $L = 11$ dB due to the low value of load resistance $R_L = 50\ \Omega$ relative to the very high output impedance $| R_L^0 | \gg R_N \approx 600\ \Omega$ for this junction ar-
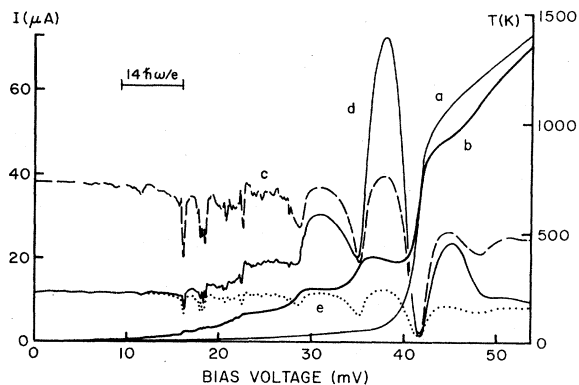

FIG. 16. Experimental curves for a 115-GHz SIS mixer using a 14-element series array of ~ 6-μm^2 Pb-alloy tunnel junctions: a, unpumped dc I-V characteristic, and b, dc I-V curve with applied LO power 0.375 μW showing a region of negative differential resistance. Curves c—e show the output of the 1.4-GHz IF radiometer with c a noise source applied to the mixer's IF port, showing a region of reflection coefficient greater than unity, d a calibrated 115-GHz signal source applied at the mixer's input, and e no applied signal; all for a LO power of 0.375 μW (Kerr et al., 1981).

ray. Much improved conversion efficiencies could, therefore, have been achieved by better matching on the IF output.

At first sight, it might be thought that operation with very high gain in this negative-differential-resistance mode would be beneficial. According to Eq. (3.22), the conversion efficiency may be arbitrarily increased when G_L^0 is negative by designing the mixer so that the load conductance $G_L \approx -G_L^0$ at the operating point. However, it may easily be seen from Eqs. (3.17) and (3.24) that

$$(G_S + G_S^0) = (G_L + G_L^0)(G_{\omega\omega} + G_S)/(G_{00} + G_L) . \quad (3.39)$$

The properties of the mixer at the signal port will therefore become singular when $G_L \to -G_L^0$. According to Eq. (3.25), the signal power "reflected" from the mixer will tend towards infinity. In a more general treatment it can be shown that the reflection coefficient at the image port and at every harmonic sideband port, here assumed shorted, will tend towards infinity as well (Feldman, 1982). This is clearly an unstable situation, which must be avoided. It is even dangerous to operate in the negative-resistance region with low or moderate gain. The negative resistance at dc implies a negative output impedance over at least some range of low frequencies, and the mixer is liable to oscillate somewhere within this range. It is interesting, however, to note that quasiparticle tunnel junctions could potentially be used as high-frequency reflection amplifiers, rather than as mixers, if the tuning circuits were properly designed (Lee, 1982).

Fortunately, a very large conversion gain is not required in order to approach quantum-limited sensitivity in the millimeter-wave region. The "temperature" of a single quantum $T = \hbar\omega/k$ corresponds to a few degrees Kelvin at these frequencies, and a conversion gain of $L^{-1} = 2$—4 is sufficient to reduce the contribution of a $T_{\rm IF} \approx 10$ K amplifier below this level. An optimized SIS millimeter-wave receiver might, therefore, be designed to operate with very large, but still positive, output impedance and a modest conversion gain, achieved in part through an IF impedance transformation.

This discussion of the quantum performance characteristics for quasiparticle mixers in terms of a simplified model has not dealt with the question of mixer noise temperature. From a practical point of view, this is not a significant omission because extensive experimental data and computer simulations have demonstrated that T_M tends to be very small in these devices when the conversion efficiency is high. It may at first seem mysterious that the noise should be so small, since the local oscillator drive induces substantial currents through the junction, which should produce shot noise. That this shot noise can indeed be very small can be understood from an argument first discussed by Uhlir (1958) for a classical p-n junction mixer with an exponential diode I-V characteristic. For a very large LO drive, the conductance of this device approaches its maximum only during a short interval of the LO cycle, and the combination of dc bias and LO current is passed almost entirely in a short burst during this interval near the turning point in the cycle. The resulting

Fourier components $G_{0\omega}$ and $G_{\omega 0}$ in Eq. (3.32) for such a classical mixer can thereby be seen to approach the values for G_{00} and $G_{\omega\omega}$, respectively, producing efficient heterodyne conversion. Shot noise occurs because the current flow results from discrete events, which are statistically independent; even if the average rate is uniform, there will be fluctuations due to the statistical variation in the total during a given interval. In the presence of only a dc current, the mean-square noise current in a bandwidth B about the output frequency would be given by the familiar shot-noise result of Eq. (3.8), which may be rewritten in the form

$$\langle I_n^2 \rangle = 2eI_{\text{dc}}B = 2\left[e\left[\frac{I_{\text{dc}}}{eB}\right]^{1/2}B\right]^2 . \tag{3.40}$$

A bandwidth B corresponds to a sampling time interval $\sim 1/B$ during which it is possible to make independent measurements of the current. The average number of electrons passing through the barrier during this interval is $N = I_{\text{dc}}/eB$. The fluctuations about this mean value will then be of order $\sqrt{N}$ when the individual events are randomly distributed throughout this time interval. When the current through the junction is passed during a sharp spike, whose duration is short on the time scale of all relevant frequencies in a mixer, however, the number of electrons passing through the barrier during each cycle at these frequencies will be accurately determined. Deviations from the mean value of the time-dependent current due to the random nature of the independent events during the current pulse cannot be resolved by the mixer under these conditions, and the shot noise is therefore effectively suppressed.

A complete description of shot noise in a heterodyne mixer requires detailed analysis, and a theory of noise in quasiparticle tunnel junctions is summarized in Sec. IV.E. The argument presented here, however, is intended to demonstrate that efficient heterodyne conversion and low noise are not incompatible, but in fact tend to go hand-in-hand.

IV. QUANTUM MIXER THEORY

In this section a systematic quantum generalization of microwave mixer analysis is presented, which describes the performance of nonlinear quasiparticle tunnel junctions as detectors and mixers (Tucker, 1979). The basis of this quantum mixer theory is the transfer Hamiltonian formulation of tunneling originally put forward by Cohen, Falicov, and Phillips (1962). In this approach, the effect of the coupling through a tunnel barrier is included via an additional term in the system Hamiltonian:

$$H_T = \sum_{kq\sigma}(T_{kq}c_k^\dagger c_q + T_{kq}^* c_q^\dagger c_k)$$

$$= H_T^+ + H_T^- . \tag{4.1}$$

Here c_k and c_q are second-quantized operators representing Bloch states for electrons on the left- and right-hand

sides of the junction, respectively, and the spin indices have been suppressed for simplicity. Terms in H_T^+ thus transfer electrons from right to left across the barrier, while those in H_T^- correspond to tunneling in the opposite direction. The matrix elements that characterize barrier penetration between states of comparable energy are given by (Bardeen, 1961)

$$T_{kq} = -\frac{\hbar^2}{2m}\int dS(\psi_k^* \nabla \psi_q - \psi_q \nabla \psi_k^*) , \tag{4.2}$$

where ψ_k and ψ_q are the appropriate Schrödinger wave functions calculated for the left- and right-hand systems separately, assuming a barrier of infinite width, and the surface overlap integral may be evaluated over any plane lying within the junction. The current flow through the barrier is then to be evaluated by including the transfer Hamiltonian of Eq. (4.1) to lowest order, utilizing time-dependent perturbation theory.

The result obtained in Sec. IV.A for the average quasiparticle tunneling current may be written in the form (Werthamer, 1966)

$$\langle I(t) \rangle = \text{Im} \int_{-\infty}^{\infty} d\omega' d\omega'' W(\omega')W^*(\omega'')$$
$$\times e^{-i(\omega'-\omega'')t}j(V_0 + \hbar\omega'/e) . \tag{4.3}$$

Here the effect of a time-dependent potential $V(t)$ across the junction is expressed in terms of the Fourier transform of the phase factor:

$$\int_{-\infty}^{\infty} d\omega' W(\omega')e^{-i\omega't} = \exp\left[-\frac{ie}{\hbar}\int^t dt'[V(t')-V_0]\right] , \tag{4.4}$$

where the dc bias voltage V_0 has been explicitly removed for convenience. This function represents the additional time dependence introduced coherently onto the wave function for every electron quasiparticle state on the ungrounded side of the junction, and may be seen to be the appropriate generalization of Eq. (3.2) to an arbitrary applied potential.

The physical response of the tunnel junction is completely characterized by the complex function $j(V)$. For the special case of a time-independent potential, Eq. (4.4) gives $W(\omega) = \delta(\omega)$, and the result of Eq. (4.3) for the tunneling current must reduce to the dc I-V characteristic of the junction:

$$I_{\text{dc}}(V_0) = \text{Im}\,j(V_0) . \tag{4.5}$$

Thus $\text{Im}\,j(V)$ may be directly measured.

The real part of the response function $\text{Re}\,j(V)$ characterizes the reactive portion of the tunneling current, and it can be related to the dissipative part $\text{Im}\,j(V)$ through a Kramers-Kronig transform which reflects the requirement of causality. This Kramers-Kronig transform of the dc I-V curve may be defined in the form

$$I_{\text{KK}}(V) \equiv \text{Re}\,j(V) = P\int_{-\infty}^{\infty}\frac{d\bar{V}}{\pi}\frac{I_{\text{dc}}(\bar{V}) - \bar{V}/R_N}{\bar{V} - V} . \tag{4.6}$$

Here it is assumed that the dc current becomes Ohmic in the limit of large bias voltage, exhibiting a normal resistance R_N. The arbitrary subtraction of the second term in the integrand of Eq. (4.6) is allowed because only the nonlinear portion of $I_{dc}(V)$ need be considered in evaluating the reactive part of the response. All physical quantities depend on differences between values of $Re j(V)$ and not on its absolute magnitude. The particular definition chosen in Eq. (4.6) turns out to be very convenient, however, both conceptually and for computational purposes as well. In this form, the nonlinear region of $I_{dc}(V)$ which gives rise to the reactive response may be approximately bounded when computing the Kramers-Kronig transform $I_{KK}(V)$. It should be pointed out that the reactances calculated in terms of $I_{KK}(V)$ are nonclassical, and are present in addition to the ordinary junction capacitance. This effect is negligible so long as photon energies $\hbar\omega/e$ are small compared to the voltage scale of the dc nonlinearity. The current can then be described as an instantaneous classical modulation of the dc I-V characteristic. In the quantum regime, however, the time-dependent current becomes a nonlocal function of the applied voltage, as described in Sec. IV.G. The quantum reactances computed using $I_{KK}(V)$ must then be included in order to obtain a physically consistent description of the tunneling process.

The form of Eq. (4.3) for the quasiparticle tunneling current was originally derived by Werthamer (1966), and is based upon an early calculation by Ambegaokar and Baratoff (1963) of the Josephson effect. When both electrodes of the junction are superconductors, a second term must be added in order to describe the coherent tunneling of Cooper pairs. The structure of the time-dependent response in Josephson junctions has been investigated theoretically by Werthamer (1966), Harris (1974,1975), and many others, and the results of these studies provide a detailed understanding of the complex and beautiful phenomena associated with the pair tunneling. The single-electron quasiparticle contribution to the tunneling current given by Eq. (4.3), however, was for many years perceived as comparatively uninteresting, and only recently has it been appreciated that new and remarkable quantum effects can occur by these processes as well. Here we are concerned exclusively with quasiparticle tunneling phenomena under conditions where the Josephson pair tunneling is either absent or suppressed. In typical SIS mixer diodes, this suppression takes the form of a substantial capacitance, which shunts the pair current at the Josephson frequency $\omega_J = 2eV_0/\hbar$ generated by the applied dc bias voltage. An external magnetic field is also applied in some cases to reduce the overall magnitude of the pair tunneling by inserting flux quanta into the junction. A basic hypothesis of the quantum mixer theory is that pair tunneling may be ignored, and this assumption will break down in SIS junctions for low dc bias voltages or when the capacitance of the junction is small.

Equations (4.3)—(4.6) completely characterize the ac response of a single-particle tunnel junction. It is remarkable that no microscopic calculation is required. The en-

tire physical response for a particular junction is contained in its measured dc I-V characteristic, so long as that characteristic represents only quasiparticle tunneling. This ability to project accurately the complex ac behavior of a tunnel junction using only its measured dc current gives the theory an extraordinary predictive power.

A. Microscopic theory

The transfer Hamiltonian description of Eq. (4.1) arose historically in response to direct observations of the superconductor energy gap in the tunneling experiments by Giaever (1960a,1960b). A new method was required in order to include consistently the many-body correlations that occur between superconducting electrons within the tunneling framework. Bardeen (1961) introduced the idea of considering exact wave functions for electrons on each side of the junction when the barrier is infinitely wide. An approximate expression for the tunneling matrix element is then calculated in Eq. (4.2) due to the small overlap of these exponentially decaying wave functions representing right- and left-side Bloch states within the barrier region. Cohen, Falicov, and Phillips (1962) utilized this picture to construct a theory in which the total system Hamiltonian for the tunnel junction is given by

$$H = H_R^0 + H_L^0 + eV(t)N_L + H_T \ . \tag{4.7}$$

Here $H_{L,R}^0$ represents the full many-body Hamiltonians for the left- and right-hand electrodes in the absence of coupling through the barrier. Modulation of the junction is included via a time-dependent potential multiplying the left-side number operator N_L, while the right side is taken to be grounded. Finally, the coupling between the two systems by tunneling is represented through the transfer Hamiltonian of Eq. (4.1), using any convenient set of Bloch wave functions for the electrons on both sides.

The tunneling current is obtained by the artifice of calculating the time derivative of the right-side number operator:

$$I = e\frac{dN_R}{dt} = i\frac{e}{\hbar}[H_T,N_R]$$
$$= i\frac{e}{\hbar}(H_T^+ - H_T^-)$$
$$= I_+ + I_- \ . \tag{4.8}$$

Notice that the current operator separates naturally into two pieces. Here I_+ transfers electrons from right to left, while I_- is its Hermitian conjugate. Electrons are supplied and extracted through electrical contacts to each side of the junction at the rate determined from Eq. (4.8) in order to preserve macroscopic charge neutrality.

The modulation by the applied potential is assumed to be sufficiently slow and weak that both bulk regions remain close to equilibrium. This will not be true under all conditions. Considerations of nonequilibrium effects in quasiparticle tunneling between superconductors may

be found in Entin-Wohlman (1980), Yu and Entin-Wohlman (1981), and Yu (1984). Here, the density matrix describing the uncoupled system is taken to be

$$\rho_0 = \frac{\exp[-\beta(H^0 - \mu N)]}{\text{Tr}\{\exp[-\beta(H^0 - \mu N)]\}} . \qquad (4.9)$$

In the absence of coupling through H_T, the left and right electrodes are independent, and the density matrix factors accordingly. The addition of the potential term to the left-side Hamiltonian is offset by the change in chemical potential:

$$\mu_L(t) = \mu + eV(t) , \qquad (4.10)$$

so that the thermal equilibrium ensemble of Eq. (4.9) remains unaffected. The only impact of the applied potential on the uncoupled system then appears as a simple phase modulation of all left-side single-particle operators:

$$c_k(t) = c_k^0(t)\exp\left[-i\frac{e}{\hbar}\int^t dt' V(t')\right]$$

$$= c_k^0(t)e^{-i(eV_0/\hbar)t}\int_{-\infty}^{\infty} d\omega' W(\omega')e^{-i\omega' t} . \qquad (4.11)$$

Here $c_k^0(t)$ denotes the Heisenberg operator for a left-side Bloch state in the absence of an applied potential, and the Fourier transform of the ac-induced phase modulation is given according to Eq. (4.4).

This coherent modulation of the quantum-mechanical phase for all Bloch states on the left side of the junction appears directly in the forward and reverse components of the current operator. Inserting the form of Eq. (4.11) into Eqs. (4.1) and (4.8) yields

$$I_-(t) = I_-^0(t)\exp[-i(eV_0 t/\hbar)]\int_{-\infty}^{\infty} d\omega' W(\omega')e^{-i\omega' t} , \qquad (4.12)$$

$$I_+(t) = I_-^\dagger(t) .$$

The expectation value for the total current is calculated by including the coupling through the transfer Hamiltonian to first order, using time-dependent perturbation theory. The standard calculational technique employs the interaction representation. The operators of the system are taken to evolve according to the Heisenberg picture with the unperturbed Hamiltonian H^0. The interaction is then included via an additional time-development operator, which depends only upon the weak perturbation according to

$$i\hbar\frac{d}{dt}U_I(t) = H_T(t)U_I(t) . \qquad (4.13)$$

To first order, this time-development operator may be approximated

$$U_I(t) \approx 1 + \frac{1}{i\hbar}\int_{-\infty}^t dt' e^{\eta t'} H_T(t') , \qquad (4.14)$$

where in the exponential factor $\eta \to 0^+$ is included to turn on the perturbation adiabatically. The current through the barrier is then given by

$$\langle I(t)\rangle = \text{Tr}[\rho_0 U_I^{-1}(t)I(t)U_I(t)]$$

$$\approx \frac{1}{i\hbar}\int_{-\infty}^t dt' e^{\eta t'}\langle[I(t),H_T(t')]\rangle_0$$

$$= \text{Im}\int_{-\infty}^t dt' e^{\eta t'}\frac{2i}{e}\langle[I_+(t),I_-(t')]\rangle_0 . \qquad (4.15)$$

The expectation values in the integrand are to be evaluated for the uncoupled system using the equilibrium density matrix of Eq. (4.9).

Explicitly withdrawing the time dependences of the current operators in Eq. (4.12) induced by the applied potential, we may write the result of Eq. (4.15) for the tunneling current according to the form quoted in Eq. (4.3). The complex response function for the tunnel junction is thus found to be given by

$$j(V) = \int_{-\infty}^t dt' e^{\eta t'}\frac{2i}{e}\langle[I_+^0(t),I_-^0(t')]\rangle_0$$

$$\times e^{+i(eV/\hbar)(t-t')} . \qquad (4.16)$$

The current commutator that appears in this expression depends only upon the time difference for the equilibrium system, and so may be represented in the form

$$\chi_{+-}''(t-t') = \frac{1}{2}\langle[I_+^0(t),I_-^0(t')]\rangle_0 . \qquad (4.17)$$

In terms of the Fourier transform of this function, the current response of the tunnel junction in Eq. (4.16) may be written

$$j(V) = \frac{4}{e}\int_{-\infty}^{\infty} d\bar{\omega}\frac{\chi_{+-}''(\bar{\omega})}{\bar{\omega} - eV/\hbar - i\eta} . \qquad (4.18)$$

An examination of the symmetry properties of the current commutator in Eq. (4.17) reveals that $\chi_{+-}''(\omega)$ is real and antisymmetric. The real and imaginary components of the current response function are thus seen from Eq. (4.18) to be related through a Kramers-Kronig transform. Explicitly identifying $\text{Im}j(V) = I_{\text{dc}}(V)$ as the dc current in Eq. (4.3), when $W(\omega) = \delta(\omega)$ and there is no applied ac potential, then leads to the results quoted in Eqs. (4.5) and (4.6), with

$$I_{\text{dc}}(V) = \frac{4\pi}{e}\chi_{+-}''(eV/\hbar) . \qquad (4.19)$$

The subtraction of the limiting Ohmic conductance from the nonlinear dc I-V characteristic within the integrand of Eq. (4.6) removes a formal divergence in the definition of the Kramers-Kronig transform, and the observable current in Eq. (4.3) may be seen to remain unaffected by this choice.

The result derived in Eq. (4.19) may be used to generate predictions for the dc tunneling current based on a microscopic model for each electrode, and this procedure is illustrated in the following section for an ideal SIS junction between identical superconductors. In practice, the experimentally measured I-V curve can be inserted into Eqs. (4.5) and (4.6) to determine the current response function

$j(V)$, and no microscopic calculation is required. The formal development outlined here in terms of the current components defined by Eq. (4.8) and their correlation functions is essential, however, to a systematic inclusion of noise within this framework.

Just as the entire ac response may be expressed in terms of the dc I-V curve and its Kramers-Kronig transform, it will be shown that all noise properties of the tunnel barrier may be calculated using the equilibrium anticommutator:

$$\phi_{+-}(t-t')=\tfrac{1}{2}\langle [I_+^0(t),I_-^0(t')]_+\rangle_0 . \qquad (4.20)$$

Employing the grand canonical ensemble of Eq. (4.9), this quantity may be related to the corresponding commutator determining the response function in Eq. (4.17) by inserting a complete set of eigenstates (Rogovin and Scalapino, 1974):

$$\phi_{+-}(\omega)=\coth(\beta\hbar\omega/2)\chi''_{+-}(\omega)$$

$$=\frac{e}{4\pi}\coth(\beta\hbar\omega/2)I_{\mathrm{dc}}(\hbar\omega/e) . \qquad (4.21)$$

Expressions of this type are known as Kubo relations, and are widely employed in analyzing fluctuation phenomena (Kubo, 1959). Such relations can be considered generalizations of the well-known Callen-Welton (1951) fluctuation-dissipation theorem.

B. dc I-V curve for an ideal SIS junction

A microscopic expression for the dc tunneling current of a SIS junction can be obtained by utilizing Green's functions and the techniques of many-body theory. This calculation was initially performed by Ambegaokar and Baratoff (1963), and is summarized for the quasiparticle component of the tunneling current in Tucker (1979, Appendix A). The result of this microscopic calculation gives

$$I_{\mathrm{dc}}(V)=\frac{2\pi e}{\hbar^2}\sum_{kq\sigma}\int_{-\infty}^{\infty} d\omega_1 d\omega_2 \, |\,T_{kq}\,|^2 A_L(k,\omega_1)A_R(q,\omega_2)[f(\hbar\omega_1)-f(\hbar\omega_2)]\delta(eV/\hbar+\omega_1-\omega_2) . \qquad (4.22)$$

Here $f(\varepsilon)=(e^{\varepsilon/kT}+1)^{-1}$ is the Fermi factor describing the equilibrium occupation of quasiparticle states of energy ε on either side relative to the chemical potential.

The quantities $A_{L,R}(k,\omega)$ appearing in this equation are the single-particle spectral distribution functions for the left- and right-side electrodes. The spectral distribution function represents the weighted probability for creating an excitation with energy $\hbar\omega$ when an electron of momentum k is either added to or removed from the ground state of the system:

$$A(k,\omega)=\sum_m |\,\langle m\,|\,c_k^\dagger\,|\,0\rangle\,|^2\delta(\omega-\omega_m^{n+1})$$

$$+\sum_m |\,\langle m\,|\,c_k\,|\,0\rangle\,|^2\delta(\omega-\omega_m^{n-1}) . \qquad (4.23)$$

Here the sum is over a complete set of energy eigenstates (see, for example, Schrieffer, 1964). The first term sums over states of the $n+1$ electron system, whose energies with respect to the n electron ground state are written in the form

$$E_m^{n+1}-E_0^n=\mu+\hbar\omega_m^{n+1} . \qquad (4.24)$$

When $k>k_F$ in a normal degenerate Fermi system, the sum in Eq. (4.23) will be dominated near the Fermi surface by a single term, whose frequency equals the energy of the long-lived quasiparticle excitation of momentum k. The second term in Eq. (4.23) sums over states of the $n-1$ electron system, where

$$E_0^n-E_m^{n-1}=\mu+\hbar\omega_m^{n-1} . \qquad (4.25)$$

The quantity $\hbar\omega_m^{n-1}$ is thus defined as the *negative* of the excitation energy for the $n-1$ electron system. When

$k<k_F$ the spectral distribution will be dominated in a normal degenerate Fermi system by a single negative-frequency component representing the quasihole excitations near the Fermi surface.

The spectral distribution function for a normal metal in the vicinity of the Fermi surface is simply

$$A_{\mathrm{normal}}(k,\omega)=\delta(\omega-\varepsilon_k/\hbar) , \qquad (4.26)$$

where ε_k is the single-particle excitation energy referenced to the chemical potential: positive for quasiparticles, and negative for quasiholes. Substitution of this form into Eq. (4.22) immediately yields an expression for the tunneling current between two normal electrodes given by Fermi's golden rule.

The spectral distribution function is most useful, however, for including correlations within the superconducting ground state in a calculation of the tunneling current (see Schrieffer, 1964). The BCS theory is based upon an electronic ground-state wave function of the form

$$|\,\psi_0\rangle=\prod_k(u_k+v_k c_{k\uparrow}^\dagger c_{-k\downarrow}^\dagger)\,|\,0\rangle . \qquad (4.27)$$

The creation operators represent Bloch states of the normal metal, and the superconductor ground state is seen to be characterized by coherent pairing in the occupation of states $(k\uparrow)$ and $(-k\downarrow)$: they are either both empty or both occupied. The probability that the individual pair $(k\uparrow,-k\downarrow)$ is occupied within the BCS ground state is given by the function

$$v_k^2=1-u_k^2=\tfrac{1}{2}(1-\varepsilon_k/E_k) . \qquad (4.28)$$

The value of E_k turns out to be the energy needed to

create a quasiparticle excitation of the superconductor with momentum k:

$$E_k = (\varepsilon_k^2 + \Delta^2)^{1/2} , \tag{4.29}$$

and the spectrum thus contains an energy gap Δ at the Fermi surface in the superconducting state. The form of this quasiparticle energy spectrum is illustrated in Fig. 17, along with the occupation probability v_k^2 for pairs in the ground state.

The quasiparticle excitations of the ground state contain a single unpaired electron of momentum k. The amplitude that such a state can be reached by inserting an additional electron of momentum k is seen to be u_k according to Eq. (4.27), since the portion of the BCS ground state already containing a pair with this momentum is unavailable by the Pauli exclusion principle. Similarly, the amplitude is v_k for obtaining an unpaired quasihole by removing an electron of momentum k from an occupied pair. The spectral distribution function of Eq. (4.23) is therefore given according to the BCS theory by

$$A(k,\omega) = u_k^2 \delta(\omega - E_k/\hbar) + v_k^2 \delta(\omega + E_k/\hbar) . \tag{4.30}$$

In the neighborhood of the Fermi surface, u_k and v_k are each nonvanishing, and the single-particle excitations thus have both a particlelike and a holelike component. The dependence of $A(k,\omega)$ is on the squares of the matrix elements, however, and so no "coherence factors" of the form $u_k v_k$ enter into determining the quasiparticle tunneling current. Substituting the results of Eqs. (4.28) and (4.30) into Eq. (4.22) readily yields an expression for the dc current between two superconductors:

FIG. 17. (a) Quasiparticle energy E_k with respect to the Fermi energy for single-particle excitations of the superconducting ground state, plotted as a function of wave vector. The energy $E_k = (\varepsilon_k^2 + \Delta^2)^{1/2}$ differs from the normal-state value $|\varepsilon_k|$ only very near k_F. The gap Δ_0 is the minimum energy required to inject or withdraw an unpaired electron. (b) The average occupation number $\langle n_k \rangle$ for individual Block states within the BCS ground state. Pair correlations alter the normal state over a very small region at the Fermi surface. (After Schrieffer, 1964.)

$$I_{dc}(V) = \frac{4\pi e}{\hbar} N^2(0) |T|^2 \int_0^\infty d\varepsilon_k d\varepsilon_q \{ [f(E_k) - f(E_q)] \delta(eV + E_k - E_q) + [f(E_k) - f(-E_q)] \delta(eV + E_k + E_q)$$

$$+ [f(-E_k) - f(E_q)] \delta(eV - E_k - E_q) + [f(-E_k) - f(-E_q)] \delta(eV - E_k + E_q) \} . $$

$$\tag{4.31}$$

Here $N(0)$ represents the density of states for each spin near the Fermi surface in the normal state, and the tunneling matrix element $T_{kq} = T$ is assumed to be independent of energy in this region. The various terms in the integrand in Eq. (4.31) may be seen to characterize tunneling processes between particlelike states with energies $+E_k$ or $+E_q$ and holelike states with energies $-E_k$ or $-E_q$ on opposite sides of the barrier. Since all dependence on the coherence factors has canceled out of the calculation, the net result of Eq. (4.31) may be represented by the simplified band diagram in Fig. 1(b) using the effective density of states given in Eq. (1.2).

Analytic expressions have been derived by Werthamer (1966) for the quasiparticle tunneling current in Eq. (4.31) between two BCS superconductors in the limit of zero temperature. The result for an ideal SIS junction between identical superconductors is shown graphically in Fig. 18.
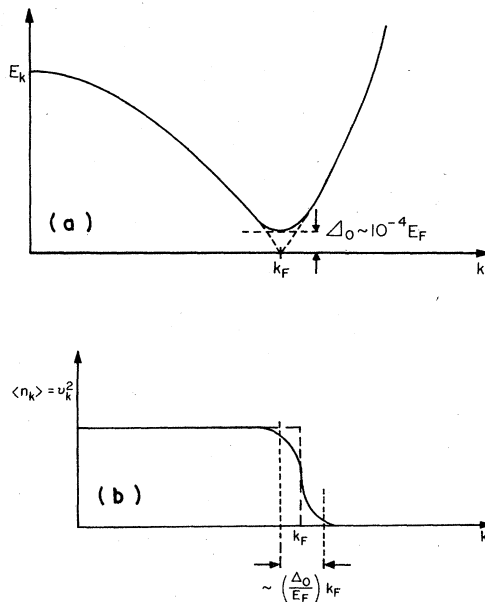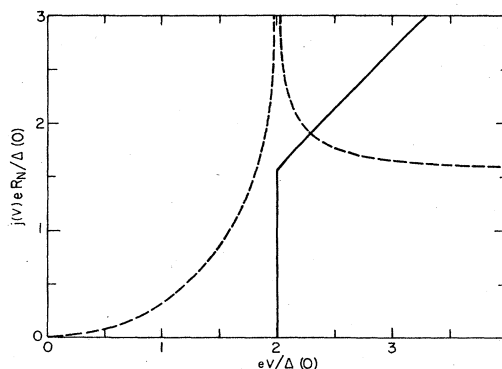

FIG. 18. Quasiparticle current response function $j(V)$ for an ideal SIS junction between identical superconductors in the low-temperature limit $kT \ll \Delta$. The solid line is the dc I-V characteristic $\mathrm{Im} j(V) = I_{dc}(V)$, and the dashed curve is its Kramers-Kronig transform $\mathrm{Re} j(V) = I_{KK}(V)$.

The solid line shows the ideal dc I-V curve $I_{dc}(V)$, with its infinitely sharp onset of quasiparticle tunneling at the gap voltage $eV=2\Delta$. The dashed curve represents the Kramers-Kronig transform $I_{KK}(V)$, which determines the reactive ac response. This function contains a mild logarithmic singularity at the gap voltage that is smoothed into a peak in real junctions by rounding of the current onset over a finite voltage region. The arbitrary constant involved in the definition of $I_{KK}(V)$ has been chosen here so that the value of this function vanishes at $V=0$. The dc current $I_{dc}(V)$ is, of course, an odd function of the applied voltage, and so its Kramers-Kronig transform $I_{KK}(V)$ will be even. These two functions give the dissipative and reactive components, respectively, of the total response function $j(V)$ for the ideal SIS tunnel junction at zero temperature.

C. Local oscillator waveform

The first step in constructing a quantum mixer theory is to solve self-consistently for the large-amplitude local oscillator waveform impressed across the tunnel junction. In general, this is an extremely difficult task, which requires consideration of all harmonics of the applied local oscillator frequency. Ingenious methods have been employed to deal with this problem in classical mixer theory, such as the multiple reflection method of Kerr (1975) and the voltage update method of Hicks and Khan (1982). These methods have recently been adapted for analysis of SIS mixers (Hicks et al., 1985). Both techniques require that the junction's response be treated in the time domain (Sec. IV.G) rather than using the frequency domain Eq. (4.3). However, the mathematical complexity involved in obtaining a complete solution to the large-signal problem, together with uncertainties in the values of the termination impedances seen by the diode at the various harmonics, usually precludes this approach.

Rather than discussing the general problem, for the remainder of this section we shall make the simplifying assumption that only the sinusoidal ac voltage at the applied local oscillator frequency need be considered, i.e., that any current generated at a higher harmonic frequency is short circuited. This condition is commonly achieved in practical SIS mixers by the relatively large geometrical capacitance of the junctions. The capacitance can be tuned out at the signal frequency by a movable backshort, and this configuration has the virtue of preventing the conversion of signal power into the unwanted harmonic sidebands. The effect of harmonic frequencies on the performance of practical SIS mixers is discussed in Secs. V.B and VI.A.

When all harmonics are assumed shorted, the time-dependent voltage across the tunnel barrier will be of the form

$$V(t)=V_0+V_{LO}\cos\omega t \ . \qquad (4.32)$$

The additional phase factor multiplying the Schrödinger wave function for each quasiparticle state on the left side

of the barrier due to the local oscillator is given by

$$\exp\left[-\frac{ie}{\hbar}\int^t dt' V_{LO}\cos\omega t'\right]=\exp[-i(eV_{LO}/\hbar\omega)\sin\omega t]$$

$$=\sum_{n=-\infty}^{\infty} J_n(eV_{LO}/\hbar\omega)e^{-in\omega t} \ . \qquad (4.33)$$

The Fourier transform of this phase factor defined by Eq. (4.4) then becomes

$$W(\omega')=\sum_{n=-\infty}^{\infty} J_n(eV_{LO}/\hbar\omega)\delta(\omega'-n\omega) \ . \qquad (4.34)$$

Substituting this result into Eq. (4.3) for the induced tunneling current gives

$$I_{LO}(t)=\text{Im}\sum_{n,m=-\infty}^{\infty} J_n(\alpha)J_{n+m}(\alpha)e^{+im\omega t}j(V_0+n\hbar\omega/e)$$

$$=a_0+\sum_{m=1}^{\infty}(2a_m\cos m\omega t+2b_m\sin m\omega t) \ , \qquad (4.35)$$

where the amplitude of the local oscillator waveform is contained in the argument of the Bessel functions:

$$\alpha=eV_{LO}/\hbar\omega \ . \qquad (4.36)$$

The average current induced by the local oscillator thus contains components at all the various harmonic frequencies, with magnitudes given by

$$2a_m=\sum_{n=-\infty}^{\infty} J_n(\alpha)[J_{n+m}(\alpha)+J_{n-m}(\alpha)]I_{dc}(V_0+n\hbar\omega/e) \ , \qquad (4.37)$$

$$2b_m=\sum_{n=-\infty}^{\infty} J_n(\alpha)[J_{n+m}(\alpha)-J_{n-m}(\alpha)]$$

$$\times I_{KK}(V_0+n\hbar\omega/e) \ .$$

The expressions derived here for a_0 and $2a_1$ are seen to reproduce the results quoted in Eqs. (3.3) and (3.5) for the dc tunneling current and the dissipative component of the current induced at the applied frequency.

In the classical limit, the quantum energy $\hbar\omega/e$ is small compared to the voltage scale of the dc nonlinearity. The above results may then be shown (Tucker, 1979) to reduce to a simple time-dependent modulation of the dc I-V curve:

$$I_{LO}^{cl}(t)=I_{dc}(V_0+V_{LO}\cos\omega t)$$

$$=a_0^{cl}+\sum_{m=1}^{\infty} 2a_m^{cl}\cos m\omega t \ , \qquad (4.38)$$

where

$$2a_m^{cl}=\frac{2}{\pi}\int_0^\pi d(\omega t)\cos m\omega t I_{dc}(V_0+V_{LO}\cos\omega t) \ . \qquad (4.39)$$

The simple Fourier transform in Eq. (4.39) for the various current components is seen to be replaced in Eq. (4.37) by

complicated Bessel series expressions, which involve the dc current $I_{dc}(V_0+n\hbar\omega/e)$ displaced from the dc bias voltage by integral multiples of $\hbar\omega/e$. It is this feature of the quantum theory that accounts for the dissipative absorption and emission of particular numbers of photons in the tunneling process. Note that the quantum expression for the tunneling current, Eq. (4.35), also contains additional reactive terms, which depend upon the Kramers-Kronig transform $I_{KK}(V)$ of the dc I-V characteristic, and these quantum reactances vanish in the classical limit. In the high-frequency quantum regime, however, the current is a nonlocal function of the applied voltage, and the instantaneous current will not be in phase with the voltage. The reactive components involving $I_{KK}(V)$ must then be included to obtain a physically consistent description of the tunnel junction.

The equivalent circuit for the mixer at the LO frequency ω is illustrated in Fig. 19. The local oscillator is represented by a current generator with complex amplitude $\mathscr{I}_{LO}$ and an effective source admittance $Y_\omega = G_\omega + iB_\omega$ determined by the input waveguide and mounting structure. The susceptance B_ω will include a contribution ωC due to the junction's geometrical capacitance. With the assumption that the higher harmonics of the local oscillator are short circuited, the only physically relevant component of the large-signal ac current through the tunnel junction is $\mathrm{Re}(I_{LO}^\omega e^{+i\omega t})$. Thus the dissipative and reactive currents defined in complex notation by

$$I_{LO}^\omega = I'_{LO} + iI''_{LO} \tag{4.40}$$

may be obtained directly from Eq. (4.37):

$$I'_{LO} = \sum_{n=-\infty}^{\infty} J_n(\alpha)[J_{n-1}(\alpha)+J_{n+1}(\alpha)]I_{dc}(V_0+n\hbar\omega/e), \tag{4.41}$$

$$I''_{LO} = \sum_{n=-\infty}^{\infty} J_n(\alpha)[J_{n-1}(\alpha)-J_{n+1}(\alpha)]I_{KK}(V_0+n\hbar\omega/e). $$

According to Fig. 19, the circuit equation may be written in the form

$$\mathscr{I}_{LO} = I_{LO}^\omega + Y_\omega V_{LO}. \tag{4.42}$$

The total local oscillator power incident on the mixer diode is equal to the available power from the current source:
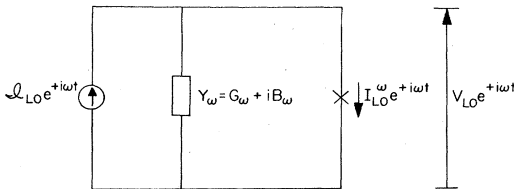

FIG. 19. Large-signal equivalent circuit for a heterodyne mixer. The LO is applied at frequency ω; all higher harmonics $2\omega, 3\omega, \ldots$, are assumed to be short circuited.

$$P_{LO} = \frac{|\mathscr{I}_{LO}|^2}{8G_\omega}$$

$$= \frac{1}{8G_\omega}[(I'_{LO}+G_\omega V_{LO})^2+(I''_{LO}+B_\omega V_{LO})^2]. \tag{4.43}$$

The large-signal problem, within the context of this model, then consists of an iterative solution to Eqs. (4.41) and (4.43) in order to determine the amplitude V_{LO} of the local oscillator waveform across the junction in terms of the incident power P_{LO} and the effective source admittance Y_ω created by the mixer mounting configuration.

D. Small-signal admittance matrix

The small-signal mixing properties of the tunnel junction may be calculated once the amplitude of the local oscillator waveform has been determined. A schematic diagram of a general heterodyne mixer is shown in Fig. 20. Strong pumping at the LO frequency ω mixes the output frequency ω_0 with all sidebands:

$$\omega_m = m\omega+\omega_0, \quad m=0,\pm1,\pm2,\ldots. \tag{4.44}$$

Each of these sidebands is represented in Fig. 20 by a mixer port with a termination admittance Y_m. The incoming signal at frequency $\omega_S=\omega_1$ is represented by a current generator $\mathscr{I}_S$ with a source admittance $Y_S=Y_1$. The function of the mixer diode is to convert this incoming signal power to the output frequency ω_0, and couple it into the load admittance $Y_0=Y_L$ representing the first-stage IF amplifier.

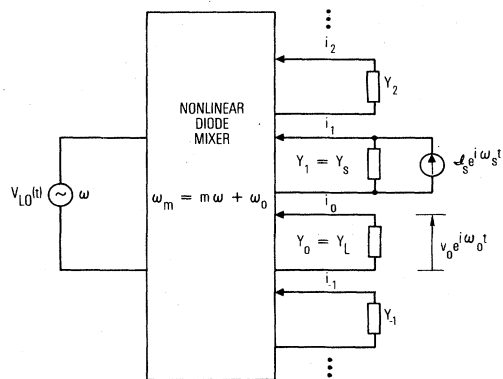The voltages and currents at the sideband frequencies may be represented in the form

FIG. 20. Schematic diagram of a general fundamental heterodyne mixer, with applied LO frequency ω, signal frequency $\omega_S=\omega_1$, and IF output at ω_0. The equivalent embedding networks at all of the sideband frequencies $\omega_m=m\omega+\omega_0$ are indicated, with termination admittances Y_m.

$$v_{\text{sig}}(t) = \text{Re} \sum_{m=-\infty}^{\infty} v_m e^{+i\omega_m t} ,$$

$$i_{\text{sig}}(t) = \text{Re} \sum_{m=-\infty}^{\infty} i_m e^{+i\omega_m t} . \tag{4.45}$$

These voltage and current components will be linearly related for small signals by an admittance matrix

$$i_m = \sum_{m'} Y_{mm'} v_{m'} . \tag{4.46}$$

The values of the admittance matrix elements are determined by the large-signal solution, and depend on the strength of the local oscillator and the nonlinear dc I-V characteristic of the tunnel junction. They are calculated by expanding the total current through the tunnel barrier and identifying those terms that are linear in the small-signal voltages.

The total voltage and current across the tunnel barrier may be written in the form

$$V(t) = V_0 + V_{\text{LO}}(t) + v_{\text{sig}}(t) ,$$

$$\langle I(t) \rangle = I_{\text{LO}}(t) + i_{\text{sig}}(t) . \tag{4.47}$$

The inclusion of $v_{\text{sig}}(t)$ in the applied voltage in Eq. (4.4) requires additional terms in the time-dependent phase factor, which multiply the result of Eq. (4.33) for $V_{\text{LO}}(t)$ alone. Retaining only terms to first order in the sideband voltage components $v_{m'}$, we generalize Eq. (4.34) to

$$W(\omega') = \sum_{n=-\infty}^{\infty} J_n(eV_{\text{LO}}/\hbar\omega) \left[\delta(\omega'-n\omega) + \sum_{m'=-\infty}^{\infty} \frac{e}{2\hbar\omega_{m'}} [v_m^* \cdot \delta(\omega'-n\omega-\omega_{m'}) - v_{m'} \cdot \delta(\omega'-n\omega+\omega_{m'})] \right] . \tag{4.48}$$

Inserting this result into Eq. (4.3) for the total current, and again retaining only terms linear in the sideband voltages $v_{m'}$, we find the admittance matrix elements that give the signal currents i_m in Eq. (4.46) to be

$$Y_{mm'} = G_{mm'} + iB_{mm'} , \tag{4.49}$$

where

$$G_{mm'} = \frac{e}{2\hbar\omega_{m'}} \sum_{n,n'=-\infty}^{\infty} J_n(\alpha)J_{n'}(\alpha)\delta_{m-m',n'-n} \{ [I_{\text{dc}}(V_0+n'\hbar\omega/e+\hbar\omega_{m'}/e) - I_{\text{dc}}(V_0+n'\hbar\omega/e)]$$

$$+ [I_{\text{dc}}(V_0+n\hbar\omega/e) - I_{\text{dc}}(V_0+n\hbar\omega/e-\hbar\omega_{m'}/e)] \} \tag{4.50}$$

and

$$B_{mm'} = \frac{e}{2\hbar\omega_{m'}} \sum_{n,n'=-\infty}^{\infty} J_n(\alpha)J_{n'}(\alpha)\delta_{m-m',n'-n} \{ [I_{\text{KK}}(V_0+n'\hbar\omega/e+\hbar\omega_{m'}/e) - I_{\text{KK}}(V_0+n'\hbar\omega/e)]$$

$$- [I_{\text{KK}}(V_0+n\hbar\omega/e) - I_{\text{KK}}(V_0+n\hbar\omega/e-\hbar\omega_{m'}/e)] \} . \tag{4.51}$$

The elements of the small-signal admittance matrix in this model are seen to separate into real and imaginary parts, which depend only upon the dissipative and the reactive components, respectively, of the junction response.

In the classical limit, the photon energies $\hbar\omega/e$ at all frequencies of interest will be small compared to the voltage scale of the dc I-V nonlinearity. The modulation due to the local oscillator in Eq. (4.38) then produces a time-dependent conductance

$$G^{\text{cl}}(t) = \frac{d}{dV_0} I_{\text{dc}}(V_0 + V_{\text{LO}}\cos\omega t)$$

$$= \sum_{m=-\infty}^{\infty} G^{\text{cl}}(m\omega)e^{im\omega t} \tag{4.52}$$

and a small-signal admittance matrix

$$Y_{mm'}^{\text{cl}} = G^{\text{cl}}[(m-m')\omega] . \tag{4.53}$$

The quantum expression of Eq. (4.50) for the real part of the admittance matrix may be shown to reduce to this result in the classical limit, while the reactive elements given by Eq. (4.51) are found to vanish (Tucker, 1979). The mathematical complexity of the quantum expressions arises from considering effects due to absorption or emission of particular numbers of photons during the tunneling process; and this is unnecessary in the low-frequency classical regime.

Once the admittance matrix elements $Y_{mm'}$ relating the small-signal currents and voltages at the various sideband frequencies have been determined, the analysis of mixer performance is straightforward. In general, there may be incoming radiation applied to the diode at any of the sideband ports in Fig. 20. An arbitrary set of current generators $\{\mathscr{I}_m\}$ placed at each sideband port ω_m of the mixer will produce small-signal current and voltage components across the junction satisfying

$$\mathcal{I}_m = i_m + Y_m v_m$$

$$= \sum_{m'} (Y_{mm'} + Y_m \delta_{m,m'}) v_{m'} . \qquad (4.54)$$

Inverting these equations, one obtains the signal voltages produced by this arbitrary set of current generators,

$$v_m = \sum_{m'} Z_{mm'} \mathcal{I}_{m'} , \qquad (4.55)$$

where, in matrix notation,

$$||Z_{mm'}|| = ||Y_{mm'} + Y_m \delta_{m,m'}||^{-1} . \qquad (4.56)$$

In particular, the output voltage at ω_0 may be written in the form

$$v_0 = Z_{00} \sum_m \lambda_{0m} \mathcal{I}_m , \qquad (4.57)$$

where the quantity

$$\lambda_{0m} = Z_{0m}/Z_{00} \qquad (4.58)$$

does not depend upon the output load termination $Y_0 = Y_L$. This conclusion is obtained by explicitly performing the matrix inversion in Eq. (4.56), and will prove useful in analyzing the noise properties of the mixer. The effect of a current source $\mathcal{I}_m$ at frequency ω_m is thus equivalent at the output to a fictitious source $\lambda_{0m}\mathcal{I}_m$ of frequency ω_0, which depends upon the properties of the mixer but not on the value of $Y_0 = Y_L$.

In a fundamental heterodyne mixer, the incoming signal may be represented by $\mathcal{I}_1 = \mathcal{I}_S$ at frequency $\omega + \omega_0$, as illustrated in Fig. 20. The total signal power available at the input is therefore

$$P_{\text{in}} = |\mathcal{I}_S|^2/8G_S . \qquad (4.59)$$

The power that is frequency down-converted and delivered into the output load may be written in the form

$$P_{\text{out}} = \tfrac{1}{2} G_L |v_0|^2 = \tfrac{1}{2} G_L |Z_{01}|^2 |\mathcal{I}_S|^2 . \qquad (4.60)$$

The conversion efficiency of the mixer is then given by

$$L^{-1} = \frac{P_{\text{out}}}{P_{\text{in}}} = 4 G_S G_L |Z_{01}|^2 . \qquad (4.61)$$

In these expressions, G_S and G_L represent the real parts of the source and load admittances Y_S and Y_L, respectively. The conversion efficiency is therefore readily calculated in terms of the small-signal admittance matrix $Y_{mm'}$ and the terminations Y_m of the diode at each of the sideband frequencies.

E. Noise properties

The combination of dc bias voltage and local oscillator waveform in Eq. (4.32) produces large tunneling currents through the junction at frequency multiples $m\omega$ of the LO drive. The total current has an expectation value given by Eqs. (4.35)—(4.37). Because this current results from the tunneling of individual quasiparticles, however,

fluctuations about the average will produce noise currents at other frequencies; and some of this shot noise will be mixed into the output of the receiver. The theory presented in this section is based conceptually upon Uhlir's (1958) beautiful analysis of shot nose in p-n junction frequency converters.

The shot noise in a tunnel junction mixer may be analyzed by placing a noise generator $[I(t) - \langle I(t) \rangle]$ in parallel with an idealized "noiseless" mixer, where $I(t)$ is the current operator for the tunnel junction. The average current $\langle I(t) \rangle = I_{\text{LO}}(t)$ is given by Eq. (4.35), and the noise generator characterizes the fluctuations about this mean value. Over a long time interval T, which will become infinite at the end of the calculations, the Fourier transform of the current operator may be defined

$$I(t) = \int_{-\infty}^{\infty} d\omega \, I_T(\omega) e^{-i\omega t}, \quad -\frac{T}{2} \le t \le \frac{T}{2} ,$$

$$\qquad (4.62)$$

$$I_T(\omega) = \int_{-T/2}^{T/2} \frac{dt'}{2\pi} e^{+i\omega t'} I(t') .$$

Since the expectation value $I_{\text{LO}}(t)$ of the local oscillator current contains no components at the sideband frequencies $\omega_m = m\omega + \omega_0$, the noise source $[I(t) - \langle I(t) \rangle]$ can be represented by placing a set of current generators $\delta I_m(t)$ at each terminal of the heterodyne mixer illustrated in Fig. 20, with amplitudes given by

$$\delta I_m(t) = \int_{\omega_m - \pi B}^{\omega_m + \pi B} d\omega' [\, I_T(\omega') e^{-i\omega' t}$$

$$+ I_T(-\omega') e^{+i\omega' t}\,] . \qquad (4.63)$$

Here B represents the IF bandwidth about ω_0. Noise components at frequencies outside this interval about each sideband will not be mixed into the load and can be neglected. The ideal "noiseless" mixer on which these current sources are placed now contains no fluctuations. The current operators of Eq. (4.63) are, therefore, transformed by the same matrix Eq. (4.55) that relates the expectation values of the sideband voltages to the external sources. The effect of a current generator at frequency ω_m may be represented at the output by an equivalent source, as in Eq. (4.57), whose strength is determined by the parameter λ_{0m} defined in Eq. (4.58). The entire set of current sources in Eq. (4.63) is thus equivalent to a single such source at the output frequency:

$$\delta I_0^{\text{eff}}(t) = \int_{\omega_0 - \pi B}^{\omega_0 + \pi B} d\omega' [\, I_T^{\text{eff}}(\omega') e^{-i\omega' t}$$

$$+ I_T^{\text{eff}}(-\omega') e^{+i\omega' t}\,] , \qquad (4.64)$$

with

$$I_T^{\text{eff}}(\omega') = \sum_m \lambda_{0m}^* I_T(m\omega + \omega') . \qquad (4.65)$$

The parameter λ_{0m}^* appears conjugated in this expression because the sign convention used to define the Fourier transform in Eq. (4.62) is opposite to that of Eq. (4.45) for the time dependence of the sideband voltages and

currents. This reflects the difference between standard conventions adopted for Fourier transforms in electrical engineering and quantum physics, and every effort has been made to preserve their appropriate use.

The time-averaged mean-square noise current represented by the effective source in Eq. (4.64) is a measure of the noise produced by the local oscillator that appears within the output bandwidth:

$$\langle [\delta I_0]^2 \rangle_{\mathrm{LO}} = \lim_{T \to \infty} \frac{1}{T} \int_{-T/2}^{T/2} dt \langle [\delta I_0^{\mathrm{eff}}(t)]^2 \rangle$$

$$= B \lim_{T \to \infty} \frac{4\pi^2}{T} \langle [I_T^{\mathrm{eff}}(\omega_0), I_T^{\mathrm{eff}}(-\omega_0)]_+ \rangle$$

$$= B \sum_{m,m'} \lambda_{0m} \lambda_{0m'}^* H_{mm'} . \tag{4.66}$$

Because these are operator equations, the ensemble average in this expression involves the anticommutator of the effective current fluctuations at $\pm\omega_0$. The quantity $H_{mm'}$ is known as the current correlation matrix:

$$H_{mm'} = \lim_{T \to \infty} \frac{4\pi^2}{T} \langle [I_T(-\omega_m), I_T(\omega_{m'})]_+ \rangle . \tag{4.67}$$

The elements of this matrix may be calculated by inserting the time-dependent phase factor of Eqs. (4.33) and (4.34) induced by the local oscillator into Eq. (4.12) for the current operators in the forward and reverse directions. The result is

$$I_-(t) = I_-^0(t) \sum_{n=-\infty}^{\infty} J_n(eV_{\mathrm{LO}}/\hbar\omega) e^{-i(n\omega + eV_0/\hbar)t} ,$$

$$I_+(t) = I_-^\dagger(t) . \tag{4.68}$$

Here $I_\pm^0(t)$ represents the Heisenberg operators for the current components in the equilibrium system. The sum of these two pieces is the total current operator of Eq. (4.8), whose Fourier transform defined in Eq. (4.62) may be substituted into Eq. (4.67) to give an expression for the current correlation matrix. After considerable manipulation, the result may be written in terms of the Fourier transform of the equilibrium anticommutator defined in Eqs. (4.20) and (4.21), to give

$$H_{mm'} = e \sum_{n,n'=-\infty}^{\infty} J_n(eV_{\mathrm{LO}}/\hbar\omega) J_{n'}(eV_{\mathrm{LO}}/\hbar\omega) \delta_{m-m',n'-n}$$

$$\times \{ \coth[\beta(eV_0 + n'\hbar\omega + \hbar\omega_{m'})/2] I_{\mathrm{dc}}(V_0 + n'\hbar\omega/e + \hbar\omega_{m'}/e)$$

$$+ \coth[\beta(eV_0 + n\hbar\omega - \hbar\omega_{m'})/2] I_{\mathrm{dc}}(V_0 + n\hbar\omega/e - \hbar\omega_{m'}/e) \} . \tag{4.69}$$

A standard measure of the sensitivity of a heterodyne mixer is the minimum detectable power: the incident signal power required in order to produce an output equal to the noise output. The signal generator $\mathscr{I}_S$ at the input port in Fig. 20 is equivalent, according to Eq. (4.57), to a current source $\lambda_{01}\mathscr{I}_S$ at the output frequency whose square may be expressed in terms of the available incident power Eq. (4.59) in the form

$$\langle [\delta I_0]^2 \rangle_{\mathrm{sig}} = \tfrac{1}{2} |\lambda_{01}|^2 |\mathscr{I}_S|^2$$

$$= 4G_S |\lambda_{01}|^2 P_{\mathrm{in}} . \tag{4.70}$$

Equating this to the mean-square noise in Eq. (4.66) yields a minimum detectable power $P_{\mathrm{in}} = kT_M^{\mathrm{LO}} B$, with a mixer noise temperature given by

$$kT_M^{\mathrm{LO}} = \frac{1}{4G_S |\lambda_{01}|^2} \sum_{m,m'} \lambda_{0m} \lambda_{0m'}^* H_{mm'} . \tag{4.71}$$

This contribution to the total mixer noise temperature T_M represents the shot noise generated by the combination of dc bias voltage and the local oscillator waveform impressed across the tunnel junction. An additional source of noise in a practical mixer can arise because thermal fluctuations in the dissipative terminations $\mathrm{Re} Y_m = G_m$ at the various sideband frequencies in Fig. 20 may be mixed into the output. Noise of this type can be included in the theory without difficulty, although great care is usually taken to ensure that such effects are minimized in practice. One additional noise source that is not included within this semiclassical theory is the "quantum noise" due to quantization of the electromagnetic fields, and this contribution is discussed in Sec. VI.E. General uncertainty principle arguments give a lower bound to the noise temperature of order $T_M \approx \hbar\omega/k$ for any heterodyne mixer. This quantum limit may be approached in practical SIS heterodyne mixers, since calculations based upon Eq. (4.71) often yield a local oscillator shot-noise contribution $T_M^{\mathrm{LO}} < \hbar\omega/k$ in regions of high conversion efficiency; and experimental measurements of mixer noise temperature in many instances give values within small factors of this nominal quantum limit.

F. Simplified heterodyne mixer model revisited

A simplified model was developed in Sec. III.B to illustrate the new quantum effects that are observed in SIS quasiparticle mixers at high frequencies. In this section, the complete quantum mixer theory will be applied to construct a heterodyne receiver model using the three-frequency approximation in the low IF limit. It will be

seen that the results of the simplified model are recovered in the special case where the signal and image frequency terminations are equal and all reactances are neglected.

As before, the tunnel barrier is assumed to have sufficient capacitance so that all harmonics $2\omega, 3\omega, \ldots$, of the local oscillator are effectively shorted, along with their associated sidebands. The waveform impressed across the junction by the local oscillator will then be sinusoidal, and its amplitude V_{LO} may be determined from the incident power P_{LO} and the source admittance $Y_\omega = G_\omega + iB_\omega$ through a self-consistent solution to Eqs. (4.41) and (4.43). The only unshorted sideband frequen-

cies are the signal, output, and image frequencies, ω_1, ω_0, and ω_{-1}, respectively. The second assumption is that the output frequency is sufficiently small compared to the local oscillator frequency that the approximation $\omega_1 \approx \omega \approx -\omega_{-1}$ may be used in evaluating the small-signal admittance and current correlation matrices, and that the quantum energy $\hbar\omega_0/e$ is so small that the response of the tunnel barrier at the output frequency is essentially classical. The signal and image frequency terminations, however, are not necessarily equal.

With these assumptions, the admittance matrix elements given in Eqs. (4.50) and (4.51) simplify to

$$G_{00} = \sum_{n=-\infty}^{\infty} J_n^2(\alpha)\frac{d}{dV_0}I_{dc}(V_0+n\hbar\omega/e) ,$$

$$G_{10} = G_{-10} = \tfrac{1}{2}\sum_{n=-\infty}^{\infty} J_n(\alpha)[J_{n-1}(\alpha)+J_{n+1}(\alpha)]\frac{d}{dV_0}I_{dc}(V_0+n\hbar\omega/e) ,$$

$$G_{01} = G_{0-1} = \frac{e}{\hbar\omega}\sum_{n=-\infty}^{\infty} J_n(\alpha)[J_{n-1}(\alpha)-J_{n+1}(\alpha)]I_{dc}(V_0+n\hbar\omega/e) , \qquad (4.72)$$

$$G_{11} = G_{-1-1} = \frac{e}{2\hbar\omega}\sum_{n=-\infty}^{\infty} [J_{n-1}^2(\alpha)-J_{n+1}^2(\alpha)]I_{dc}(V_0+n\hbar\omega/e) ,$$

$$G_{1-1} = G_{-11} = \frac{e}{2\hbar\omega}\sum_{n=-\infty}^{\infty} J_n(\alpha)[J_{n-2}(\alpha)-J_{n+2}(\alpha)]I_{dc}(V_0+n\hbar\omega/e) ,$$

and

$$B_{00} = B_{01} = B_{0-1} = 0 ,$$

$$B_{10} = -B_{-10} = \tfrac{1}{2}\sum_{n=-\infty}^{\infty} J_n(\alpha)[J_{n-1}(\alpha)-J_{n+1}(\alpha)]\frac{d}{dV_0}I_{KK}(V_0+n\hbar\omega/e) ,$$

$$B_{11} = -B_{-1-1} = \frac{e}{2\hbar\omega}\sum_{n=-\infty}^{\infty} [J_{n-1}^2(\alpha)-2J_n^2(\alpha)+J_{n+1}^2(\alpha)]I_{KK}(V_0+n\hbar\omega/e) , \qquad (4.73)$$

$$B_{1-1} = -B_{-11} = \frac{e}{2\hbar\omega}\sum_{n=-\infty}^{\infty} [J_{n-2}(\alpha)J_n(\alpha)-2J_{n-1}(\alpha)J_{n+1}(\alpha)+J_n(\alpha)J_{n+2}(\alpha)]I_{KK}(V_0+n\hbar\omega/e) .$$

In these expressions, the parameter $\alpha = eV_{LO}/\hbar\omega$ characterizes the amplitude of the local oscillator waveform.

The conversion efficiency of the mixer is determined by the small-signal admittance matrix elements $Y_{mm'} = G_{mm'} + iB_{mm'}$, together with the external terminations Y_1, Y_0, Y_{-1} seen by the tunnel junction at the signal, output, and image frequencies, as illustrated in Fig. 20. These termination admittances are added along the diagonal of the 3×3 admittance matrix, as in Eq. (4.56), and the combination is then inverted to yield the 3×3 impedance matrix $Z_{mm'}$ which characterizes the conversion properties of the complete mixer. The load admittance $Y_0 = G_L$ at the output frequency will ordinarily be real, and represents the conductance of the IF amplifier as seen by the tunnel junction. The source admittance $Y_1 = Y_S$ at the signal frequency and the image termination $Y_{-1} = Y_I$ depend upon the design of the mixer mount. For a double-sideband mixer, $Y_S = Y_I^*$. For a single-sideband mixer, the real part of Y_I is either zero (shorted) or infinite (open). In general the performance of a mixer depends

upon both Y_S and Y_I in addition to G_L. Inversion of the 3×3 augmented admittance matrix in Eq. (4.56) is, of course, straightforward for arbitrary values of these terminations.

The double-sideband mixer, in which the signal and the image frequencies are equivalent, presents a commonly realized special case. Under these conditions, $Y_1 = Y_{-1}^* = Y_S = G_S + iB_S$, and the result of Eq. (4.61) for conversion efficiency leads to the expression

$$L^{-1} = L_0^{-1} 4\eta g_S g_L \frac{(\xi+g_S)^2+(b_S-\gamma)^2}{[(\xi+g_S)(1+g_S)+(b_S^2-\gamma^2)]^2}$$
$$\times \frac{1}{(g_L+g_L^0)^2} . \qquad (4.74)$$

The dimensionless parameters appearing here are defined in terms of the admittance matrix elements and the source and load terminations by

$$L_0 = \frac{2G_{10}}{G_{01}}, \quad \eta = \frac{2G_{01}G_{10}}{G_{00}(G_{11}+G_{1-1})},$$

$$g_S = \frac{G_S}{G_{11}+G_{1-1}}, \quad g_L = \frac{G_L}{G_{00}},$$

$$\xi = \frac{G_{11}-G_{1-1}}{G_{11}+G_{1-1}}, \quad \beta = \frac{B_{10}}{G_{10}}, \quad (4.75)$$

$$\gamma = \frac{B_{1-1}}{G_{11}+G_{1-1}}, \quad b_S = \frac{B_{11}+B_S}{G_{11}+G_{1-1}}.$$

The output conductance of the mixer is real in this case, and is obtained by subtracting the load conductance from the total mixer conductance at the output frequency:

$$G_L^0 = \frac{1}{Z_{00}} - G_L . \quad (4.76)$$

This quantity is simply the slope of the dc $I\text{-}V$ curve in the presence of the local oscillator drive. In dimensionless units, the result obtained in this model for the output conductance may be written in the form

$$g_L^0 = \frac{G_L^0}{G_{00}} = 1 - \eta \frac{(\xi+g_S)+\beta(b_S-\gamma)}{(\xi+g_S)(1+g_S)+(b_S^2-\gamma^2)} . \quad (4.77)$$

These results of the complete theory for a double-sideband mixer are seen to be identical to the simplified model discussed in Sec. III.B, if all reactive elements are neglected. When β, b_S, and γ are all set equal to zero, Eq. (4.74) for the conversion efficiency reduces to the form of Eq. (3.27), and the result of Eq. (4.77) for the out-

put conductance becomes identical to the expression obtained in Eq. (3.28). The correspondence between the dimensionless parameters defined in Eq. (4.75) and their counterparts in Eq. (3.26) may be verified by noting the following relationships among the series expressions of Eq. (4.72) and those of Eq. (3.36) for the conductance components of the small-signal admittance matrix:

$$G_{\omega 0} = 2G_{10},$$

$$G_{0\omega} = G_{01}, \quad (4.78)$$

$$G_{\omega\omega} = G_{11}+G_{1-1}.$$

It is interesting to note that the reactive terms will disappear from Eqs. (4.74) and (4.77) if the mixer is adjusted so that $b_S = \gamma$. The quantity b_S contains the termination susceptance B_S, which is, in principle, a free experimental parameter. Therefore the simpler expressions of Eqs. (3.27) and (3.28) are always exact for at least one possible tuning condition. This is not in general the optimum tuning condition (Feldman, 1982), but often represents a good approximation for efficient conversion in practical SIS mixers. In most model calculations performed thus far, the numerical impact of the quantum reactive terms on predicted performance has indeed been found to be very small.

To complete this analysis of a quasiparticle mixer in the three-frequency and low IF approximation, the elements of the current correlation matrix in Eq. (4.69) reduce within these assumptions to

$$H_{00} = 2e \sum_{n=-\infty}^{\infty} J_n^2(\alpha)\coth[(eV_0+n\hbar\omega)/2kT]I_{\mathrm{dc}}(V_0+n\hbar\omega/e),$$

$$H_{10} = H_{-10} = H_{01} = H_{0-1} = e \sum_{n=-\infty}^{\infty} J_n(\alpha)[J_{n-1}(\alpha)+J_{n+1}(\alpha)]\coth[(eV_0+n\hbar\omega)/2kT]I_{\mathrm{dc}}(V_0+n\hbar\omega/e),$$

$$(4.79)$$

$$H_{11} = H_{-1-1} = e \sum_{n=-\infty}^{\infty} [J_{n-1}^2(\alpha)+J_{n+1}^2(\alpha)]\coth[(eV_0+n\hbar\omega)/2kT]I_{\mathrm{dc}}(V_0+n\hbar\omega/e),$$

$$H_{1-1} = H_{-11} = 2e \sum_{n=-\infty}^{\infty} J_{n-1}(\alpha)J_{n+1}(\alpha)\coth[(eV_0+n\hbar\omega)/2kT]I_{\mathrm{dc}}(V_0+n\hbar\omega/e).$$

Inserting these results into Eq. (4.71) then yields an expression for the local oscillator shot-noise component of the single-sideband mixer noise temperature. For the special case of the double-sideband mixer, the single-sideband noise temperature is found to be given by

$$kT_M^{\mathrm{LO}} = \frac{1}{4G_S|\lambda_{01}|^2}[H_{00}+2(\lambda_{01}+\lambda_{01}^*)H_{10}$$

$$+(\lambda_{01}^2+\lambda_{01}^{*2})H_{1-1}+2|\lambda_{01}|^2H_{11}],$$

$$(4.80)$$

where

$$\lambda_{01} = \frac{-G_{01}}{G_{11}+G_{1-1}}\frac{(\xi+g_S)-i(b_S-\gamma)}{(\xi+g_S)(1+g_S)+(b_S^2-\gamma^2)}. \quad (4.81)$$

The results of the complete quantum mixer theory that are specific to the double-sideband model may be easily generalized to a mixer with different terminations $Y_1 = Y_S$ and $Y_{-1} = Y_I$ at the signal and image frequencies. The special case of a shorted-image sideband mixer is treated in Tucker (1979), Eqs. (6.33)—(6.40), neglecting the quantum reactances. Sollner (1981) gives the conversion efficiency for this case including the quantum reactances. [Note that the definition $b_S = (B_S+B_{11})/G_{11}$ must be used for his equation to be correct.] The output admittance in the shorted-image case is *not* in general

real. A model for another mixing mode, harmonic mixing at zero dc bias in an inversion-symmetric tunnel junction, is given in Tucker (1983, Appendix B). Infinite available conversion efficiency is possible using SIN junctions in this configuration in the quantum regime (Shen and Richards, 1981). It is also straightforward to generalize all of the equations of this section to the case where the output frequency, the IF, is *not* small.

The major assumption necessary to produce any of these relatively simple models is that higher harmonics of the local oscillator may be ignored. When this approximation cannot be made, the large-signal calculation of the local oscillator waveform impressed across the mixer diode becomes vastly complicated. The effects of such harmonics are expected to be detrimental to the mixer's performance; and evidence that this has reduced the conversion efficiency in some experiments is discussed in Sec. VI.A. Therefore the assumption of a sinusoidal local oscillator potential is expected to provide a reasonable model for most receivers of practical interest.

G. Response of a tunnel junction in the time domain

The quantum mixer theory described in this section has been constructed using Eq. (4.3) for the expectation value of the quasiparticle tunneling current. The form of Eq. (4.3) is designed to facilitate calculations in the frequency domain. Following Harris (1976), we may alternatively express the quasiparticle tunneling current in a form suitable for analysis in the time domain (Tucker, 1983, Appendix C):

$$\langle I(t)\rangle = \frac{V(t)}{R_N} + \mathrm{Im}\left[U^*(t)\int_{-\infty}^{t}dt'\bar{\chi}(t-t')U(t')\right].$$

(4.82)

The time-dependent phase factor induced by the potential across the tunnel barrier is here represented as

$$U(t)=\exp\left[\frac{-ie}{\hbar}\int_{-\infty}^{t}dt'V(t')\right],$$

(4.83)

and the response function characterizing the nonlinear behavior of the junction is found to be given by

$$\bar{\chi}(t)=\frac{2}{\pi}\int_{0}^{\infty}d\omega\left[I_{\mathrm{dc}}(\hbar\omega/e)-\frac{\hbar\omega}{eR_N}\right]\sin\omega t.$$

(4.84)

The dc $I\text{-}V$ characteristic is assumed in these expressions to be antisymmetric, $I_{\mathrm{dc}}(-V)=-I_{\mathrm{dc}}(V)$, and to approach an Ohmic resistance R_N at large bias voltages.

Equations (4.82)–(4.84) may be obtained by inserting the expression given in Eq. (4.12) for the time-dependent current operators into Eq. (4.15) for the average tunneling current. Using the equilibrium current commutator defined in Eq. (4.17) then yields

$$\langle I(t)\rangle = \mathrm{Im}\left[U^*(t)\int_{-\infty}^{t}dt'\frac{4i}{e}\chi''_{+-}(t-t')U(t')\right].$$

(4.85)

According to Eq. (4.19), the Fourier transform of the response function in this expression is directly related to the dc $I\text{-}V$ characteristic:

$$\chi(t)\equiv\frac{4i}{e}\chi''_{+-}(t)=\frac{i}{\pi}\int_{-\infty}^{\infty}d\omega\,I_{\mathrm{dc}}(\hbar\omega/e)e^{-i\omega t}.$$

(4.86)

The real function $\chi(t)$ is not well defined here because the dc tunneling current is unbounded at large argument. This difficulty may be circumvented by subtracting out the Ohmic behavior in defining the modified response function of Eq. (4.84). The outcome of this procedure gives

$$\bar{\chi}(t)=\chi(t)-\frac{2\hbar}{eR_N}\delta'(t).$$

(4.87)

Using this expression in Eq. (4.85) then yields the result quoted in Eq. (4.82) for the quasiparticle tunneling current.

The function $\bar{\chi}(t)$ is plotted in McDonald *et al.* (1980) for an ideal SIS junction at $T=0$. $\bar{\chi}(t)$ oscillates in time with the energy-gap frequency $2\Delta/h$, and its amplitude falls off only inversely with t at large times. The current can therefore depend upon the voltage history infinitely far into the past. This slow falloff in $\bar{\chi}(t)$ is a reflection of the perfectly sharp onset of quasiparticle tunneling in an ideal SIS junction. For a real junction, the nonlinearity occurs over a finite voltage range and $\bar{\chi}(t)$ dies off within a finite time, more quickly for a more smeared nonlinearity. In the limit where $\bar{\chi}(t)$ becomes insignificantly small after a time corresponding to the applied frequency, the response will be effectively instantaneous. In this case, the tunneling current may be shown to follow a time-dependent modulation of the dc $I\text{-}V$ characteristic, and the assumptions of classical mixer theory are valid. If, on the other hand, the nonlinearity is sharp enough that $\bar{\chi}(t)$ remains significant over the rf period, then the current becomes a nonlocal function of time and the quantum theory must be used. Because the junction response is no longer instantaneous, nonlinear reactances appear in the quantum regime, and the in-phase conductance depends upon frequency as well.

This frequency dependence of the in-phase part of the response breaks important symmetries obeyed in classical theory at low frequencies. The effect is illustrated by the example in Sec. III.B, where $2G_{0\omega}$ can become larger than $G_{\omega0}$ when the rf photon energy $\hbar\omega/e$ becomes greater than the voltage scale of the nonlinearity. In the language of Sec. IV.D, $G_{01}\neq G_{10}$ and the classical symmetry relation implied by Eq. (4.53) breaks down. The violation of these symmetries leads, as shown in Sec. III.B, to the possibility of conversion gain and negative differential resistance. From this point of view there is no need to attribute these effects to the nonlinear quantum reactance; and indeed in Sec. IV.F it was shown that the results of the simplified model ignoring these reactances could be recovered, within its assumptions, for a particular choice of tuning. Nevertheless, the time-domain representation of the tunneling current clearly demonstrates that the frequency dependence of the conductance and the appear-

ance of the quantum reactance are inseparable results of the noninstantaneous response of the tunnel junction at high frequencies.

V. EXPERIMENTAL MIXERS

The history of SIS mixers has been one of rapid progress, with the most striking new results achieved almost simultaneously in a few laboratories. It had long been clear to a number of researchers working with Josephson junctions that quasiparticle tunneling in these devices offered the prime requirement for a superior mixer: a sharp resistive nonlinearity. But the relatively large capacitance of the SIS junctions available prior to the mid 1970s was discouraging. It was not until 1978 that the first mention of the possibility of SIS millimeter-wave mixers appeared in the literature (Richards, 1978).

Shortly thereafter, three different laboratories reported experimental SIS mixers. Richards *et al.* (1979) measured a SSB noise temperature as low as 14 K; Dolan *et al.* (1979) demonstrated a SIS mixer at 115 Ghz; Rudner and Claeson (1979) found 5.8-dB conversion loss. Even at that early date the potential for SIS mixers was apparent. Could all of these attributes have been combined in a single device, that SIS mixer would have been superior to the best Schottky mixer.

When the quantum theory of mixing (Tucker, 1979) was applied to analyze their performance, it became clear that SIS mixers were not limited by the classical proscription of conversion gain (Tucker, 1980). This remarkable prediction was soon verified by Shen *et al.* (1980) and by Rudner *et al.* (1981a). In both cases this demonstration was marginal: both found a SSB conversion slightly better than 3-dB loss, implying a slight gain for double-sideband operation. The quantum theory prediction was more firmly established when McGrath *et al.* (1981; see also Smith *et al.*, 1981b) and Kerr *et al.* (1981) reported infinite available conversion gain at 36 and 115 GHz, respectively. This meant that arbitrarily high small-signal gain could be achieved with an appropriately matched IF load. McGrath *et al.* (1981) actually realized a +4.3-dB conversion gain, still an experimental record.

The progress in building practical receivers using SIS mixers has been equally impressive. At least four millimeter-wave observatories, at the time of this writing, routinely utilize SIS receivers.

The experimental results thus far achieved with SIS mixers are reviewed here in some detail. Most of the junctions employed were fabricated using a variation of the Pb-alloy technology developed at IBM (Broom *et al.*, 1980, and other articles in the same journal issue). These junctions are designed to be stable over long periods of time and with frequent cycling between room temperature and liquid-helium temperature (so long as they are protected from humidity and from severe electrical shock).

A. SIS mixer results

The initial experiments on SIS mixers and receivers have been carried forward in a few major laboratories, and the results are summarized in this section by research group.

1. Berkeley

The Berkeley group's experiments, all at 36 GHz, were carried out using a measurement system designed for the quantitative evaluation of mixer parameters, rather than for use as a low-noise receiver. A diagram of their mixer block is shown in Fig. 21. This is a standard Schottky mixer mount, described in Sec. II.A, which has been modified to provide a wider tuning range. The junction substrate is placed across a full-height *Ka*-band waveguide. The two rf tuning elements are an adjustable stub $3\lambda/4$ in front of the junction and a sliding backshort behind it. At the rf entrance to the mixer block a high-loss cold attenuator (not shown in Fig. 21) is inserted to prevent room-temperature radiation and noise due to the oscillators from saturating the mixer.

The IF output from the mixer is amplified by a string of room-temperature transistor amplifiers, centered on a frequency of 50 MHz, having an input noise temperature of $T_{\text{IF}} \approx 50$ K. Even though this is an extremely low value of T_{IF} for room-temperature amplifiers, these amplifiers must be precisely calibrated as a function of input impedance, frequency, temperature distribution along the IF cable, etc., in order to extract the mixer noise temperature from Eq. (2.1) with reasonable precision. The Berkeley group accomplished this by installing three identical IF cables into their Dewar, one terminated with a short circuit to measure IF cable losses and one terminated in a 50-Ω cold load to provide a noise source for calibrating the IF amplifiers, in addition to the one connected to the SIS mixer.

The first Berkeley experiments (Richards *et al.*, 1979) used $\sim 5\text{-}\mu\text{m}^2$ area Pb(In,Au) SIS junctions of the type illustrated in Fig. 21. The unpumped dc *I-V* curve of one
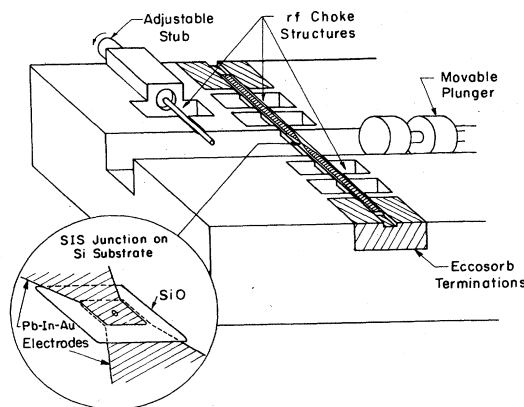

FIG. 21. Mixer block and SIS junction mounting configuration used in 36-GHz experiments at Berkeley (Richards *et al.*, 1979).

such junction, shown in Fig. 2(a), has the quasiparticle current rise at the energy gap smeared over a range of perhaps twice $\hbar\omega/e$ in voltage. Nevertheless, the mixer conversion response curve, Fig. 2(e), displays a distinct modulation on the quantum voltage scale $\hbar\omega/e$. Figure 2(e) is the first demonstration of nonclassical mixing behavior in published experimental data. The best result from these experiments was a mixer conversion loss of 8.0 dB with better than 14-K SSB noise temperature, for an $R_N = 100$ Ω junction with $\omega R_N C \sim 2$. The noise temperature was determined by comparing the curves of Fig. 2(c) and 2(d).

Subsequently the Berkeley group (Shen et al., 1980) used Pb(Bi) junctions with a much sharper energy-gap current rise. A typical junction was ~ 9 μm^2 in area, had $R_N = 22$ Ω, and apparently had $\omega R_N C$ on the order of unity. In these experiments the small modulation seen in Fig. 2(e) now dominated the mixer conversion trace, and maximum conversion was obtained on the fifth peak below the energy-gap voltage. The best result was a reported 2.0-dB conversion loss with better than 3-K SSB noise temperature, although this noise temperature figure has not been repeated in subsequent publications. The mixer was noted to begin to saturate at an input signal power of 30 pW, which is equivalent to room-temperature radiation in a 7-GHz bandwidth. This dynamic range is uncomfortably small, but still satisfactory for many applications.

In a further series of experiments, the Berkeley group (McGrath et al., 1981; Smith et al., 1981b) used Sn junctions of about 10 μm^2 area, with typical $R_N = 22$ Ω and $\omega R_N C \sim 7$. Even though the energy-gap current rise of these Sn junctions appears perhaps somewhat less sharp than for their previous Pb(Bi) junctions, the results, shown in Figs. 13–15, are distinctly more dramatic. The pumped dc I-V curve, which for the Pb(Bi) junctions of Fig. 2(b) appeared featureless, is now clearly modulated on a voltage scale $\hbar\omega/e$. This modulation is so strong that the pumped curve shows a region of negative differential resistance in Fig. 13 on the first step below the energy-gap voltage. Since, in the limit of zero IF, the output impedance of the mixer is equal to the dc differential resistance, this means that essentially infinite conversion gain is available into an appropriately matched low-frequency load. The gain would be limited only by saturation of the large output signal. Furthermore, as the mixer was tuned towards increasing differential resistance, approaching this negative-resistance region, the measured mixer conversion gain into the 50-Ω IF load increased, as shown in Fig. 15. The maximum conversion efficiency was achieved on the first step below the gap in Fig. 14, and corresponded to a 4.3±1 dB gain. The SSB noise temperature at this point was 9±6 K, the same noise temperature measured in later experiments (van Kempen et al., 1981) using Pb-alloy junctions. The same mixer began to saturate with 1.5-pW input signal power (Smith and Richards, 1982). This experiment clearly establishes the excellence of SIS mixers, with the practical caveats that Sn junctions do not properly recycle to room

temperature, and that the dynamic range here is impractically small.

No other group has to date demonstrated actual conversion gain from a SIS mixer. What distinguishes these Sn junction results from the earlier Pb(Bi) junction results? One likely factor, discussed in Sec. VI.A, is the large $\omega R_N C$ product, coupled with the ability to tune out the capacitance at the signal frequency, which allows this mixer to operate near the energy-gap voltage and better take advantage of the nonlinearity. In addition, the Sn junctions had an extremely high dynamic resistance below the gap, as seen in Fig. 13, and this may also be important.

Most recently, the Berkeley group (McGrath et al., 1985) has constructed a (30–40)-GHz SIS mixer test apparatus which provides a much greater measurement accuracy. The mixer input is thermal radiation from a cryogenic variable-temperature rf load, and the mixer output is compared to a variable-temperature IF load. Using a single Pb-alloy junction in the SSB mode, their most precise result was $T_M = 9.2\pm0.9$ K with $L = 6.2\pm0.1$ dB, and the lowest noise temperature measured was $T_M = 5.6\pm2.5$ K with $L = 4.6\pm0.4$ dB. This last figure represents a mixer noise of only three times the nominal quantum limit $\hbar\omega/k$ at 36 GHz.

2. Caltech/Bell Labs

Researchers from the California Institute of Technology and from Bell Laboratories have concentrated upon developing and improving SIS receivers for millimeter-wave astronomy, for the most part at 115 GHz and more recently at 230 GHz. They have used extremely small-area Pb-alloy junctions made by the photoresist bridge method described in Sec. II.B.1 (see Fig. 7), to give an $\omega R_N C$ product of less than unity at 115 GHz in all of their reported experiments.

Their initial results (Dolan et al., 1979) used a mixer block modified from an InSb bolometric mixer, with an IF of only 2 MHz. A 0.4-μm^2 area, $R_N = 50$ Ω SIS junction was suspended across a full-height 115-GHz waveguide, with a sliding backshort and an E-H tuner as coupling elements. The mixer had a SSB noise temperature < 100 K with 10-dB conversion loss. The mixer response showed a clear modulation on the voltage scale $\hbar\omega/e$, as was true for all subsequent experiments.

As early as mid 1979, a prototype of the next-generation receiver was operating on the Bell Telephone Laboratories Telescope (Phillips et al., 1981), with a SSB receiver temperature of 400 K at 115 GHz. The LO is introduced through a 1% dielectric beam splitter, which illustrates the flexibility possible when one can be wasteful of LO power. In the SIS mixer, described by Dolan et al. (1981), the junction is suspended across a quarter-height waveguide with a single tuning element, a sliding backshort. The best mixer result was $T_M(\text{SSB}) = 62$ K with 7.6-dB conversion loss. By 1981 a modified version of this receiver had a SSB noise temperature of 130 K, using a SIS mixer with $T_M(\text{SSB}) = 80$ K and with 8-dB con-

version loss (Phillips and Woody, 1982). The current Bell Labs receiver uses the same basic design (Stark, 1983), but many of the elements of the system have been improved, and the overall performance is now extremely good. In every SIS mixer, the rf blocking structure on the IF output connection acts as a fixed tuning element; this structure was varied in these experiments to provide extra tuning flexibility. The receiver (Stark, 1984) operates at 4.2 K, is intrinsically double-sideband, and has a noise temperature measured on the telescope of less than 50-K DSB from 108 to 115 GHz. The best measured noise temperature is 28-K DSB at 112 GHz. This corresponds to a SSB receiver temperature of ~80 K, when the Fabry-Perot filter used for astronomical observations is included.

The Caltech receivers emphasize simplicity of design and operation (Woody et al., 1985). These receivers, cooled to 4.5 K by closed-cycle refrigerators, are of basically the same design as the Bell Labs receiver. An important difference is that the SIS mixers use a circular waveguide, which is much more simply and accurately machined than rectangular waveguides, but which also has a narrower range for single-mode operation and the unfortunately high waveguide impedance of ~400 Ω. A SIS junction is suspended across the circular waveguide, which immediately flares into a scalar feed horn. Behind the junction is a noncontracting adjustable backshort. The 1.4-GHz FET IF amplifiers have noise temperatures of ~10 K. The receivers operate from 85 to 115 GHz, with noise temperatures often in the range of 100- to 120-K DSB, and are generally tuned for moderate image rejection. These receivers have been in routine operation on the three telescopes of the Owens Valley Radio Observatory millimeter interferometer for more than four years, and are used for continuum and line observations and for both linked interferometry and very-long-baseline interferometry.
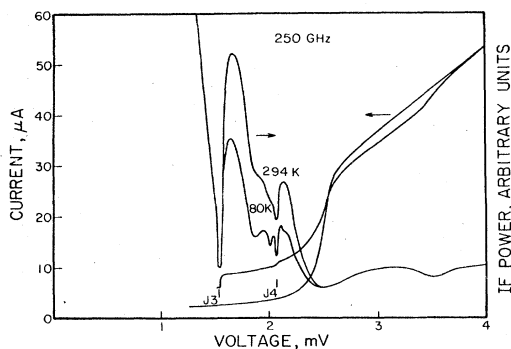

FIG. 22. Performance curves at 250 GHz for a SIS mixer using a ~0.5-μm^2 Pb-alloy junction. The unpumped and pumped (LO power ~ −43 dBm) I-V curves are shown, along with the IF output power for room temperature and liquid-nitrogen temperature loads applied at the mixer's input. At the points marked J3 and J4 the ac Josephson frequency is an integral multiple of the local oscillator frequency (Sutton, 1983).

The first 230-GHz SIS mixer was reported by Phillips et al. (1981). These results were impaired by Josephson-effect noise (Sec. VI.D); and a magnetic field large enough to suppress this noise degraded the mixer's performance as well. A more recent 230-GHz SIS receiver has, however, been more successful (Sutton, 1983). This was a version of the Caltech 115-GHz receiver with a mixer block scaled to the higher frequency, and used a 0.5-μm^2 area Pb-alloy SIS junction with $R_N = 68$ Ω ($\omega R_N C \sim 2$) suspended across the circular waveguide. The best performance obtained was a receiver noise temperature of 305 K (SSB) at 241 GHz (more sensitive than the best Schottky receivers at this frequency), with an input-to-IF conversion loss of 10.5 dB. This remarkable result bodes well for high-frequency SIS receivers. Some results from this experiment are shown in Fig. 22. Note the structures on the pumped dc I-V curve and the IF response curves at the points marked J3 and J4, which are integral multiples of the ac Josephson voltage $\hbar\omega/2e$ for this LO frequency. A magnetic field suppressed these structures, but without greatly affecting the sensitivity of the receiver.

3. Chalmers

All of the mixing experiments performed at Chalmers University of Technology, in Gothenburg, Sweden, used series arrays (see Sec. VI.B) of SIS junctions. The junctions were made in an in-house dedicated evaporation system, which allowed the testing of a large number of diverse samples to explore the physics of SIS mixing. The method of fabrication, thermal evaporation through bimetallic stencil masks, produced relatively large (~25-μm^2 area, in general) junctions connected by a relatively large series inductance. The first experiments (Rudner and Claeson, 1979) used many-junction Pb arrays mounted in microstrip and connected to a coaxial cable at 9 GHz. The best result was a conversion loss of 5.8 dB with a mixer noise temperature of (10—40)-K SSB. At this low frequency the conversion curve showed no sign of photon-assisted tunneling modulation.

The subsequent experiments at Chalmers used a novel mixer design which takes some advantage of the planar character of SIS junctions. The pattern seen in Fig. 23(a) was deposited onto a glass substrate, and includes the Pb-alloy junctions [Fig. 23(b)] and a monopole antenna for rf coupling to a full-height waveguide. When assembled [Fig. 23(c)] in the mixer block with a tuning backshort, the junctions lodge in a recess, tightly sandwiched between two ground planes, to minimize the series inductance arising from the junction interconnections.

A large number of $N = 6$ junction arrays (Rudner et al., 1981a,1981b) and $N = 36$ junction arrays (Rudner et al., 1980,1981b) were tested for mixing at 75 GHz. The 6-junction arrays were short, of length 0.035λ, but the 36-junction arrays were over half a wavelength long and thus showed little sign of photon-assisted tunneling structure in the conversion. The 6-junction arrays showed
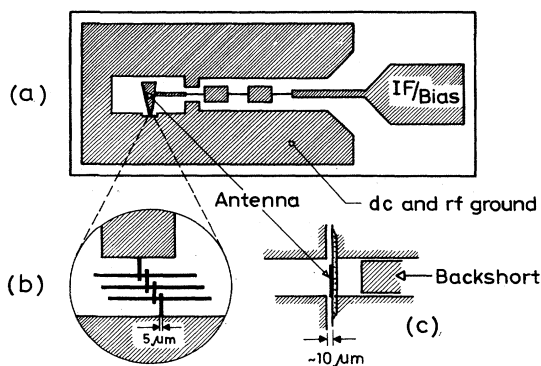
FIG. 23. Experimental configuration for a 75-GHz SIS mixer: (a) glass substrate with evaporated pattern, including (b) magnified 6-junction Pb-alloy series array within a recess, and (c) full-height waveguide with backshort and substrate in place (Rudner et al., 1981b).

distinct structure in their conversion efficiency on the voltage scale of $6\hbar\omega/e$, and in fact all published results for short ($\ll\lambda$) SIS arrays show this structure on the voltage scale $N\hbar\omega/e$ and never on the scale $\hbar\omega/e$. The 6-junction arrays generally reached their maximum conversion value on the second peak below the energy gap. A summary of the better conversion results obtained for different array structures is shown in Fig. 24, reprinted from Feldman and Rudner (1983). The best conversion for the short 6-junction arrays was (2.0 ± 0.9)-dB loss for $R_N \sim 24$ Ω, at which point $\omega R_N C = 2$ for the array. A conversion loss of 7.8 dB was reached using the 36-junction arrays. A mixer noise temperature of less than ~ 100 K was found for all of the samples measured.

More recently, a (35—50)-GHz SIS receiver (Olsson et al., 1982,1983) was built and is now operational at the Onsala Space Observatory. This receiver uses a series array of six Pb-alloy SIS junctions, each with ~ 25-μm^2
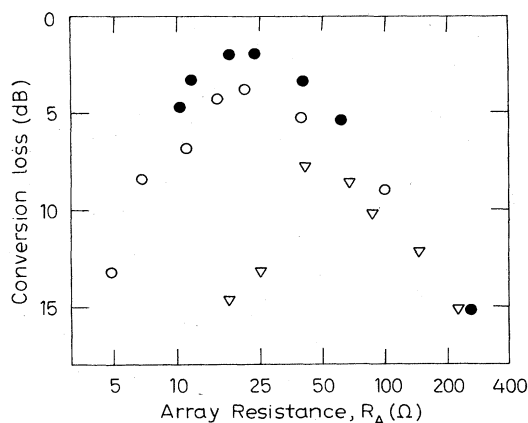

FIG. 24. Minimum conversion loss achieved using various SIS arrays for mixing at 75 GHz by Rudner et al. (1981b). Three types of arrays were tested: ●, 6-junction Pb(In) arrays; ○, 6-junction pure Pb arrays; ▽, long 36-junction pure Pb arrays (Feldman and Rudner, 1983).

area. The optimal R_N for the array is 30—50 Ω, giving an $\omega R_N C$ product of roughly two for the array. The input signal enters the mixer through a long quasioptical lens guide terminated with a corrugated horn. The mixer output is fed to a 4-GHz IF system with a noise temperature of 22 K, whose first stage is a commercial parametric amplifier cooled to 2 K. This relatively large value for the IF is a distinct advantage for this receiver; the backshort is invariably adjusted to short out the lower sideband, so the mixer operates in a truly single-sideband mode. At 47 GHz, the mixer's conversion loss was measured to be 5 dB. The mixer noise temperature there was 11 ± 6 K, which is as good as most single-junction mixers. The receiver noise temperature varied smoothly from ~ 220 K at 35 GHz to ~ 140 K at 50 GHz, except for a resonance near 42 GHz. The receiver saturated at an input signal power of 1.7 nW, fully sufficient for radio astronomy.

4. NASA—Goddard Institute

The experiments performed at NASA—Goddard Institute for Space Studies also used series arrays of SIS junctions, in this case at 115 GHz. One distinction from the other experiments discussed here is that a 40$\times$ scale model of the mixer block was used in conjunction with computer simulations of the junctions' response to determine the optimal design of the printed circuitry immediately surrounding the junctions (Feldman et al., 1983).

In the earlier experiments (Kerr et al., 1981; Feldman et al., 1983), an array of fourteen series-connected 8-μm^2 area Pb-alloy junctions, with $R_N = 600$ Ω ($\omega R_N C \sim 10$) for the array, was mounted in a stripline circuit suspended across a quarter-height waveguide with an adjustable backshort. Note the negative-resistance region on the pumped dc I-V curve shown in Fig. 16(b). The maximum realized conversion was poor, about 11.5-dB loss, due to the drastic IF impedance mismatch. The mixer SSB noise temperature was 70 ± 40 K at the better operating points, and this was true for large positive, infinite, or negative output impedance with about ±10 K scatter.

Subsequently, the NASA—Goddard group constructed a (110—118)-GHz SIS receiver (Pan et al., 1983b) which is at present in use on the Columbia-GISS CO Sky Survey Telescope. This receiver uses a series pair of Pb-alloy junctions with $R_N = 94$ Ω and $\omega R_N C \sim 7$ for the pair. The mixer block and junction chip are illustrated in Fig. 25. Again, the junctions are mounted across a quarter-height waveguide with an adjustable backshort, but here the suspended stripline couples to a second waveguide with its own backshort to serve as a second tuning element. This configuration has the virtue of giving a highly tuned circuit to resonate the relatively large capacitance of the junctions (the instantaneous bandwidth was ~ 300 MHz) and to give large image rejection. The second backshort, however, adds perhaps an extra 2 dB of Ohmic loss to the mixer's conversion. Two leveling loops, for the LO power and the dc bias current, maintain a near-
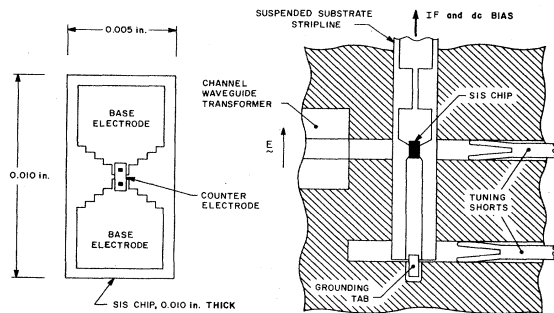
FIG. 25. Single-sideband 115-GHz receiver: schematic drawing of the 2-junction SIS chip and a cross-sectional view of the mixer block (Pan et al., 1983b).

optimum bias point during mixer adjustment and are described in Pan et al. (1983a).

The receiver's best recorded performance was a SSB noise temperature of 68 ± 3 K (with 12-dB image rejection). This is twice the sensitivity of any other receiver at this frequency. With >20 dB image rejection, the receiver had $T_R \sim 80$ K over most of its operating band. Most of this noise was due to the 1.4-GHz IF amplifier, whose noise temperature was 10.5 K, multiplied by the mixer conversion loss. That loss was measured to be 6.9 dB at 115.3 GHz, and the mixer's noise temperature at that point was inferred to be 15 ± 14 K. The 1-dB gain compression point was 4 nW, sufficient for observing an object one hundred times brighter than the sun. A scaled version of this receiver was also built (Pan et al., 1983b), for observations of the 3-K cosmic blackbody radiation at 46 GHz, which used a larger pair of junctions with $R_N = 34$ Ω and $\omega R_N C \sim 2.5$. Its SSB receiver noise temperature was 55 K. These results should firmly establish the SIS mixer as the first choice for ultra-low-noise millimeter-wave receivers.

5. West Germany/France

SIS junctions developed at the Max-Planck-Institut in Garching, West Germany, are described by Gundlach et al. (1982). These junctions have a base electrode of Pb(Bi,In) and a counterelectrode of Pb(Bi). A typical I-V characteristic is shown in Fig. 26, curve 1. Note the large value of the energy-gap voltage, which is typically 3.45 mV at a temperature of 2 K. This is considerably higher than for any other junction reviewed in this paper. Also, the current rise at the gap voltage is extremely sharp, indicating that these junctions should be very well suited for SIS mixers.

After an early concentration on video detection, mixing experiments were performed at 70 GHz (Hartfuss and Gundlach, 1981b). The SIS junction, with $R_N \sim 18$ Ω and $\omega R_N C$ approximately unity, was placed across a full-height waveguide with both a sliding backshort and an adjustable stub for tuning. The best result was 3.7-dB
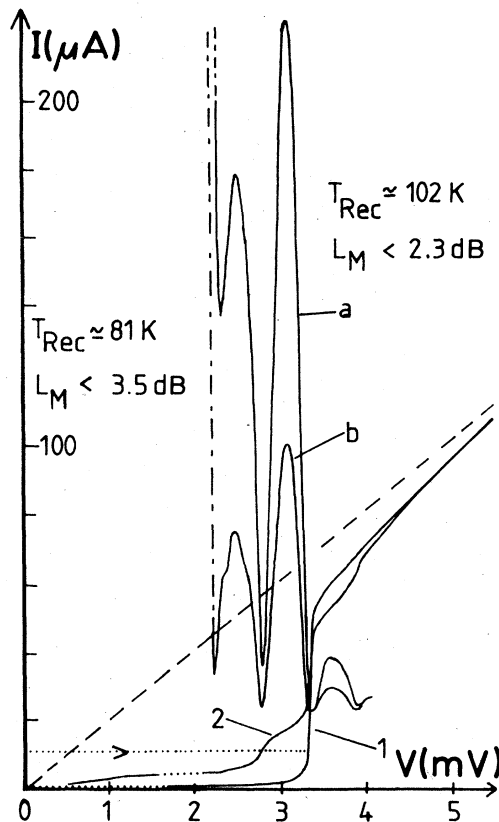

FIG. 26. Performance curves for a 150-GHz SIS mixer using a ~ 0.7-μm^2 Pb-alloy junction: 1, unmodulated and 2, modulated dc I-V curve in the presence of the LO, and IF output noise power with a a hot load and b a cold load applied at the mixer's input, where for curves a and b one vertical division corresponds to 21.5 K at the mixer output (Ibruegger et al., 1984).

conversion loss and a SSB mixer noise temperature of <100 K.

These experiments were continued (Blundell et al., 1982) at the Institut de Radio Astronomie Millimétrique (IRAM) in Grenoble, France, with the aim of building competitive SIS receivers for 80–100 GHz and more recently for the 150-GHz frequency range. A quarter-height waveguide with a single tuning backshort was used. Only DSB measurements were reported, even though the IF was a relatively high 4 GHz and the junction capacitance was in some cases large enough (the $\omega R_N C$ product was as much as ten) to expect that the receiver operated in the SSB mode. In the lower frequency range (Blundell et al., 1983) the best result was a receiver noise temperature of 73-K DSB at 92 GHz, for a 2-μm^2 junction with $R_N = 54$ Ω (i.e., $\omega R_N C \sim 3$). In the upper frequency range (Ibruegger et al., 1984) the best result was a receiver noise temperature of 81-K DSB at 141 GHz (see Fig. 26), for a 0.7-μm^2 junction with $R_N = 51$ Ω (i.e., $\omega R_N C \sim 1.3$). In both cases $T_{IF} \approx 16$ K. These receivers are slated for installation at the IRAM 30-m telescope in Spain.

Two unusual aspects of these experiments were noted. At both frequencies the best performance of the SIS mixers was obtained on the second photon-assisted tunneling step below the energy gap, whereas one would expect that the first step would be superior, especially above 100 GHz. Also, the experimenters note that almost all of the SIS junctions that they tested at both 100 and 150 GHz, covering a very wide range of R_N and of $\omega R_N C$, gave approximately the same receiver sensitivity.

In a separate application (Hartfuss and Tutter, 1983b), a SIS mixer is being used in Garching as a calibration channel of a conventional receiver for the measurement of electron cyclotron emission from fusion experiments.

6. Other laboratories

The first SIS mixer experiments using Nb-based junctions were performed at Cornell University (Callegari and Buhrman, 1982). The edge of a Nb film was oxidized and covered by a Pb(Bi) counterelectrode. This process produced extremely tiny junctions, typically 3×0.15 μm^2, which were suspended across an eighth-height waveguide with a sliding backshort and were irradiated at 55 GHz. The junctions tested had either very high or very low resistance. The high-resistance junctions had quite sharply nonlinear I-V curves. One, with $R_N = 600$ Ω and $\omega R_N C = 5$, had its best conversion of 7.4-dB loss on the first photon step $above$ the energy-gap voltage. The low-resistance junctions were considerably less sharply nonlinear and had their best conversion at lower voltages. An $R_N = 8$ Ω junction ($\omega R_N C = 0.16$) gave 7-dB conversion loss with $T_M \leq 27$ K SSB. In light of the severe mismatch at both input and output of the mixer, these results must be considered extremely encouraging.

Further Nb-based SIS mixer experiments were reported from the Soviet Union (Gubankov et al., 1982,1983). Again, the Nb was oxidized and covered with Pb(Bi), but in this case the junction was of much larger area, ~ 15 μm^2, so its capacitance was very large ($\omega C = 0.6$ Ω^{-1}, R_N not quoted). The junction was suspended across a full-height Ka-band waveguide with a sliding backshort and a tuning stub, and gave a conversion loss of 4 ± 3 dB when irradiated at 50 GHz.

A very recent (90–120)-GHz SIS mixer developed at the National Radio Astronomy Observatory (D'Addario, 1984) is the first to use integrated circuit tuning techniques. The junction substrate sits in a milled channel with one metallized end sticking into a full-height waveguide to act as a coupling probe. Two adjustable waveguide tuning elements are provided by a movable backshort and a second sliding short placed in a side channel located half a guide wavelength in front of the substrate. On the substrate is a 6-μm^2 Pb-alloy SIS junction and integrated circuitry for rf and IF coupling; five layers of photolithography are used. The circuitry includes a transmission line, which appears as an inductive shunt at the junction, and which is designed to cancel the junction's capacitive susceptance at the rf frequency.

This works well enough that for the two samples tested, with R_N equal to 48 and 74 Ω and hence $\omega R_N C$ equal to ~ 6 and ~ 10, the mixer is intrinsically double-sideband, using a 1.4-GHz IF. In fact, the mixer is so broadband that it is badly saturated by an input temperature of 50 K. Therefore the performance of the mixer was measured using a variable-temperature waveguide load maintained between 8 and 20 K. All of the measurements quoted for the two junctions, at various frequencies, gave a realized SSB conversion of 3-dB loss, with at most unity available gain. The DSB mixer noise temperature was between 20 and 40 K. Four-junction SIS arrays were less completely tested. The measurements were made at a physical temperature of 3.1 K, achieved with a closed-cycle refrigerator.

B. Comparing theory and experiment

All of the qualitative predictions of the quantum theory of mixing have been repeatedly verified in the experiments discussed above. For instance, the SIS mixer conversion efficiency is modulated with a dc voltage periodicity $\hbar\omega/e$ ($N\hbar\omega/e$ for N-junction series arrays). A relatively small local oscillator power is required for a SIS mixer. As the LO power is increased, the conversion efficiency increases to its maximum and then oscillates as a function of P_{LO} until, at larger powers, the junction's nonlinearity begins to be washed out. Conversion gain has been achieved, and induced negative differential resistance has been observed as well. The mixer noise temperature is very small, often a few times the nominal quantum limit $\hbar\omega/k$.

In this section we shall discuss the $quantitative$ predictions of quantum mixer theory, and in particular their range of applicability and agreement with experimental results. Once confidence in the theory is established, it can be a powerful tool for the design and optimization of practical mixer circuits. For any particular experiment, the theory can predict how much improvement is to be expected from modifications of the tuning structures, the use of different SIS junctions, etc.

In $principle$, it is a simple matter to use the theory to predict quantitatively the behavior of a given experimental mixer. The only data required are the junction's unpumped dc I-V curve and the complex embedding impedances seen by the junction at all relevant frequencies. This last is generally understood to include the junction's own geometrical capacitance. Given this information, the theory of Sec. IV predicts the mixer's performance, most notably the conversion efficiency and the noise temperature, as a function of the applied LO power and dc voltage, for comparison with the experimental results. The predictive power of the quantum theory of mixing is extraordinary in that all of the quantitative predictions of the theory are specific to a particular nonlinear tunnel junction, characterized by its dc I-V curve, rather than applying to a general class of devices.

The emphasis in this section will be on the conversion

efficiency, because it is difficult to make a meaningful comparison of noise temperature results with theory. One reason for this is that the theory's prediction of mixer noise temperature is incomplete; it does not include quantum noise, and it is not certain how this should be included. Another more practical reason is that the predicted noise is generally so small that it is difficult to perform noise temperature measurements with sufficient precision. The quoted errors in noise temperature measurements are usually of the same order as the measured noise temperature itself.

In *practice*, a complete calculation of a quantum mixer's performance requires an extremely complicated self-consistent solution to obtain the large-amplitude local oscillator waveform, as noted in Sec. IV.C. This has only recently been performed by Hicks *et al.* (1985), who treat the SIS junction's large-signal response in the time domain (Sec. IV.G) rather than using the frequency-domain equation, Eq. (4.3). The results of this complete calculation are not yet extensive enough to justify general conclusions.

Every other quantum theory calculation of mixer properties has relied upon a number of simplifying assumptions, of varying accuracy. First, all of the harmonics of the LO, and the sidebands of those harmonics, are usually assumed to be short circuited. This is known as the three-port mixer approximation, because, except for the LO whose voltage amplitude can be taken as real, three frequencies, the signal, the image, and the IF, remain to be analyzed. Second, the classical IF approximation is always made: The output frequency is assumed to be small enough that the junction response at the IF is essentially classical. The IF is further assumed to be sufficiently small compared to the LO frequency that the approximation $\omega_S \approx \omega \approx \omega_I$ may be used in the calculations. In fact, the IF is generally taken to be effectively at zero frequency, so that the complex embedding admittance seen by the junction at the LO and at its sidebands are all equal. The high-frequency source admittance, $G_S + iB_S$, and the (real) IF load conductance G_L are then the only experimental quantities required in order to characterize the mixer's environment. Equations (4.74) and (4.77) are used to calculate the conversion efficiency. In some very few cases, less restrictive assumptions are made.

Even with this drastic simplification, a major problem remains: for most experiments G_S and B_S are difficult to determine. Each published paper deals with this problem in a different manner. In many papers all reactances are ignored; that is, B_S, which includes the geometrical capacitance, is assumed to cancel exactly the conversion effects of the nonlinear quantum reactance when the backshort and other tuning structures are adjusted for efficient mixing. This appears to be a valid procedure in many circumstances (Feldman, 1982).

One technique for determining G_S and B_S from experimental data is the "method of intersecting circles" of Shen (1981). For a given dc current point on the pumped I-V curve, Eq. (3.3) is inverted (by computer) to give the LO voltage amplitude, $V_\omega = V_{LO}$. The complex LO

current I^ω_{LO} can then be found from Eqs. (4.40) and (4.41). Knowing these quantities, one considers the LO power equation, Eq. (4.43), as a circle in (G_S, B_S) space whose radius and central coordinates are functions of P_{LO}, V_{LO}, and I^ω_{LO}. This circle is the locus of values of G_S and B_S which will result in the measured dc current. This same procedure can be repeated for many points along the pumped I-V curve, or for many different values of P_{LO}, to produce many circles in (G_S, B_S) space. If the experiment data are precisely known and the three-port model is valid (all LO harmonics shorted), then all of these circles must intersect in the one point which gives the actual LO termination admittance, $G_S + iB_S$. A pumped I-V curve calculated wih G_S and B_S determined by this method is shown in Shen (1981), and it is in reasonable but not exact agreement with the experimental curve.

The beauty of this technique is that G_S and B_S can be obtained from a limited amount of easily accessible experimental data. Unfortunately, in some cases at least, it is of limited accuracy and may leave large ambiguities in the determination of G_S and B_S. One of us (M.J.F.) attempted to apply this technique to a SIS mixer for which it is known, in retrospect (Feldman *et al.*, 1983), that the three-port model is quite precisely valid. The resulting circles in (G_S, B_S) space, unlike the three idealized circles in Shen (1981), Fig. 6, did not intersect in a single point. Rather, they tended to delineate *two* loosely defined regions. The reason for this ambiguity must be that small errors in measuring the pumped dc current are magnified by the calculation. Nevertheless, the method of intersecting circles should be valuable to find a first approximation for G_S and B_S. Note that this method gives no information about the signal and image port embedding admittances when these are not equal to the LO port admittance.

The first attempt to calculate a working mixer's conversion efficiency (Shen *et al.*, 1980) was not very successful. Whereas the experimental conversion reached a maximum of 2-dB loss at the fifth photon step below the energy gap and declined as the energy-gap voltage was approached, the calculated conversion efficiency, with G_S and B_S from the intersecting circle method, became extremely large near the energy-gap voltage. On the assumption that significant harmonic effects depressed the experimental conversion near the energy-gap voltage, these authors subsequently applied a five-port mixer model (Richards and Shen, 1980). The calculated conversion efficiency curve no longer diverged in this case, and the agreement with the experimental conversion was within a factor of 2, but still the shapes of the two curves were quite dissimilar.

The technique used to perform the five-port mixer analysis is explained by Shen and Richards (1981). First, it is necessary to know the embedding impedance at the second harmonic frequency and its sidebands, as well as the fundamental terminations. The simplest assumption, used by these authors, is that the SIS junction's own capacitance is the primary component of the harmonic ter-

mination. The most difficult aspect of the five-port analysis is the determination of the LO waveform. In addition to the fundamental voltage V_{LO}, one must consider the second harmonic voltage, with components in phase and out of phase with V_{LO}. Therefore the result of Eq. (4.34) is generalized to a product of three Bessel function series. These series must be summed separately by computer for each iteration of the computation, in which the juction response is compared with the embedding network response to converge (hopefully) to a self-consistent solution, which gives the complex second harmonic voltage. Once the self-consistent LO waveform is obtained, the five-port small-signal analysis, which induces the IF together with the sidebands of both the fundamental and second harmonic frequencies, is a straightforward generalization of the three-port solution.

A much simpler approach to comparing experimental data with the three-port model was taken by Dolan et al. (1981). No attempt was made to ascertain the embedding impedances. Rather, these authors ignored all reactances, assumed the signal and image terminations to be equal, and plotted the predicted conversion efficiency against dc voltage for a wide range of values G_S, between 20 and 200 Ω. Their results agreed with the general shape of the experimental conversion curve, but the predicted conversion was more than 5 dB too large on the first photon step below the energy-gap voltage. These results, and those above, indicate that some important element is missing from the theoretical model for these experiments.

A more extensive series of experiments demonstrated the quantitative accuracy of predictions based on the quantum theory of mixing (Rudner et al., 1981a,1981b). A large number of 6-junction arrays were tested as SIS mixers; the maximum experimental conversion obtained for some of these is shown in Fig. 24. The unpumped dc I-V curve of each array was used in the theory to predict the size of each of the conversion peaks. All reactances were ignored in the calculations, and the value $1/G_S=50$ Ω was ascertained by reflection measurements. The predicted conversion was in every instance larger than the respective experimental result. The discrepancy between the predicted and the experimental conversion loss is shown in Fig. 27. This figure includes the results for the first and the second conversion peaks below the energy-gap voltage, for all of the Pb(In) arrays tested, except for two arrays in which the junctions were clearly heterogeneous. Additional, less complete, data from the third conversion peaks and from 6-junction pure Pb arrays are not shown, but those data fit along the trends seen in Fig. 27.

In one region of Fig. 27, the second peak conversion for those arrays having less than ~25 Ω normal resistance, there is excellent agreement between theory and experiment. More data were in fact available in this region. Figure 9 of Feldman and Rudner (1983) shows this region, the dashed area in our Fig. 27, with a magnified scale, and includes a total of thirteen data points, the others derived from the third conversion peak for the same samples and from the pure Pb arrays. Each of these thirteen data points represents a completely independent ex-
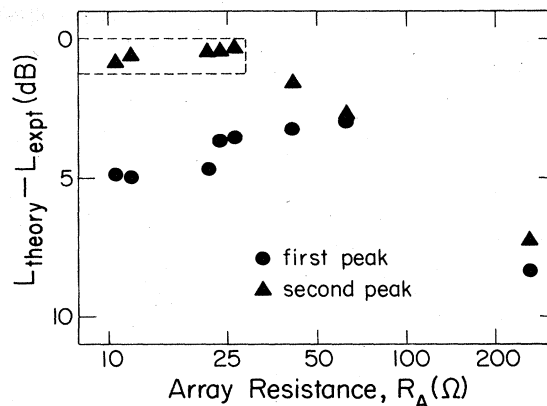

FIG. 27. Discrepancy between the optimum theoretical and experimentally observed conversion loss at 75 GHz for each Pb(In) SIS series array tested by Rudner et al. (1981a,1981b), shown for both the first and second mixing peaks below the energy-gap voltage (Feldman and Rudner, 1983).

periment; each experimental result is predicted by the quantum theory, using no adjustable parameters, with a discrepancy of 0.5 ± 0.3 dB. (A discrepancy of ~0.5 dB was expected from antenna mismatch measurements.) These thirteen points included all of the available data in this region. It is clear that, for this experiment, the quantum theory of mixing quite accurately predicts the conversion efficiency for those arrays with $R_A \lesssim 25$ Ω, except on the first photon peak below the energy-gap voltage.

Note that all of these SIS arrays had the same junction areas and hence about the same capacitance. Therefore the $\omega R_N C$ product, which measures how effectively the capacitance is able to shunt the junction currents, is directly proportional to R_A ($\omega R_N C \sim 2$ for $R_A=25$ Ω in this experiment). Figure 27 indicates that the theoretically calculated results are valid only for smaller R_A and hence smaller $\omega R_N C$, and the authors conclude that their experimental structures were not capable of resonating the array capacitance for larger $\omega R_N C$. The unresonated capacitance would increase the conversion loss for large R_A, as seen in Fig. 24, and hence would create the considerable discrepancy in the theoretical calculation seen in Fig. 27 for large R_A.

But what is the cause of the first peak discrepancy seen in Fig. 27, of up to 5 dB for low $\omega R_N C$? A similar effect—the experimental conversion efficiency appears to be severely depressed near the energy-gap voltage for low $\omega R_N C$ junctions—was seen in the other experiments discussed immediately above. In Fig. 27 the relative depression of the first peak disappears above $\omega R_N C \sim 4$. We shall use these results in Sec. VI.A to argue that harmonic conversion effects are important near the energy-gap voltage for low $\omega R_N C$ junctions.

A more elaborate technique for determining the mixer embedding impedance from internal experimental evidence is illustrated in Fig. 28 for a ~115-GHz mixer (Phillips and Dolan, 1982). The pumped dc I-V curve is calculated for many values of G_S and B_S and compared
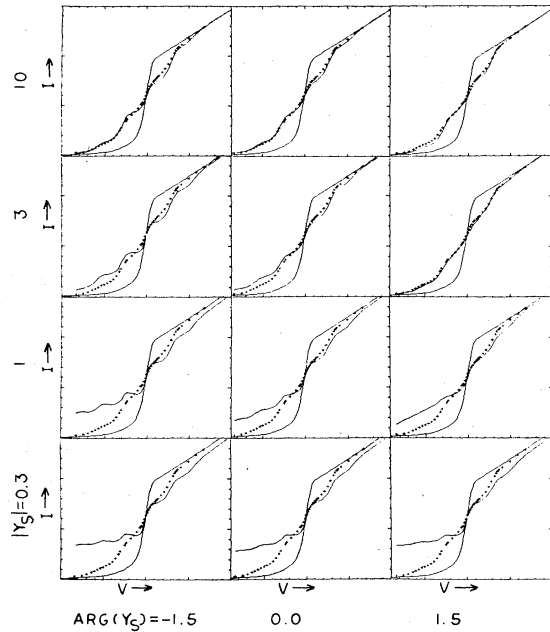
FIG. 28. The experimental unpumped (solid curve) and pumped (crosses) dc I-V curves for a Pb(In) junction in a $\sim$115-GHz SIS mixer are repeated in each box. The latter curve is to be compared to the various theoretical pumped I-V curves, which are calculated with the LO power as a free parameter, for the given values of amplitude and phase of the source admittance Y_S (Philips and Dolan, 1982).

to the corresponding experimental curve to find the best detailed fit. The applied LO power is a free parameter adjusted in each case to give the experimental current at the center of the first photon step. This method is essentially a generalization of the intersecting circles method to include all points on the pumped I-V curve, and its success will also depend upon the assumption that all LO harmonics are unimportant. If the signal and image port embedding impedances are not equal to the LO port admittance, the admittance must be separately determined by applying this technique at all three frequencies.

Phillips and Dolan (1982) used the values of the parameters determined by means of Fig. 28 to compute the results shown in Figs. 29 and 30. Figure 29 shows the pumped dc I-V curve calculated for the G_S, B_S, and LO power giving the best fit (curve C), as well as the calculated results for half that LO power (curve B) and twice that power (curve D), all compared to the corresponding experimental data. Figure 30 shows the conversion loss of their mixer calculated using the best-fit parameters from Fig. 28, again compared to the experimental values. The agreement is in all cases excellent. Note, however, that the only other extensive attempt to employ this three-parameter-fit method to an experimental mixer (Phillips and Woody, 1982) gave discrepancies of up to 2 dB between the predicted and experimental conversion losses. McGrath et al. (1981) also used this technique to calculate their mixer's conversion efficiency, at a single operating point.
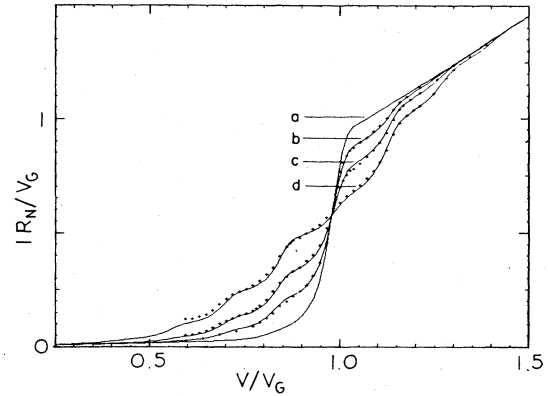

FIG. 29. dc I-V curves in reduced units for the SIS junction shown in Fig. 28, for several values of applied LO power near 115 GHz: curve a, zero power; curve c, the same LO power as in Fig. 23; curve b, 3 dB less than c; curve d, 3 dB more than c. The crosses are experimental data, and the corresponding solid lines are calculated using the best-fit values of LO power and source admittance determined from Fig. 28 (Phillips and Dolan, 1982).

The quantum theory of mixing can serve as a powerful tool for the design and optimization of a practical SIS mixer only to the extent that the mixer embedding impedance is known. Much of this section has detailed the approximations made and the techniques that have been used to infer the embedding impedance of various experimental mixers. These were necessary because direct measurements of the embedding impedance of a millimeter-wavelength mixer mount are extremely difficult with current technology.

This unsatisfactory situation can be avoided. A low-frequency network analyzer can be used to determine the embedding impedances of a larger-scale model of the mixer block. Scale-model measurements, described in Sec. II.A for a Schottky mixer, are straightforward and accurate, and can give the harmonic embedding impedances in addition to those at the LO, signal, and image frequencies. Feldman et al. (1983) adapted this technique
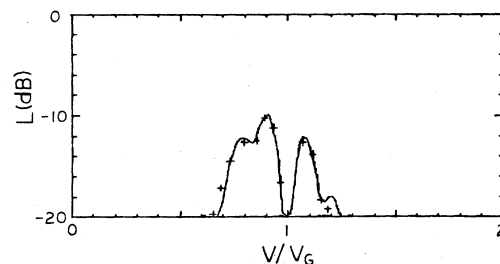

FIG. 30. Conversion loss as a function of reduced bias voltage for the $\sim$115-GHz SIS mixer characterized in Figs. 28 and 29. The experimental values are represented by crosses, and the solid line is calculated using the parameters determined from Fig. 28 (Phillips and Dolan, 1982).

to a 40× scale model of their SIS mixer block. For this experiment the harmonic impedances were not needed because the sample, a 14-junction array, had a large enough capacitance ($\omega R_N C = 10$) to ensure that the three-frequency approximation was valid.

Relying upon the scale model, Feldman et al. (1983) used experimental SIS mixer results to make a detailed test of the predictions of the quantum theory of mixing. The experimental conversion efficiency and the pumped dc current were measured at both the first and the second photon steps below the gap voltage, for nine different positions of the backshort spanning almost half a guide wavelength. Then using the complex embedding impedances at the LO, signal, and image frequencies, measured on the scale model as functions of backshort position, Feldman et al. calculated the LO voltage from Eqs. (4.41) and (4.43), the pumped dc current from Eq. (3.3), and the conversion efficiency from equations analogous to Eqs. (4.74) and (4.77) (generalized to allow unequal signal and image impedances), all as functions of backshort position. The results are shown in Fig. 31. It is clear that the quantum theory of mixing is quite successful in quantitatively predicting the experimental results, at least for this large-capacitance SIS array.

The largest uncertainties regarding Fig. 31 were in the measured values of the array capacitance and the LO
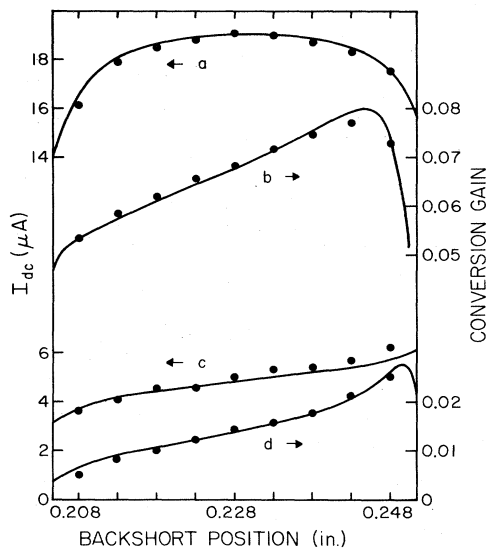

FIG. 31. Performance curves for a 115-GHz SIS mixer using a 14-element series array of ~ 2.5-μm^2 Pb-alloy junctions with array capacitance $C = 22.5 \pm 2.0$ fF: a, the dc current and b, the conversion gain, both measured at a dc bias voltage on the first photon peak below the gap and with constant $P_{LO} = 180 \pm 40$ nW, for nine backshort positions spanning almost half a guide wavelength. Curves c and d are the same as a and b, respectively, but measured on the second mixing peak. There are 36 experimental points, and the solid lines are theoretical predictions calculated for $C = 22.5$ fF and $P_{LO} = 173$ nW (Feldman et al., 1983).

power, which were known to an accuracy of about $\pm 10\%$ and $\pm 25\%$, respectively. The excellent agreement seen in Fig. 31 was obtained for the nominal values of C and P_{LO}, but allowed a range of variation of these quantities of only about $\pm 2\%$ and $\pm 5\%$, respectively. It is interesting to note, therefore, that this procedure can be inverted: the quantum theory of mixing can be fitted by computer to experimental mixer measurements to determine a SIS junction's capacitance with greater precision than by previously available techniques (for instance that of Magerlein, 1981).

The experiments discussed thus far in this section test the quantitative predictions of the quantum theory of mixing only at applied frequencies less than one-fifth of the energy gap. In a more recent experiment (Winkler, 1984; Winkler et al., 1985), aluminum junctions were measured at 75 GHz, which is more than 80% of the gap frequency $2\Delta_{Al}/h \approx 90$ GHz, using the mixing design illustrated in Fig. 23 in a He dilution refrigerator. The samples were arrays of six junctions, each of area ~ 25 μm^2. Both Al(In)-oxide-Al (SIS) and Al(In)-oxide-Ag (SIN) junctions were tested. A SIS array with $R_N = 620$ Ω and $\omega R_N C = 27$ gave a maximum conversion of 10-dB loss, while a SIN array with $R_N = 320$ Ω and $\omega R_N C = 23$ gave a maximum conversion of 28-dB loss. In spite of these large values of conversion loss, mainly due to severe impedance mismatch, the authors were able to compare their results to the quantum theory predictions, using a scale model to determine the source impedance. For both of these samples, the mixer conversion loss and the pumped dc current plotted against bias voltage agreed quite well with the theory. This is the first time that such a comparison has been made for SIN junctions. Josephson-effect noise (Sec. VI.D) was not a problem for the SIS junctions because of the large relative capacitance and because a magnetic field could be used to suppress the Josephson currents. These results give confidence that the quantum theory predictions for mixer conversion remain valid at applied frequencies approaching the energy gap, so long as Josephson pair tunneling can be neglected.

A number of authors have calculated the theoretical performance of SIS mixers (in general, double-sideband), using the equations of Sec. IV over a wide range of parameters, without an immediate application to experimental results. Shen and Richards (1981) addressed the case of the ideal SIS junction at $T = 0$ (see Fig. 18). The infinite-gain and the unity-gain contours were plotted against G_S and P_{LO}, ignoring all reactances, for a variety of reduced frequencies and dc voltages. The region of parameter space for which the calculated mixer noise temperature due to shot noise falls below $\hbar\omega/k$ was given as well. With the same assumptions Sollner (1981) plots some results for the shorted-image single-sideband case. Sollner and Powell (1983) plot the conversion efficiency versus frequency for a variety of synthetic I-V characteristics intended to represent realistic SIS junctions. These results disagree with all others in that the conversion efficiency never becomes infinite. Zorin (1985) plots

the shot-noise temperature for some special cases, as well as for synthetic I-V characteristics. Other papers have based their calculations upon measured Pb-alloy junction I-V curves. Phillips and Woody (1982) plot conversion efficiency against G_S and B_S at 112 GHz. Hartfuss and Tutter (1983a) plot conversion efficiency against G_S and the LO voltage amplitude, at 88 GHz, for several choices of B_S. These authors (Phillips and Woody, 1982; Hartfuss and Tutter, 1984) have also presented similar results for the mixer noise temperature, including the quantum noise contribution through some questionable assumptions. D'Addario (1984) calculates the conversion efficiency for two measured I-V curves in the DSB mode, with the image shorted, and with the image open circuited. The *open*-circuit image case gives the best result for the parameters considered. These various calculations can be valuable for general reference.

C. Other mixing modes

Subharmonic pumping is a favored technique for Schottky diode mixers. Most commonly, two diodes are mounted back-to-back to give inversion symmetry, and are pumped at approximately one-half of the signal frequency. This has the advantages that sufficient LO power is more easily obtainable at the lower frequency and that the symmetry of the device prevents the noise sidebands of the LO from appearing at the mixer output. These considerations are not important for SIS mixers, whose very small LO requirement permits any commercial LO source, with its noise sidebands, to be greatly attenuated. Nevertheless, the likelihood that the fundamental SIS mixer results described above were degraded by harmonic effects, especially near the energy-gap voltage where the I-V curve has an approximate inversion symmetry, suggested that a SIS harmonic mixer might be worthwhile to attempt.

After Richards and Shen's (1980) discussion of SIS harmonic mixing at the gap voltage, the Berkeley group (Smith et al., 1981a,1983) operated their Sn-based mixer, which had achieved 4.3-dB conversion gain in the fundamental mode (described in Sec. V.A.1), in this harmonic mixing mode. With an 18-GHz LO, they measured 3.2-dB conversion loss for a 36-GHz signal. As expected, the maximum conversion occurred quite near the energy-gap voltage. These results are encouraging, although no measure of the noise temperature was quoted.

A SIS' tunnel junction, made from two different superconductors with unequal energy gaps Δ and Δ', can have a negative resistance on its umpumped I-V curve at voltages above $|\Delta - \Delta'|/e$. Roesler and deZafra (1982) suggested that this structure can be utilized for a high-gain mixer. Smith et al. (1983) measured the mixing properties of a SIS' junction that showed this negative-resistance region, but it was not clear that the negative resistance had any effect on their results. A practical application of the SIS' junction's negative resistance appears doubtful, for two reasons. First, the structure has a very small am-

plitude in current, so on general grounds one expects that it would saturate at very low powers. Second, even if saturation can be avoided, experience with other devices having an intrinsic negative resistance, such as tunnel diodes, indicates that extreme care must be taken with the junction's embedding environment to prevent oscillations and other noisy phenomena.

VI. DISCUSSION OF SIS MIXER PERFORMANCE

We have reviewed the quantum theory of mixing and the various experiments which, on the whole, give confidence that this theory is appropriate for describing quasiparticle mixing in SIS tunnel junctions. But both the theory itself and the application of the theory to practical mixers are based upon a number of assumptions and approximations which will not be perfectly satisfied in all situations. In this section we shall discuss several topics that fall outside the scope of the simplest models.

One example is the assumption that the significant currents through the tunnel junction are due to single-particle tunneling. For the theory to describe realistically an experimental mixer it is required that all other current mechanisms in the active element, for instance superconducting pair tunneling, multiparticle tunneling, and resistive leakage currents, not be important in the interesting region of parameter space. This appears to be true in most cases. Multiparticle tunneling (Wilkins, 1969)—the simultaneous tunneling of two or more quasiparticles, unpaired, through the barrier in a single process—is discussed for SIS mixers by Rudner et al. (1981b). It is in general not an important effect. Another example is the implicit assumption that the local oscillator waveform is perfectly cyclic. As with any sufficiently nonlinear device, however, a SIS junction may respond chaotically under certain circumstances. Hicks and Feldman (1983) found chaotic solutions in a time-domain analysis (Sec. IV.G) of a SIS mixer, for very small values of $\omega R_N C$. Whether chaotic noise can be a problem for realistic SIS mixer parameters has not been determined.

A. Optimum $\omega R_N C$ product

The quantum mixer theory treats the nonlinear effects of single-particle tunneling currents. In a SIS junction there is also a considerable displacement current due to the geometrical capacitance. The SIS junction has the form of a parallel-plate capacitor with the narrow separation between its superconducting electrodes filled with a relatively high-dielectric-constant insulator. This linear capacitance is included in a theoretical calculation simply by treating it as an element of the embedding impedance, the linear circuit surrounding the junction. Experimentally the capacitance acts as a parasitic element that tends to short-circuit the desired junction nonlinearity. Because of this the lateral side of a SIS millimeter-wave mixer junc-

tion is constrained to be quite small, measured, at most, in micrometers. Before such small junctions were available, an effective SIS mixer was not possible.

The standard measure of the parasitic effect of the geometrical capacitance is the junction $\omega R_N C$ product, the ratio of the junction's normal-state resistance to its capacitive impedance. Note that $\omega R_N C$ is actually *independent* of the area of a junction, because R_N and C scale oppositely with area. Rather, for a given type of SIS junction, $R_N C$ depends only upon the thickness of the tunnel barrier: thinner barriers, and hence larger Josephson critical current densities, give smaller values of $R_N C$. A graph of $R_N C$ versus Josephson critical current density for Pb-alloy tunnel junctions is given by Harris and Hamilton (1978). Once a SIS junction is considered for a device application, R_N is constrained to be in a relatively narrow range for reasonable input and output impedance matching. To achieve a smaller $\omega R_N C$ product for a SIS mixer therefore requires using smaller junctions *and* thinner barriers. Considerable research at present is aimed at making SIS junctions of very small area and with very high Josephson critical current densities, and this should not be a limiting factor for SIS mixers at high frequencies.

Although it is clear that too large an $\omega R_N C$ product will prevent effective SIS mixing, the optimum value of $\omega R_N C$ is still in question. One might assume that $\omega R_N C$ should be less than unity to prevent the capacitance from dominating the junction's dynamics. Two obvious qualifications are necessary. First, it is the SIS junction's input impedance in the mixing mode, rather than R_N, which should properly be compared to its capacitive impedance. The input impedance, given by Eq. (3.24) for the simplified model, is a complicated function of the mixer's operating point, but it is generally of the same order as R_N. Second, since a SIS junction's electrodes are superconducting, with very small rf resistance, any capacitance can in principle be almost perfectly resonated by an external tuning circuit. Still, insofar as the capacitance serves no constructive purpose, $\omega R_N C$ should be made as small as possible, certainly no larger than about unity.

There is strong evidence that this view is incorrect, and that the junction capacitance *does* play a constructive role in practical SIS mixers. It was noted by Feldman and Rudner (1983) that experiments using SIS junctions with very small $\omega R_N C$ products tended to give relatively poor mixer conversion, and, on the other hand, that two most promising SIS mixer experiments (McGrath *et al.*, 1981; Kerr *et al.*, 1981) had $\omega R_N C \sim 10$. These results are explained by the hypothesis that the large junction capacitance improves the conversion efficiency by suppressing harmonic conversion effects.

The quantum mixer theory in the three-port approximation predicts that a SIS mixer's conversion efficiency is largest for dc bias voltages relatively close to the energy-gap voltage, in most cases on the first conversion peak below the gap. But the three-port approximation ignores harmonic conversion effects, by assuming that all currents at the harmonic and harmonic sideband frequen-

cies are short circuited. A large junction capacitance (which should of course be tuned out at the signal frequency) assures that these currents are in fact short circuited. And, indeed, when $\omega R_N C$ is large, the three-port theory agrees very well with experiment (Feldman *et al.*, 1983).

When $\omega R_N C$ is small, there is considerable evidence that harmonic conversion effects can be important. Recall from Sec. V.B that the results from a number of experiments disagreed with the three-port mixer theory calculations, and, to generalize, the discrepancy appeared to be larger close to the energy-gap voltage. It is precisely here, near the gap voltage, that one expects the harmonic currents to be more important (Richards and Shen, 1980), due to the approximate inversion symmetry of a SIS junction's I-V curve in this region. Theoretical support for this hypothesis is given by the calculations of Richards and Shen (1980) in the five-port approximation, discussed in Sec. V.B, which predict that their mixer's conversion would be severely depressed near the gap voltage compared to the three-port model. Thus it appears that harmonic effects can reduce the conversion efficiency of a SIS mixer, most strongly near the energy-gap voltage, where the predicted conversion is largest. This would prevent a SIS mixer from realizing its full potential.

Contrary evidence is provided by the excellent performance of the current Bell Labs receiver (Sec. V.A.2), which presumably uses a SIS junction with a small $\omega R_N C$ product. Moreover, the good three-port-theory fit to the experimental data of Figs. 28—30 (from Phillips and Dolan, 1982), using a similar SIS junction, tends to argue against the importance of the harmonic frequencies.

A thorough investigation of this question will require a SIS quantum mixer analysis that explicitly includes the higher harmonics, like that of Hicks *et al.* (1985), mentioned in Sec. IV.C. Until this is done one can only roughly estimate how large a capacitance is required to suppress the harmonics. Figure 27 (discussed in Sec. V.B), supported by auxiliary data (Feldman and Rudner, 1983, Fig. 9), shows good agreement between experiment and three-port mixer calculations for those arrays having low resistance, and hence low $\omega R_N C$, *except* at the first conversion peak below the energy-gap voltage. On the first peak the experimental conversion appears to be depressed by about 5 dB, which is comparable to other experiments using low $\omega R_N C$ junctions (Shen *et al.*, 1980; Dolan *et al.*, 1981). For larger array resistance in Fig. 27, above about $R_{array} = 50 \ \Omega$ ($\omega R_N C \sim 4$), this relative depression of the first conversion peak disappears. This is presumably due to the suppression of harmonic conversion effects by the larger *relative* capacitance. Therefore, on the basis of this one series of experiments, it is tentatively inferred that optimized SIS mixers should be designed with $\omega R_N C \gtrsim 4$.

The choice of $\omega R_N C \gtrsim 4$ rather than $\lesssim 1$ relaxes somewhat the requirement of very small SIS junction area. However, it places much more stringent requirements on a SIS mixer's tuning circuits, which must be able to compensate the large capacitance at the signal frequency.

B. Arrays

Many SIS mixer experiments have employed a series array of junctions, rather than a single junction, as their active element. This greatly increases the versatility of SIS mixers, with apparently little cost in complexity or performance. Mixing with SIS arrays has been reviewed by Feldman and Rudner (1983).

The most important advantage of array mixers is that they afford a greatly increased dynamic range. Single-junction SIS mixers generally saturate at a very low signal power, in one extreme case about a picowatt (quoted in Smith and Richards, 1982), but the dynamic range increases as the square of the number of junctions in series. Additional advantages arise from the larger size (discussed below) of arrayed junctions. Josephson-effect noise (Sec. VI.D) is more readily suppressed by an applied magnetic field in larger junctions. The arrays of larger junctions are also less susceptible to electrical transients, and they can be made with less sophisticated equipment and techniques. These are crucial factors for many laboratories.

Most of the disadvantages of using arrays are apparent. Since the same currents must flow through all of the junctions in series, any heterogeneity in the arrayed junctions' characteristics will cause the voltages to divide unevenly among them. If this effect is large enough, it will interfere with the mixer's performance and make theoretical comparisons almost impossible. In past experiments, though, the array heterogeneity appears to have been acceptably small. Another consideration is that the series inductance along an array will be larger, for a given overall device impedance. More disconcerting, however, is the possibility, raised by the experiments of van Kempen et al. (1981), that SIS array mixers have higher noise temperatures than single-junction mixers, contrary to the simple theoretical arguments given below.

The most straightforward way to understand the behavior of a series array of N SIS junctions is to postulate an "equivalent single junction," a junction with the same barrier thickness but whose area is only $1/N$ of the area of a typical junction in the array. The equivalent single junction then has an I-V characteristic identical to that of the array, but reduced in both current scale and voltage scale by the factor N. All of its impedances, both real and imaginary, are equal to those of the array. The equivalent single junction is *not* one of the junctions in the array; it is the junction one would expect to most closely simulate the mixing behavior of the entire array, if placed in the same environment.

It is useful to review the argument from Feldman and Rudner (1983) that leads to the concept of the equivalent single junction, giving the conditions necessary for an array to behave in this simple manner. Figure 32(a) is an equivalent circuit for an array of SIS junctions, connected by small series inductances, with each element consisting of a nonlinear resistance, a nonlinear reactance, and a capacitance. To simplify Fig. 32(a) one must make certain assumptions.
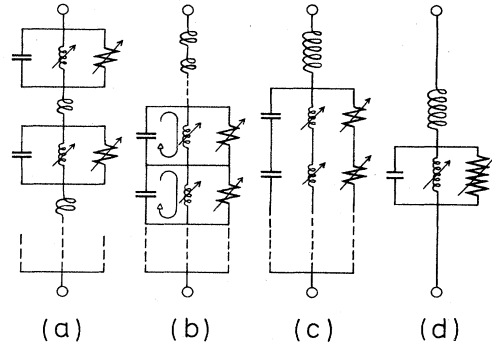

(a)   (b)   (c)   (d)

FIG. 32. Construction illustrating that, with certain assumptions, the equivalent circuit for a series array of N SIS junctions reduces to that for a single element with all impedances multiplied by N.

First, assume that the current is in phase all along the array, i.e, that the total current at every position along the array is the same. This will certainly be true for an experimental array that is very short compared to the effective wavelength at the frequencies of interest. If the currents are in phase along the array, then the ordering of the array elements is not important, and Fig. 32(a) is equivalent to Fig. 32(b).

Second, assume that all of the elements of the array are identical. If this is true, then the two example current loops drawn in Fig. 32(b) carry equal currents. This means that the total current carried by the horizontal connecting bars between the array elements is zero. These bars can thus be eliminated, so that Fig. 32(b) becomes Fig. 32(c). The impedances are then added in series to give Fig. 32(d).

Although Fig. 32(d) is identical in form to a single element of Fig. 32(a), it does not represent a physically realizable junction. The voltage scale in Fig. 32(d) is N times that for a single junction, so, for instance, its energy-gap voltage is N times the single-junction value. To replace the equivalent circuit in Fig. 32(d) by a real junction one must reduce its voltage scale, and also its current scale to maintain impedance levels, by the factor N. The resulting junction is then the "equivalent single junction" of the array.

This argument leads to three important conclusions regarding array devices that obey these assumptions. First of all, no complexity is introduced because $N > 1$. Second, note that an array *differs* from its equivalent single junction in that it requires N times the current and N times the voltage. Therefore an array behaves like a single junction with N^2 times the power. The required LO power and the saturation power will both scale as N^2. Noise powers are discussed below. Third, since the equivalent single junction has the same R_N and C as the entire array, it must be N times smaller in area than any one junction in the array. These last two attributes of arrays, larger power flow and larger junction size, lead to the advantages mentioned previously.

The equivalent-single-junction picture of arrays is borne out very well in practice, so much so that in Sec. V very little notice was taken as to whether an experiment used single junctions or SIS arrays. In fact, two of the most detailed analyses of SIS mixers (Rudner et al., 1981b; Feldman et al., 1983) were performed for array mixers, and found in good agreement with the quantum theory by postulating an equivalent single junction. This indicates that the two assumptions made above, (1) that the current is in phase all along the array, and (2) that all of the elements of the array are identical, are well enough satisfied for these experiments. This is fortunate, because whenever either of these assumptions is clearly violated the SIS mixer performance deteriorates (Rudner et al., 1981b). Moreover, an exact solution for the equations of a *heterogeneous* array would be exceedingly difficult, even for the case $N = 2$.

We have not yet considered the noise properties of arrays. If array mixers are noisier than single-junction mixers, then arrays will not be widely used. But there is good reason to believe that the noise temperature of an array mixer should *not* be necessarily worse than that of a single-junction mixer.

Consider first the effects of shot noise in classical mixer theory. Shot noise is the predominant contribution to the noise temperature of most SIS mixers. Figure 33(a) represents a series array of identical elements, each with characteristic impedance Z. An instantaneous current I through the array generates shot noise in each of the elements with mean-square amplitude $\langle i_n^2 \rangle = 2eIB$. These shot-noise generators are not correlated. Figure 33(a) can also be represented by the Thévenin equivalent circuit Fig. 33(b), where $\langle v_n^2 \rangle = 2eIB |Z|^2$. The noise sources are added incoherently to produce Fig. 33(c), with $\langle V_n^2 \rangle = 2eIBN |Z|^2$. Since the total impedance of the array is NZ, Fig. 33(c) can be transformed to the Norton equivalent circuit of Fig. 33(d), giving $\langle I_n^2 \rangle = 2eIB/N$. This result must be compared to the shot noise of the array's equivalent single junction, which passes the current I/N and hence has a shot-noise generator of mean-square amplitude $\langle i_n^2 \rangle = 2e(I/N)B$, exactly equal to that for the entire array. The shot-noise current for an array is therefore equal to that of its equivalent single

junction. It is clear that an even simpler construction suffices for any Johnson noise component, generally represented as a series voltage noise generator.

This is, admittedly, a heuristic demonstration. But any noise mechanism operating within an individual junction should be treatable in the same fashion. Even quantum noise, discussed in Sec. VI.E, which has not yet been solved for the SIS mixer, must eventually be represented by one or more noise generators, using an equivalent circuit such as those suggested by Haus and Mullen (1964), in order to allow the output noise to be calculated. The quantum noise-equivalent circuit could then be treated exactly like the equivalent circuits for shot noise or thermal noise. Under these reasonable assumptions, it appears to be a general result that the noise properties of an array are no worse than those of its equivalent single junction. Thus, although signal and LO powers scale as N^2 for an array, noise powers are expected to be independent of N.

Contrary to this expectation, there is some experimental evidence that SIS array mixers do in fact have higher noise temperatures. van Kempen et al. (1981) measured the mixing properties of 1-, 10-, and 50-junction SIS arrays at 36 GHz. These arrays were made with the same oxide thickness, and the areas of the individual junctions were chosen so that the three samples were "equivalent," each with the same total normal-state resistance of 55 Ω. As expected, the three samples gave roughly the same conversion: the conversion efficiency for the $N = 50$ junction array was more than two-thirds that for the single junction. But the mixer noise temperature showed a dramatic dependence upon N. The measured SSB mixer noise temperature for the 1-, 10-, and 50-junction arrays were 9.8 ± 5, 34 ± 12, and 85 ± 25 K, respectively. Thus, in this experiment, the mixer noise temperature increased roughly as $\sqrt{N}$.

This experiment has recently been repeated by McGrath et al. (1985), using an apparatus that allows much greater accuracy in noise measurements, with distinctly different results. The performance of a 36-GHz SSB mixer was characterized using series arrays of $N = 1$, 5, 10, and 50 Pb-alloy tunnel junctions, all with approximately the same total normal-state resistance. Those with $N = 1$, 5, and 10 showed similar noise temperatures $T_M \approx 8 - 9 \pm 1$ K, with conversion efficiencies $L^{-1} \approx 0.2$, while the $N = 50$ array had a somewhat larger $T_M = 16.3 \pm 0.6$ K and a lower $L^{-1} \approx 0.1$. The mixer noise temperature in these experiments thus depends only weakly, if at all, upon N, and the apparent contradiction with the earlier results of van Kempen et al. (1981) is puzzling. The more recent work used junctions with $\omega R_N C \sim 3$ rather than ~ 1.5, was in the purely SSB mode rather than being roughly DSB, showed more variation among the arrays in conversion efficiency, and had somewhat poorer overall conversion efficiency.

The question of excess noise in SIS array mixers is an important one in view of the greater dynamic range afforded by the longer arrays, and this should be an active area for further theoretical and experimental investigation in the near future.
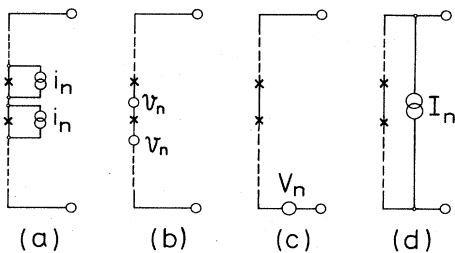

FIG. 33. Construction illustrating that the shot noise for a series array is identical to that for an equivalent single junction, not shown, with the same total impedance as the array.

C. LO power and saturation power

A simple intuitive argument (Feldman and Rudner, 1983) is remarkably successful in predicting the required LO power for SIS mixers. If a SIS junction or array is to be effective as a mixer, then the amplitude of the rf voltage swing V_{LO} around the dc bias voltage V_{dc} must be at least large enough to sample the nonlinearity at the energy-gap voltage: $V_{LO} > V_g - V_{dc}$. In particular, if the mixer is operating on the nth conversion peak below the energy-gap voltage, then $V_{LO} > (n - \frac{1}{2})N\hbar\omega/e$. A closer estimate of V_{LO} is given by the observation (Rudner et al., 1981b) that, to a very rough approximation, the conversion at peak n varies like the Bessel function $J_n(\alpha)$. Thus the conversion on peak n is optimized when $V_{LO} \approx N\hbar\omega\alpha_n/e$, where α_n is the value that maximizes $J_n(\alpha)$. Also to rough approximation, the LO input impedance of a double-sideband SIS mixer is on the order of its normal-state resistance R_N. Therefore the optimum LO power required for a double-sideband SIS mixer is

$$P_{LO} \approx (N\hbar\omega\alpha_n/e)^2/2R_N . \qquad (6.1)$$

This formula successfully predicts the optimum P_{LO} for all published SIS mixers for which the necessary information is available, except for the single-sideband result of Pan et al. (1983b). It is found to correctly estimate the observed P_{LO} to within 2 dB, covering a very wide range in published experimental values for P_{LO} from 1 nW to 30 μW. Note that the required P_{LO} increases as the square of the number of junctions arrayed and also as the square of the operating frequency, everything else held constant.

A SIS quantum mixer will begin to saturate for an input signal power larger than a certain value P_{sat}. All of the calculations in this paper have assumed that the input signal amplitude is small enough to be treated as a perturbation on the applied LO drive. The equations for the sideband currents are expanded to first order in the signal voltage, and therefore the IF output power is linearly related to the rf signal power. When the signal power is increased beyond the value P_{sat}, this assumption is no longer perfectly true, and the mixer response begins to saturate.

The gain-versus-bias voltage curve of a SIS mixer consists of a series of peaks, each of width $N\hbar\omega/e$, along the V_{dc} axis. The mixer is normally operated at a value of V_{dc} corresponding to the top of the largest of these gain peaks. The IF response of the mixer can be considered as a low-frequency modulation of the instantaneous bias point around this value of V_{dc}. Smith and Richards (1982) recognized that if this IF voltage swing is large enough, the instantaneous bias point will sample regions of slightly lower gain, and that this will be seen as a saturation of the mixer's response. Specifically, saturation at the IF port begins to occur when the amplitude of the IF voltage swing V_{IF} equals some small fraction of the width of the gain peak: $V_{IF} = \gamma_0 N\hbar\omega/e$. The quantity γ_0, small compared to unity, depends upon the allowable gain compression and can be calculated from the mea-

sured gain-versus-voltage curve for a particular SIS mixer by treating the effective gain as an average of the instantaneous gain over the IF voltage swing. Since the IF output power of the mixer is $V_{IF}^2/2R_L$, it is concluded that a SIS mixer with conversion gain L^{-1} begins to saturate at an input rf signal power of

$$P_{sat} = (\gamma_0 N\hbar\omega/e)^2/2L^{-1}R_L . \qquad (6.2)$$

Thus, like the required LO power, P_{sat} increases as the square of the number of junctions arrayed and also as the square of the operating frequency, everything else held constant.

Some examples are enlightening. For a SIS mixer operating with 3-dB gain, Smith and Richards (1982) estimate $\gamma_0 = 0.1$ for 0.2-dB gain compression. Equation (6.2) then predicts $P_{sat} = 2$ pW, whereas the observed 0.2-dB gain compression point occurred at 1.5 pW. The SIS receiver of Pan et al. (1983b), with 7.5-dB overall conversion loss, also gives $\gamma_0 = 0.10$ for 0.2-dB gain compression. It is interesting that γ_0 is independent of all of the factors distinguishing these experiments. For a 1.0-dB gain compression $\gamma_0 = 0.20$ and thus $P_{sat} = 2.1$ nW, whereas Pan et al. (1983b) observed the 1.0-dB gain compression point at 4 nW. The argument leading to Eq. (6.2) considered only saturation at the IF port. The good agreement with these two experiments indicates that this is the dominant saturation mechanism for SIS mixers in the quantum regime.

The range of signal power over which a receiver may be used, from the minimum detectable power to the saturation power, is called the "dynamic range." Photon fluctuation noise over a bandwidth $\Delta\nu$ limits the minimum detectable power to $\hbar\omega\Delta\nu$ in the best possible receiver (Sec. VI.E). Therefore Eq. (6.2) implies that a SIS mixer has at most a dynamic range given by

$$P_{sat}/P_{min} < \frac{\hbar\gamma_0^2}{2e^2R_L} \frac{N^2}{L^{-1}(\Delta\nu/\nu)} . \qquad (6.3)$$

This can be a rather stringent restriction. To appreciate the magnitudes involved, let us assert that a practical receiver requires a dynamic range at least of order 10^3, although a much larger value is preferred, and a fractional bandwidth on the order of one percent. Assuming $\gamma_0 \sim 0.1$ and $R_L = 50$ Ω, Eq. (6.3) then implies that $L^{-1} < N^2/4$. Thus, for this reason alone, a practical SIS receiver employing a single junction should have a gain less than unity. Here again, the potential advantage of series arrays is apparent.

D. Josephson-effect noise

A SIS mixer's output noise rises very sharply below a certain threshold bias voltage V_N. For instance, in Fig. 22 the IF output power rapidly goes off-scale below $V_N \sim 1.45$ mV, and the mixer cannot distinguish between the hot and cold inputs. Figure 34 shows the IF output noise power for one SIS mixer (Rudner et al., 1981b) with constant LO power, for various values of applied magnet-
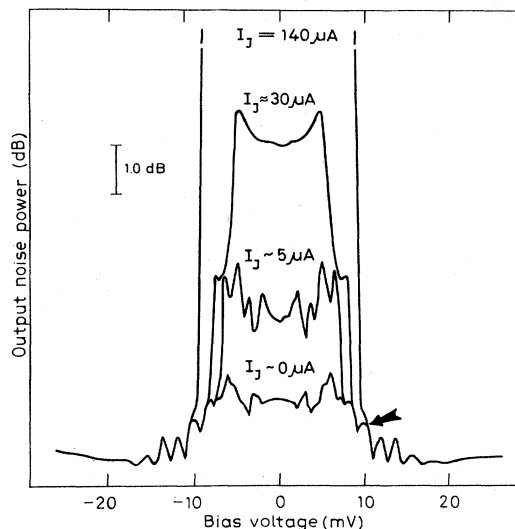
FIG. 34. Output noise power in the IF band as a function of dc bias voltage for the 75-GHz SIS mixer using a 6-junction Pb(In) series array illustrated in Fig. 23. The applied LO power is 1.11 μW, and the gap voltage is $V_g = 18$ mV for the array. The unpumped magnetic-field-depressed Josephson critical current I_J is listed, beginning with the zero-field value. The arrow indicates the noise threshold V_N for one curve (Rudner et al., 1981b).

ic field. The magnetic field depressed values of the unpumped Josephson critical current for the SIS array are listed. For larger values of bias voltage, above ~ 10 mV, the mixer is relatively quiet; the oscillatory noise seen in the figure is due to the converted rf input noise and the reflected noise from the IF circuit. But below the threshold bias voltage V_N, marked by an arrow in Fig. 34, the output IF noise suddenly becomes extremely large. When a magnetic field is applied to suppress the dc Josephson critical current I_J, the noise threshold voltage V_N is reduced, and the magnitude of the noise is diminished. In Fig. 34 the mixer output noise temperature is thereby reduced from more than 2000 K without magnetic field to about 65 K on the lowest trace. The strong magnetic field dependence implies that this noise in the region below V_N arises from the Josephson effect.

1. Explanation

The explanation of the Josephson-effect noise was first suggested by Dolan et al. (1981) and clearly established by Rudner et al. (1981a,1981b). In general, an unpumped, capacitively shunted, Josephson junction cannot be stably biased on the quasiparticle branch of its I-V curve below a certain voltage, which is called the dropback voltage V_d. If one attempts to reduce the dc voltage below this value, the voltage hysteretically switches to zero. This can be clearly seen in Fig. 22, where for this junction the switching occurs at $V_d \sim 1.2$ mV. Now consider a SIS mixer biased at a dc voltage $V_{dc} > V_d$. The

applied LO causes a voltage swing of amplitude V_{LO} around this bias point. If V_{LO} is large enough that the instantaneous voltage across a junction ever falls below V_d, the junction will switch to its zero-voltage state. The current must then increase to exceed the critical current before the junction can switch back to its quasiparticle branch. This hysteresis loop will be traversed on every cycle of the rf field.

According to this interpretation of the Josephson-effect noise, the threshold bias voltage V_N for a given level of LO power is simply

$$V_N = V_d + V_{LO} .\tag{6.4}$$

Rudner et al. (1981a,1981b) verified this relationship by showing that V_N increases linearly with $(P_{LO})^{1/2}$ for small P_{LO} and that, in the limit of zero P_{LO}, V_N is indeed equal to V_d. This was true for a variety of samples in various magnetic fields. A magnetic field applied to a SIS junction reduces V_d and hence reduces V_N by Eq. (6.4). It is, moreover, reasonable to suppose that the magnitude of the Josephson-effect noise diminishes when a magnetic field suppresses I_J because then less time is spent in traversing the hysteresis loop.

What is the cause of the switching at V_d? The generally accepted explanation is that the ac Josephson oscillations make it impossible to maintain a stable bias point at a voltage below V_d. This problem was first examined by McCumber (1968) and by Stewart (1968). Their model assumed that the quasiparticle branch could be represented in the region of interest by a simple linear resistance R. Then, using the Josephson equations (2.2) and (2.3), the total current through a capacitively shunted SIS junction is given by

$$I = \frac{\hbar C}{2e} \frac{d^2\varphi}{dt^2} + \frac{\hbar}{2eR} \frac{d\varphi}{dt} + I_J \sin\varphi .\tag{6.5}$$

This equation cannot in general be solved analytically. By numerical integration it is possible to show that for a constant I less than some critical value I_d, the only solution is $\varphi = \sin^{-1}(I/I_J) = $ const. Thus for $I < I_d$ no solution exists with nonzero average voltage, and it is not possible to sit on the quasiparticle branch. I_d/I_J is found to be a simple function of the parameter $\beta_c = 2eI_J R^2 C/\hbar$; and this relationship is given graphically by McCumber (1968). In the limit of small I_d/I_J, which is the only region of interest for building a practical SIS mixer, the critical value of dc current is given to first order by $I_d = I_J(2/\beta_c)^{1/2}$. If I_d is identified with the dropback voltage through $I_d = V_d/R$, then the result may be written

$$V_d = k V_{pl} ,\tag{6.6}$$

where the plasma voltage $V_{pl} = (\hbar I_J/2eC)^{1/2}$ is the Josephson voltage $\hbar\omega_{pl}/2e$ given by the resonance frequency of the Josephson inductance $\hbar/2eI_J$ with the capacitance, and where $k = \sqrt{2}$ for this linear model.

This simple result for I_d is very sensitive to the assumption of a linear quasiparticle current. Any other assumed quasiparticle current, including that appropriate to

a real SIS junction, will give quite a different value of I_d. This has been the topic of much investigation in recent years (e.g., Tarutani and Van Duzer, 1983; Murayama, 1983) because of its relevance to Josephson-effect computer elements. It is interesting to note that a parabolic quasiparticle current $I = aV^2$ gives an equation analogous to Eq. (6.5) which *can* be solved analytically for I_d (Stewart, 1974). Although the result for I_d is very different from the linear-current case, once again $V_d \equiv (I_d/a)^{1/2} = V_{pl}\sqrt{2}$ in the limit of small I_d/I_J. This last result has not to our knowledge been noted in the literature. Could this be evidence that V_d is in general independent of the form of the quasiparticle current, for small I_d?

The junctions used for SIS mixing experiments yield somewhat larger values of the proportionality constant than the analytic value $k = \sqrt{2}$. Rudner *et al.* (1981b) verified Eq. (6.6), with $k = 3.0$, showing that V_d was indeed proportional to $(I_J)^{1/2}$ for a few samples with various magnetic fields. Shen (1981) quotes the value $k \approx 3.5$ for his junctions. The data given both by Dolan *et al.* (1981) and by Sutton (1983) imply $k \approx 2.1$. It is possible that the experimental values for k are larger than the analytic result because noise in real junctions forces the instantaneous voltage into the region of instability from an otherwise stable bias point.

2. High-frequency limitation

The Josephson-effect noise is not a problem at the relatively low frequencies of most SIS experiments reported thus far. The mixer is biased securely above V_N, and the unstable region is never entered. But for high-frequency operation the Josephson-effect noise imposes severe design limitations on SIS mixers. Recall from Eq. (6.4) that the mixer must operate at a bias voltage $V_{dc} > V_d + V_{LO}$. This condition becomes harder to fulfill at higher frequencies for three reasons. First, the optimum bias point is approximately $V_{dc} = V_g - \hbar\omega/2e$, which decreases with frequency. Second, the optimum value of α should be relatively insensitive to frequency, so $V_{LO} = \hbar\omega\alpha/e$ must increase with frequency. Third, a mixer design is scaled by maintaining a constant R_N and $\omega R_N C$, so C should decrease with increasing frequency; and therefore V_d increases as $\sqrt{\omega}$ by Eq. (6.6). In other words, a straightforward scaling of a SIS mixer to higher frequencies causes the optimum bias point to approach and eventually enter the Josephson-effect noise region, making low-noise mixing impossible.

This argument can be quantified. The upper frequency limit for SIS mixing occurs when $V_{dc} \approx V_g - \hbar\omega/2e = V_N$, which, with Eq. (6.4), becomes

$$V_g - \hbar\omega/2e = kV_{pl} + \hbar\omega\alpha/e . \tag{6.7}$$

Since for lead junctions at low temperature $I_J R_N \cong 0.2\pi V_g$ (Ginsburg *et al.*, 1976), the plasma voltage can be written

$$V_{pl} \cong \left[\frac{\hbar\omega}{e} \frac{\pi}{10} \frac{V_g}{\omega R_N C} \right]^{1/2} . \tag{6.8}$$

If the quantity $\omega R_N C$ is considered to be a design constant independent of frequency, Eq. (6.7) is a quadratic equation in $\sqrt{\hbar\omega}$ whose solution is

$$\hbar\omega_{max} = eV_g \left[\frac{\sqrt{x + \alpha + 1/2} - \sqrt{x}}{\alpha + \frac{1}{2}} \right]^2 , \tag{6.9}$$

where

$$x = \frac{k^2\pi}{40\omega R_N C} . \tag{6.10}$$

This, then, is the approximate upper frequency limit for SIS quasiparticle mixing with Pb-based junctions in the conventional mode. For junctions made of other materials the numerical constant in the definition of x will be different, by at most 15% (Ginsberg *et al.*, 1976).

The upper frequency limit given in Eq. (6.9) increases for smaller x, for smaller α, and for larger V_g. For a generous numerical estimate we choose $k = 2.1$ as in Sutton (1983), the rather low value $\alpha = 1.0$, and $V_g = 3$ mV. Then if $\omega R_N C = 2$ the upper frequency limit for a SIS mixer is estimated to be 250 GHz. For $\omega R_N C = 10$, which would require sophisticated tuning structures, the upper frequency limit becomes 350 GHz. Note that the upper frequency limit increases proportionally to V_g, so that eventual SIS junctions made of very-high-T_c superconductors, such as NbN, should work to roughly twice these frequencies.

The limit for high-frequency SIS mixers imposed by Eq. (6.9) is not at all absolute. There are a number of possible ways a mixer might be designed to extend this limit, such as the recent suggestion by Imai *et al.* (1985) of using SIS junctions with an insulator containing magnetic impurities. In addition, Eq. (6.9) is derived from purely classical arguments, which are appropriate only at low frequencies. The extrapolation to establish a high-frequency limit must be incorrect, at least in its details. For one thing, Eq. (6.4) assumes that the LO voltage samples the junction I-V curve as a classical waveform, oscillating smoothly between $V_{dc} - V_{LO}$ and $V_{dc} + V_{LO}$, when in fact the LO voltage samples the I-V curve only at quantized photon points separated by $\hbar\omega/e$. Also, at high frequencies the dropback switching time (see McDonald *et al.*, 1980) becomes comparable to $1/\omega_{LO}$, and this must affect the junction dynamics. The switching behavior of a Josephson junction driven at high frequencies requires more study.

There is little experimental evidence at present to test Eq. (6.9). Only Sutton (1983) has reported detailed results at 230 GHz and above. For the data given in that paper, Eq. (6.9) predicts an upper frequency limit of a little over 200 GHz, and yet Sutton tested his SIS mixer up to ~400 GHz. The interpretation of this experiment, however, is problematic: in our Fig. 22 the conversion appears to result from Josephson-effect mixing as well as quasiparticle

mixing. Indeed, Sutton notes that Josephson-effect mixing contributions become severe at frequencies of 230 GHz and above. Equation (6.9) does not apply to Josephson mixing.

Serious attention should be paid to the possibility of employing Josephson-effect mixing in SIS junctions. As discussed in Sec. II.B.2, essentially all of the work on Josephson mixing, both theoretical and experimental, has been concentrated upon point-contact Josephson junctions. A major problem in this work has been the downconversion of noise from higher harmonic sidebands. The larger capacitance afforded by SIS Josephson junctions should ameliorate, and may completely eliminate, this problem. If this is the case, Josephson-effect mixing could become the favored mode at frequencies approaching the energy gap.

The most straightforward way to avoid the Josephson-effect noise limitation is to suppress the Josephson critical current with a magnetic field. As noted in the discussion of Fig. 34 at the beginning of this section, a magnetic field reduces V_d and hence V_N and also reduces the magnitude of the noise. To suppress I_J to zero requires a magnetic field large enough to place one flux quantum within a SIS junction, and so smaller junctions require larger fields for an equal effect. Unfortunately, the junctions used for high-frequency single-junction SIS mixers are in general so small that the required fields are large enough to begin to destroy the bulk superconductivity of the thin films, and so degrade SIS mixer performance. Phillips et al. (1981) show a very clear example of this at 230 GHz. This problem can be circumvented by using a series array of SIS junctions in place of a single junction. The larger size of the arrayed junctions allows a weaker magnetic field to suppress I_J and hence avoid the Josephson-effect noise. This is a strong incentive for using series arrays for high-frequency SIS mixers. An alternative possibility is to employ a single small-area "edge" junction (Sec. II.B.1) with one long dimension.

E. Quantum noise

There is a fundamental lower limit to the noise temperature of any high-gain linear amplifier, $T_N \geq \hbar\omega/2k$. The term "high-gain linear amplifier" refers to any device whose output radiation field is linearly related to its input signal field with a large multiplication of photon number, and which preserves the phase information of the input. This definition includes the mixers described in this paper as well as classical mixers. The irreducible noise, generally called "quantum noise," arises as a result of the uncertainty principle.

The problem of quantum noise in tunnel junction mixers has not been solved. Even though the theory presented in this paper can be called the "quantum theory of mixing," in that the charge carriers have been quantized, the radiation fields are treated as classical fields in Sec. IV, and so the noise temperature of a tunnel junction mixer given in Eq. (4.71) has no absolute lower limit. This expression can approach zero, and is found to be ex-

tremely small compared with $\hbar\omega/k$ over a wide and quite realistic range of parameters. A complete quantum theory of tunnel junction mixers must quantize the radiation fields as well as the charge carriers, and then, it is expected, the quantum noise limitation will result. Nevertheless, we shall see that Eq. (4.71) does contain some traces of the quantum noise.

Experimental SIS mixers are, indeed, approaching the quantum noise limit. For example, McGrath et al. (1985) measured a mixer noise temperature of 3.5 ± 1.5 times $\hbar\omega/k$ at 36 GHz. There is a strong expectation that more precise measurement techniques and further exploration of experimental parameter space will improve on previous results. Therefore a discussion of quantum noise in tunnel junction mixers is timely. But since no specific theory exists for tunnel junction mixers, this discussion must be a more general one. We shall rely for the most part upon the concepts of quantum noise in linear amplifiers that were developed up to the early 1960s, when it had become clear that both maser amplifiers and parametric amplifiers had limiting noise temperatures of $\hbar\omega/2k$. This early work is now discussed in standard textbooks, for instance Robinson (1974). A recent and quite thorough treatment is given by Caves (1982).

The concept of "noise temperature" has become widely used because it is a convenient shorthand for noise power. The standard definition of noise temperature is as follows: T_N is the temperature of the input termination of a noise-free equivalent of a device, which would result in the same output noise power as the actual device connected to a noise-free input termination. Unfortunately, this definition has two serious problems when applied to a noise temperature near the quantum limit. First, it is ambiguous; it is not clear whether or not the idealized noise-free input termination should include zero-point fluctuation noise. Second, under this definition the noise temperature is not simply proportional to power, because the full Planck blackbody radiation formula must be used rather than the linear Rayleigh-Jeans limit. Thus noise temperatures are not additive, and equations such as Eq. (2.1) must be rejected. To avoid these problems we shall use the term "noise temperature" to signify the input-equivalent noise power which a device adds to an incident signal, expressed as a temperature by equating it to $kT_N\Delta\nu$. Then T_N is directly determined, with no quantum correction factor, by the standard hot/cold load technique, so long as the hot and cold loads are themselves in the Rayleigh-Jeans limit.

1. Heffner's treatment

A familiar form of the uncertainty principle states that if one measures the energy E of a system and the precise time t at which the system possesses this energy, the uncertainties in these quantities are related by $\Delta E \Delta t \geq \hbar/2$. If E is the energy in a signal wave packet at some central frequency ω, then E is related to the number of quanta in the wave packet by $E = n\hbar\omega$, and the phase of the signal is $\varphi = \omega t$. This leads to the equation

$$\Delta n \Delta \varphi \geq \tfrac{1}{2} \qquad\qquad (6.11)$$

relating the uncertainties in the simultaneous measurement of the quantities n and φ. Thus one cannot measure both the amplitude and the phase of a sinusoidal signal precisely.

Most radiation-sensitive devices fall into either of two distinct categories. At one extreme is the ideal photon detector, such as an x-ray counter, which can count arriving quanta with no uncertainty ($\Delta n \to 0$) but which gives no phase information at all ($\Delta \varphi \to \infty$). An amplifier, on the other hand, attempts to reproduce its input radiation field with larger amplitude while maintaining the phase information, subject to Eq. (6.11). One may also imagine other types of radiation-sensitive devices with varying degrees of phase sensitivity (Serber and Townes, 1960; Caves, 1982).

The arrival time of the photons at a photon detect will of course fluctuate, if only because of the zero-point vacuum fluctuations. Nevertheless, an ideal detector is usually considered noiseless, in the sense that it adds no noise to these fluctuations already present in its input. A compelling heuristic argument given by Heffner (1962) shows that a high-gain linear amplifier *cannot* be noiseless in this same sense. A noiseless linear amplifier would perfectly reproduce its input (including fluctuations) with larger amplitude: n_i photons received at its input would produce $n_0 = G n_i$ output photons, where G is the (integral) amplifier photon gain, and further, the output phase φ_0 would be equal to the input phase φ_i plus some constant phase shift θ. Both G and θ can be precisely determined at large signal levels. The amplifier output quantities can be measured with an uncertainty $\Delta n_0 \Delta \varphi_0 = \tfrac{1}{2}$. But since the amplifier is noiseless, this means that the input signal quantities have been measured with an uncertainty $\Delta n_i \Delta \varphi_i = \tfrac{1}{2} G^{-1}$, which violates the uncertainty relation Eq. (6.11) if $G > 1$. The conclusion is that a linear amplifier must add noise to its input signal, to remain consistent with the uncertainty principle.[1]

Heffner carried his argument further to show that an ideal high-gain linear amplifier, one that minimizes the product $\Delta n \Delta \varphi$ to $\tfrac{1}{2}$, has a minimum total output noise, referred to its input, equivalent to one photon per unit bandwidth of the input signal radiation. Since the input radiation is itself accompanied by one-half photon of zero-point vacuum fluctuations, the process of amplification has somehow added a minimum of one-half photon of input-equivalent noise.

---

[1]Caves (1982,1983) takes exception to this argument on the grounds that it requires the hypothesis of a noise-free input signal, which in itself violates the principles of quantum mechanics. As presented here, though, Heffner's argument concerns the *measurability* of an arbitrary input signal, including its inherent fluctuations.

2. Caves's treatment

A very different argument given by Caves (1982) finds the same result as Heffner and has the virtue of being more mathematically explicit. Caves's argument is based upon the commutation relations for the conjugate variables describing the input and output modes of an amplifier. We shall give a brief account of an already abridged version of this argument found in Caves (1983).

The complex amplitudes of the input and output signals of an amplifier are written $\hat{x}_1 + i\hat{x}_2$ and $\hat{y}_1 + i\hat{y}_2$, respectively. If the amplifier is linear, its evolution equations must be of the general form

$$\hat{y}_1 = G_1 \hat{x}_1 + G_1 \hat{a}_1 ,$$

$$\hat{y}_2 = G_2 \hat{x}_2 + G_2 \hat{a}_2 , \qquad (6.12)$$

where $\hat{a}_1$ and $\hat{a}_2$ have zero expectation value and commute with $\hat{x}_1$ and $\hat{x}_2$. The operators $\hat{a}_1$ and $\hat{a}_2$ are responsible for any noise added by the amplifier. In general (but not necessarily) the term "linear amplifier" connotes a device that treats both quadrature phases identically. Then $G_1^2 = G_2^2 = G$, the commonly defined photon number gain of the amplifier. The total output signal is thus given by

$$|\langle \hat{y}_1 + i\hat{y}_2 \rangle|^2 = G |\langle \hat{x}_1 + i\hat{x}_2 \rangle|^2 . \qquad (6.13)$$

The total output noise is given by

$$[(\Delta y_1)^2 + (\Delta y_2)^2] = G[(\Delta x_1)^2 + (\Delta x_2)^2] + GA , \qquad (6.14)$$

where the "added noise number" $A \equiv (\Delta a_1)^2 + (\Delta a_2)^2$ represents the photon-number-equivalent noise added by the amplifier to the input signal, referred to the amplifier input. In proper units, A is the noise temperature of the amplifier.

The Hermitian operators $\hat{x}_1$ and $\hat{x}_2$ must obey the commutation relation $[\hat{x}_1, \hat{x}_2] = i/2$. This implies that the uncertainties of their expectation values obey $\Delta x_1 \Delta x_2 \geq \tfrac{1}{4}$, which further implies $(\Delta x_1)^2 + (\Delta x_2)^2 \geq \tfrac{1}{2}$. This last is the uncertainty principle, whose lower limit gives the half-quantum of zero-point input noise which appears (amplified) on the right side of Eq. (6.14). Since the same relations must be true for $\hat{y}_1$ and $\hat{y}_2$, the commutation relation can be applied to both the input and the output operators in Eq. (6.12), yielding

$$[\hat{a}_1, \hat{a}_2] = \frac{i}{2}(G^{-1} - 1) . \qquad (6.15)$$

The corresponding uncertainty principle is

$$\Delta a_1 \Delta a_2 \geq \tfrac{1}{2} |\langle [\hat{a}_1, \hat{a}_2] \rangle| = \tfrac{1}{4} |1 - G^{-1}| , \qquad (6.16)$$

and therefore

$$A \geq |1 - G^{-1}|/2 . \qquad (6.17)$$

Thus a high-gain linear amplifier has an added noise number $A \geq \tfrac{1}{2}$; it must add at least a half-quantum of

noise, referred to its input, to the half-quantum of zero-point noise already present at its input. Therefore $T_N \geq \hbar\omega/2k$. In Caves's terms, the amplifier independently enforces the uncertainty principle which is already obeyed by the input radiation. The *total* output noise in Eq. (6.14), referred to the input, is equivalent to at least one photon per unit bandwidth, the same result as found by Heffner.

Assuming that blackbody radiation at physical temperature T accompanies the input signal, the total output noise power referred to the input of a linear amplifier is

$$P_N = [A + \tfrac{1}{2}\coth(\hbar\omega/2kT)]\hbar\omega\Delta\nu , \qquad (6.18)$$

as in Caves (1982) Eq. (3.33). The second term on the right describes the blackbody radiation (Callen and Welton, 1951), including the zero-point fluctuations. It is enlightening to plot the minimum of this expression (i.e., $A = \tfrac{1}{2}$) as a function of the physical temperature T. This is done in Fig. 35, with all quantities expressed in photon units. This figure illustrates some of the various values that have been quoted for the minimum noise temperature T_N of a high-gain linear amplifier. If P_N at $T=0$ is simply expressed as a temperature by equating it to $kT_N\Delta\nu$, then $T_N = \hbar\omega/k$. If T_N is defined as the physical input temperature required to double the output noise compared to a $T=0$ input, then $T_N = \hbar\omega/k \ln2$. If T_N is defined as the physical input temperature required for a hypothetical noise-free equivalent of the amplifier to equal the noise output of the actual amplifier with $T=0$, then $T_N = \hbar\omega/k \ln3$. Finally, the (minimum) noise temperature extrapolated from high-input-temperature measurements of the amplifier's output power is $T_N = \hbar\omega/2k$. Such an extrapolation is most often used to determine experimentally the T_N of real devices. This last value, not coincidentally, is equal to the minimum noise power add-
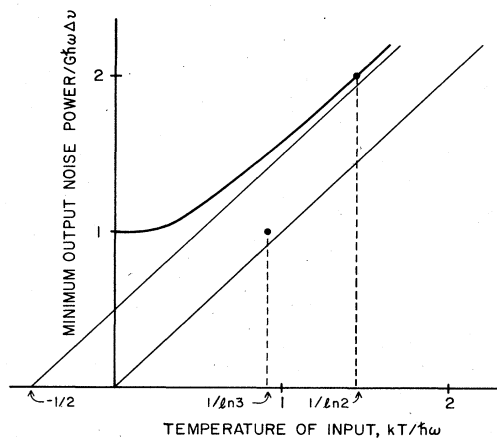
FIG. 35. The total output noise power, referred to the input, of an ideal linear amplifier with photon gain $G \gg 1$ is plotted against the physical temperature of the amplifier's input termination, in photon units (heavy curve). The light lines help in understanding the various definitions which give different values for the amplifier's "quantum noise temperature."

ed by the amplifier, expressed as a temperature by equating it to $kT_N\Delta\nu$.

3. Quantum noise in tunnel junction mixers

As already noted, the problem of quantum noise in tunnel junction mixers has not been solved. However, the tunnel junction mixer acts as a "high-gain linear amplifier" in that it is linear, it preserves the phase information of its input, and it virtually always operates with a large multiplication of photon number. Therefore one may state with some assurance that the minimum noise added by a tunnel junction mixer is at least the equivalent of a half-photon per unit bandwidth at its input. But can the tunnel junction mixer, in principle, approach this limit?

Equation (4.71) gives the contribution to the noise temperature of a tunnel junction mixer arising from shot noise in the local oscillator currents. This should be the only unavoidable source of noise except for quantum noise. In the tractable low-IF three-frequency approximation with equal signal and image termination conductance G_S (the DSB case), it is not difficult to show that the shot noise, Eq. (4.80), can indeed approach zero as a limit for one and only one choice of parameters. For an I-V curve whose nonlinearity covers a finite range in voltage this occurs if, and only if, $I_{dc}(V_0 - \hbar\omega/e) = 0$, $I_{dc}(V_0) = 0$, and $I_{dc}(V_0 + \hbar\omega/e) > 0$ (e.g., an ideal SIS junction at $T=0$); in the small LO power limit $\alpha \ll 1$; and for $G_S = eI_{dc}(V_0 + \hbar\omega/e)/2\hbar\omega$. If the output impedance of the mixer is matched, the mixer's power gain approaches infinity at this point. These conditions are, admittedly, virtually impossible to fulfill in an experiment, but are allowable in principle. (For an unlimited exponential nonlinearity in the DSB case the shot-noise contribution goes to zero only in the limit of very *large* LO power.) Although the mixer can have zero shot noise, the quantum noise limitation has not been violated. For these parameters, the zero-point fluctuations in the image termination will contribute exactly a half-quantum to the mixer's equivalent input noise power.

The question immediately arises: what happens if the image frequency is short circuited? In this case the three-frequency approximation becomes in effect a two-frequency approximation, with an infinite terminating admittance at the image (the SSB case). It is not difficult to show that the shorted-image mixer's shot-noise temperature has a distinct limiting minimum value, $T_M = \hbar\omega/2k$, and that it approaches this value for one and only one choice of parameters. For an I-V curve whose nonlinearity covers a finite range in voltage, this occurs for the same parameters as listed for the DSB case. If the output impedance of the mixer is matched, the mixer's power gain is *not* infinite, but equal to $2G_S/G_1$ at this bias point, where G_1 is the slope of the I-V curve at $V = V_0 + \hbar\omega/e$. [Tucker (1979), Eq. (7.34), shows that for an unlimited exponential nonlinearity in the large LO power limit the minimum shot noise in the SSB case also approaches $T_M = \hbar\omega/2k$.] In the shorted-image case, the image termination cannot contribute to the mixer's noise

temperature; the half-quantum of mixer equivalent input noise power required by the uncertainty principle is provided by the shot noise.

For both of the cases just considered, the tunnel junction mixer's minimum equivalent added-noise power is exactly one half-quantum, and it is natural to call this quantum noise. In the DSB case the quantum noise results from zero-point fluctuations in the image termination, while the shot-noise power can approach zero. In the SSB case, where the image noise cannot be matched into the mixer, the shot noise is finite and constitutes the quantum noise.

This discussion suggests a procedure for calculating the noise temperature of a tunnel junction mixer, in the absence of a rigorous theory for quantum noise. The noise temperature is assumed to be the sum of the shot-noise contribution, Eq. (4.71), and a thermal-noise contribution that includes zero-point fluctuations. The thermal-noise contribution is calculated by including in parallel with the terminating conductance G_i at the image frequency ω_i a current noise generator of mean-square amplitude

$$\langle i_n^2 \rangle = 2G_i \hbar \omega_i \Delta \nu \coth(\hbar \omega_i / 2kT) , \qquad (6.19)$$

where T is the physical temperature of the image termination. (The generalization to include thermal noise from the harmonic sidebands is straightforward.) This procedure succeeds in giving the anticipated minimum noise temperature in the two important limiting cases just considered. Zorin (1985) maintains that this approach is equivalent to a complete quantum-mechanical treatment.

Neither Heffner's argument nor Caves's argument identifies the origin of an amplifier's quantum noise. Nevertheless, even though it is not required in his treatment, Caves (1982) asserts that the added half-quantum of noise arises from the zero-point fluctuations in some "internal mode," whose existence, he states, is required for any linear amplifier. He gives the example of a parametric amplifier, whose only internal mode is the idler. The idler's zero-point fluctuations appear amplified at the output and are responsible for the added noise. The preceding discussion questions the generality of this interpretation. For an ideally optimized tunnel junction mixer in the DSB case, the *external* electromagnetic field fluctuations at the image frequency produce the quantum noise, and this is clearly Caves's "internal mode." But in the SSB case the quantum noise is a remnant of the *internal* shot noise, and it is hard to identify a single quantum mode that is responsible. It does not appear useful to attempt to ascribe the quantum noise in both of these cases to some irreducible internal mode. Rather, this example illustrates the impossibility in quantum mechanics of separating a measuring apparatus from the system to be measured.

VII. CONCLUSION

Recent progress in utilizing photon-assisted tunneling to approach quantum-limited detection at millimeter wavelengths has been remarkable. This success is rooted

in a deep and powerful understanding of the tunneling of electrons across a thin oxide barrier separating two metals. If a theory is judged by its ability to predict new and unexpected phenomena, then the Hamiltonian formulation of tunneling created by Bardeen (1961) and by Cohen, Falicov, and Phillips (1962) must surely be accounted a great success. This was the framework utilized by Josephson (1962), along with the BCS theory, to predict the extraordinary pair tunneling phenomena which bear his name. This same framework has now been combined with the concept of photon-assisted tunneling, due to Dayem and Martin (1962) and Tien and Gordon (1963), to obtain surprising new effects in quasiparticle tunneling as well. The successful prediction of such varied and unusual behavior, based upon phase modulation of the quantum-mechanical wave functions for both Cooper pairs and single electrons, is a very substantial theoretical achievement. It is also an important practical development, since the theory allows precise experimental control over the quantum response of superconducting tunnel junctions.

Beyond their scientific interest as quantum phenomena, both Josephson tunneling and quasiparticle tunneling have major technical applications. The quasiparticle mixers and receivers described here are destined to have a far-reaching impact, most immediately on millimeter-wave astronomy. Already, receivers with noise temperatures approaching the quantum limit are being constructed for the frequency range between 30 and 300 GHz. These techniques should eventually be extendable to both higher and lower frequencies as well, opening up a large new portion of the spectrum to quantum detection. Such receivers will, in fact, be among the most nearly ideal radiation detectors available at any frequency in view of their ultra-low operating power, very large bandwidth, and quantum sensitivity. As these advances become more widely known, other applications will surely follow. Quasiparticle mixers may, for example, be well suited to quantum nondemolition experiments for gravity wave detection.

The development of this field has required the integration of major ideas generated in several branches of science and engineering, from basic millimeter-wave techniques to the latest materials research on superconductor tunnel junctions. We believe that the combined result of this work constitutes a major advance in understanding and control of processes at the quantum level. As such, the methods described here are not simply technical innovations that will someday be superseded, but fundamentally new science that is expected to stimulate research in new directions.
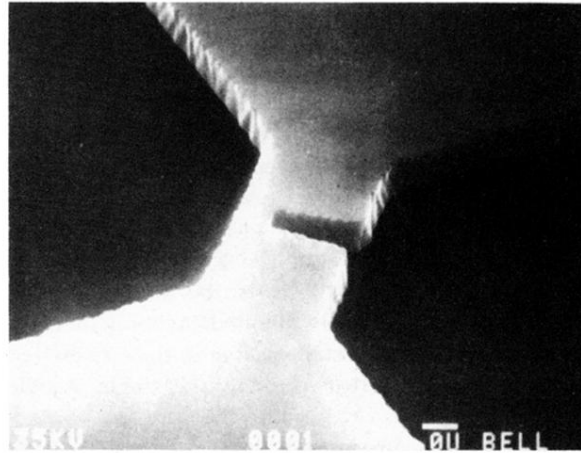
ACKNOWLEDGMENTS

with whom we have both had especially close and valuable interactions on this subject: J. Bardeen, T. Claeson, G. J. Dolan, A. R. Kerr, W. R. McGrath, S.-K. Pan, T. G. Phillips, P. L. Richards, S. Rudner, T.-M. Shen, A. D. Smith, T. C. L. G. Sollner, M. Tinkham, and D. P. Woody. One of us (J.R.T.) was supported in part by the Joint Services Electronics Program under Contract No. N00014-C-79-0424.
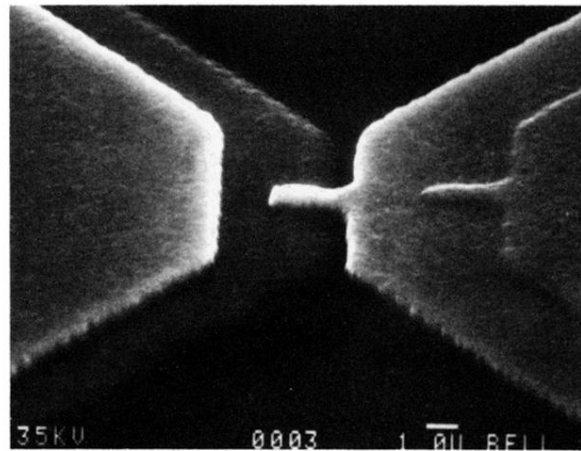
REFERENCES

Ambegaokar, V., and A. Baratoff, 1963, Phys. Rev. Lett. 10, 486.
Anderson, P. W., and A. H. Dayem, 1964, Phys. Rev. Lett. 13, 195.
Archer, J. W., 1984, Proc. IEEE 73, 109.
Bardeen, J., 1961, Phys. Rev. Lett. 6, 57.
Bardeen, J., 1980, Phys. Rev. Lett. 45, 1978.
Bardeen, J., L. N. Cooper, and J. R. Schrieffer, 1957, Phys. Rev. 108, 1175.
Barone, A., and G. Paternò, 1982, *Physics and Applications of the Josephson Effect* (Wiley, New York).
Barrett, A. H., C. J. Lada, P. Palmer, L. E. Snyder, and W. J. Welch, 1983, Report of the Subcommittee on Millimeter- and Submillimeter-Wavelength Astronomy to the National Science Foundation (unpublished).
Blaney, T. G., 1978, in *Future Trends in Superconductive Electronics* (AIP Conference Proceedings No. 44), edited by B. S. Deaver, Jr., C. M. Falco, J. H. Harris, and S. A. Wolf (AIP, New York), p. 230.
Blundell, R., K. H. Gundlach, and E. J. Blum, 1983, Electron. Lett. 19, 498.
Blundell, R., H. Hein, K. H. Gundlach, and E. J. Blum, 1982, Int. J. Infrared Millimeter Waves 3, 793.
Broom, R. F., R. Jaggi, Th. O. Mohr, and A. Oosenbrug, 1980, IBM J. Res. Dev. 24, 206.
Calander, N., T. Claeson, and S. Rudner, 1982, J. Appl. Phys. 53, 5093.
Callegari, A. C., and R. A. Buhrman, 1982, J. Appl. Phys. 53, 823.
Callen, H. B., and T. A. Welton, 1951, Phys. Rev. 83, 34.
Caves, C. M., 1982, Phys. Rev. D 26, 1817.
Caves, C. M., 1983, in *Quantum Optics, Experimental Gravitation, and Measurement Theory*, edited by P. Meystre and M. O. Scully (Plenum, New York), p. 567.
Claassen, J. H., and P. L. Richards, 1978, J. Appl. Phys. 49, 4117.
Cohen, M. H., L. M. Falicov, and J. C. Phillips, 1962, Phys. Rev. Lett. 8, 316.
D'Addario, L. R., 1984, Int. J. Infrared Millimeter Waves 5, 1419.
Danchi, W. C., F. Habbal, and M. Tinkham, 1982, Appl. Phys. Lett. 41, 883.
Dayem, A. H., and R. J. Martin, 1962, Phys. Rev. Lett. 8, 246.
Dickman, R. L., W. J. Wilson, and G. G. Berry, 1981, IEEE Trans. Microwave Theory Tech. MTT-29, 788.
Dolan, G. J., 1977, Appl. Phys. Lett. 31, 337.
Dolan, G. J., R. A. Linke, T. C. L. G. Sollner, D. P. Woody, and T. G. Phillips, 1981, IEEE Trans. Microwave Theory Tech. MTT-29, 87.
Dolan, G. J., T. G. Phillips, and D. P. Woody, 1979, Appl. Phys. Lett. 34, 347.

Entin-Wohlman, O., 1980, Phys. Rev. B 22, 5225.
Erickson, N. R., 1983, in *Digest of the Eighth International Conference on Infrared and Millimeter Waves* (IEEE cat. no. 83CH1917-4), edited by R. J. Temkin (IEEE, New York), p. M6.7.
Erickson, N. R., 1984, talk presented at the URSI Symposium on Millimeter and Submillimeter Wave Radio Astronomy, Granada, Spain (unpublished).
Feldman, M. J., 1982, J. Appl. Phys. 53, 584.
Feldman, M. J., and M. T. Levinsen, 1981, IEEE Trans. Magn. MAG-17, 834.
Feldman, M. J., S.-K. Pan, A. R. Kerr, and A. Davidson, 1983, IEEE Trans. Magn. MAG-19, 494.
Feldman, M. J., P. T. Parrish, and R. Y. Chiao, 1975, J. Appl. Phys. 46, 4031.
Feldman, M. J., and S. Rudner, 1983, in *Reviews of Infrared and Millimeter Waves, Vol. 1*, edited by K. J. Button (Plenum, New York), p. 47.
Giaever, I., 1960a, Phys. Rev. Lett. 5, 147.
Giaever, I., 1960b, Phys. Rev. Lett. 5, 464.
Giaever, I., and K. Megerle, 1961, Phys. Rev. 122, 1101.
Ginsberg, D. M., R. E. Harris, and R. C. Dynes, 1976, Phys. Rev. B 14, 990.
Gubankov, V. N., K. I. Konstantinyan, V. P. Koshelets, and G. A. Ovsyannikov, 1982, Pis'ma Zh. Tekh. Fiz. 8, 1498 [Sov. Tech. Phys. Lett. 8, 643 (1982)].
Gubankov, V. N., K. I. Konstantinyan, V. P. Koshelets, G. A. Ovsyannikov, and A. N. Vystavkin, 1983, IEEE Trans. Magn. MAG-19, 968.
Gundlach, K. H., S. Takada, M. Zahn, and H. J. Hartfuss, 1982, Appl. Phys. Lett. 41 294.
Habbal, F., W. C. Danchi, and M. Tinkham, 1983, Appl. Phys. Lett. 42, 296.
Halbritter, J., 1985, IEEE Trans. Magn. MAG-21, 858.
Harris, R. E., 1974, Phys. Rev. B 10, 84.
Harris, R. E., 1975, Phys. Rev. B 11, 3329.
Harris, R. E., 1976, Phys. Rev. B 13, 3818.
Harris, R. E., and C. A. Hamilton, 1978, in *Future Trends in Superconductive Electronics* (AIP Conference Proceedings No. 44), edited by B. S. Deaver, Jr., C. M. Falco, J. H. Harris, and S. A. Wolf (AIP, New York), p. 448.
Hartfuss, H. J., and K. H. Gundlach, 1981a, Int. J. Infrared Millimeter Waves 2, 809.
Hartfuss, H. J., and K. H. Gundlach, 1981b, Int. J. Infrared Millimeter Waves 2, 925.
Hartfuss, H. J., and M. Tutter, 1983a, Int. J. Infrared Millimeter Waves 4, 993.
Hartfuss, H. J., and M. Tutter, 1983b, in *Digest of the Eighth International Conference on Infrared and Millimeter Waves* (IEEE cat. no. 83CH1917-4), edited by R. J. Temkin (IEEE, New York), p. M1.5.
Hartfuss, H. J., and M. Tutter, 1984, Int. J. Infrared Millimeter Waves 5, 717.
Haus, H. A., and J. A. Mullen, 1964, in *Quantum Electronics*, edited by P. Grivet and N. Bloembergen (Columbia University, New York), p. 71.
Heffner, H., 1962, Proc. IRE 50, 1604.
Held, D. N., and A. R. Kerr, 1978, IEEE Trans. Microwave Theory Tech. MTT-26, 55.
Hicks, R. G., and M. J. Feldman, 1983, in *Digest of the Eighth International Conference on Infrared and Millimeter Waves* (IEEE cat. no. 83CH1917-4), edited by R. J. Temkin (IEEE, New York), p. T6.6.
Hicks, R. G., M. J. Feldman, and A. R. Kerr, 1985, IEEE

Trans. Magn. **MAG-21**, 208.

Hicks, R. G., and P. J. Khan, 1982, IEEE Trans. Microwave Theory Tech. **MTT-30**, 251.

Huang, H-C. W., S. Basavaiah, C. J. Kircher, E. P. Harris, M. Murakami, S. P. Klepner, and J. H. Greiner, 1980, IEEE Trans. Electron Devices **ED-27**, 1979.

Ibruegger, J., K. Okuyama, R. Blundell, K. H. Gundlach, and E. J. Blum, 1984, in *Proceedings of the 17th International Conference on Low Temperature Physics*, edited by U. Eckern, A. Schmid, W. Weber, and H. Wuhl (North-Holland, Amsterdam), p. 937.

Imai, S., S. Morita, A. Ishikawa, Y. Takeuti, and N., Mikoshiba, 1985, IEEE Trans. Magn. **MAG-21**, 906.

Irwin, K. E., S. E. Schwarz, and T. Van Duzer, 1981, in *Digest of the Sixth International Conference on Infrared and Millimeter Waves* (IEEE cat. no. 81CH1645-1 MTT), edited by K. J. Button (IEEE, New York), p. M-4-2.

Irwin, K. E., T. Van Duzer, and S. E. Schwarz, 1985, IEEE Trans. Magn. **MAG-21**, 216.

Josephson, B. D., 1962, Phys. Lett. **1**, 251.

Kamerlingh Onnes, H., 1911, Leiden Comm., Nos. **120b,122b,124c**.

Kerr, A. R., 1975, IEEE Trans. Microwave Theory Tech. **MTT-23**, 828.

Kerr, A. R., S.-K. Pan, M. J. Feldman, and A. Davidson, 1981, Physica **108B**, 1369.

Kerr, A. R., P. H. Siegel, and R. J. Mattauch, 1977, in *IEEE MTT-S International Microwave Symposium Digest* (IEEE cat. no. 77CH1219-5 MTT), edited by E. R. Silverstein (IEEE, New York), p. 96.

Kleinsasser, A. W., and R. A. Buhrman, 1980, Appl. Phys. Lett. **37**, 841.

Krautle, H., E. Sauter, and G. V. Schultz, 1977, Infrared Phys. **17**, 477.

Kroger, H., L. N. Smith, D. W. Jillie, and J. B. Thaxter, 1983, IEEE Trans. Magn. **MAG-19**, 783.

Kubo, R., 1959, in *Lectures in Theoretical Physics, Vol. I*, edited by W. E. Brittin and Y. Dunham (Interscience, New York), p. 120.

Kuzmin, L. S., K. K. Likharev, and V. V. Migulin, 1979, IEEE Trans. Magn. **MAG-15**, 454.

Lee, G. S., 1982, Appl. Phys. Lett. **41**, 291.

Magerlein, J. H., 1981, IEEE Trans. Magn. **MAG-17**, 286.

McColl, M., 1977, IEEE Trans. Microwave Theory Tech. **MTT-25**, 54.

McColl, M., M. F. Bottjer, A. B. Chase, R. J. Pedersen, A. H. Silver, and J. R. Tucker, 1979, IEEE Trans. Magn. **MAG-15**, 468.

McColl, M., M. F. Millea, and A. H. Silver, 1973, Appl. Phys. Lett. **23**, 263.

McColl, M., M. F. Millea, A. H. Silver, M. F. Bottjer, R. J. Pedersen, and F. L. Vernon, Jr., 1977, IEEE Trans. Magn. **MAG-13**, 221.

McCumber, D. E., 1968, J. Appl. Phys. **39**, 3113.

McDonald, D. G., R. L. Peterson, C. A. Hamilton, R. E. Harris, and R. L. Kautz, 1980, IEEE Trans. Electron Devices **ED-27**, 1945.

McGrath, W. R., A. V. Räisänen, P. L. Richards, R. E. Harris, and F. L. Lloyd, 1985, IEEE Trans. Magn. **MAG-21**, 212.

McGrath, W. R., P. L. Richards, A. D. Smith, H. van Kempen, R. A. Batchelor, D. E. Prober, and P. Santhanam, 1981, Appl. Phys. Lett. **39**, 655.

Morita, S., S. Takaki, S. Imai, Y. Takeuti, and N. Mikoshiba, 1983, IEEE Trans. Magn. **MAG-19**, 608.

Murayama, Y., 1983, Int. J. Electron. **54**, 887.

Olsson, L., S. Rudner, E. Kollberg, and C. O. Linström, 1982, *Proceedings of the 12th European Microwave Conference* (Microwave Exhibitions and Publishers, Kent), p. 270.

Olsson, L., S. Rudner, E. Kollberg, and C. O. Lindström, 1983, Int. J. Infrared Millimeter Waves **4**, 847.

Pan, S.-K., M. J. Feldman, A. R. Kerr, E. S. Palmer, J. A. Grange, and P. Timbie, 1983a, in *Digest of the Eighth International Conference on Infrared and Millimeter Waves* (IEEE cat. no. 83CH1917-4), edited by R. J. Temkin (IEEE, New York), p. M6.2.

Pan, S.-K., M. J. Feldman, A. R. Kerr, and P. Timbie, 1983b, Appl. Phys. Lett. **43**, 786.

Phillips, T. G., and G. J. Dolan, 1982, Physica **109&110B**, 2010.

Phillips, T. G., and D. P. Woody, 1982, Annu. Rev. Astron. Astrophys. **20**, 285.

Phillips, T. G., D. P. Woody, G. J. Dolan, R. E. Miller, and R. A. Linke, 1981, IEEE Trans. Magn. **MAG-17**, 684.

Predmore, C. R., A. V. Räisänen, N. R. Erickson, P. F. Goldsmith, and J. L. R. Marrero, 1984, IEEE Trans. Microwave Theory Tech. **MTT-32**, 498.

Richards, P. L., 1978, in *Future Trends in Superconductive Electronics* (AIP Conference Proceedings No. 44), edited by B. S. Deaver, Jr., C. M. Falco, J. H. Harris, and S. A. Wolf (AIP, New York), p. 223.

Richards, P. L., and T.-M. Shen, 1980, IEEE Trans. Electron Devices **ED-27**, 1909.

Richards, P. L., T.-M. Shen, R. E. Harris, and F. L. Lloyd, 1979, Appl. Phys. Lett. **34**, 345.

Richards, P. L., T.-M. Shen, R. E. Harris, and F. L. Lloyd, 1980, Appl. Phys. Lett. **36**, 480.

Robinson, F. N. H., 1974, *Noise and Fluctuations* (Oxford, London).

Roesler, R. F., and R. L. deZafra 1982, Int. J. Infrared Millimeter Waves **3**, 241.

Rogovin, D., and D. J. Scalapino, 1974, Ann. Phys. (N.Y.) **86**, 1.

Röser, H. P., and R. Wattenbach, 1984, in *Digest of the Ninth International Conference on Infrared and Millimeter Waves*, edited by K. Mizuno (Japan Society of Applied Physics), p. 304.

Rudner, S., and T. Claeson, 1979, Appl. Phys. Lett. **34**, 711.

Rudner, S., M. J. Feldman, E. Kollberg, and T. Claeson, 1980, in *SQUID '80*, edited by H. D. Hahlbohm and H. Lübbig (de Gruyter, Berlin), p. 901.

Rudner, S., M. J. Feldman, E. Kollberg, and T. Claeson, 1981a, IEEE Trans. Magn. **MAG-17**, 690.

Rudner, S., M. J. Feldman, E. Kollberg, and T. Claeson, 1981b, J. Appl. Phys. **52**, 6366.

Saleh, A. A. M., 1971, *Theory of Resistive Mixers* (MIT, Cambridge).

Schneider, M. V., 1982, in *Infared and Millimeter Waves, Vol. 6*, edited by K. J. Button (Academic, New York), p. 209.

Schrieffer, J. R., 1964, *Theory of Superconductivity* (Benjamin, Reading, Mass.), Chap. 5.

Serber, R., and C. H. Townes, 1960, in *Quantum Electronics: A Symposium*, edited by C. H. Townes (Columbia University, New York), p. 233.

Shen, T. M., 1981, IEEE J. Quantum Electron. **QE-17**, 1151.

Shen, T.-M., and P. L. Richards, 1981, IEEE Trans. Magn. **MAG-17**, 677.

Shen, T.-M., P. L. Richards, R. E. Harris, and F. L. Lloyd, 1980, Appl. Phys. Lett. **36**, 777.

Smith, A. D., R. A. Batchelor, W. R. McGrath, D. E. Prober,

and P. Santhanam, 1981a, in *Digest of the Sixth International Conference on Infrared and Millimeter Waves* (IEEE cat. no. 81CH1645-1 MTT), edited by K. J. Button (IEEE, New York), p. M-4-1.

Smith, A. D., W. R. McGrath, P. L. Richards, R. E. Harris, F. L. Lloyd, D. E. Prober, and P. Santhanam, 1983, IEEE Trans. Magn. **MAG-19**, 490.

Smith, A. D., W. R. McGrath, P. L. Richards, H. van Kempen, D. E. Prober, and P. Santhanam, 1981b, Physica **108B**, 1367.

Smith, A. D., and P. L. Richards, 1982, J. Appl. Phys. **53**, 3806.

Soerensen, O. H., B. Dueholm, J. Mygind, and N. F. Pedersen, 1980, J. Appl. Phys. **51**, 5483.

Sollner, T. C. L. G., 1981, Physica **108B**, 1365.

Sollner, T. C. L. G., and S. D. Powell, 1983, IEE Trans. Magn. **MAG-19**, 605.

Stark, A. A., 1983, in *National Radio Science Meeting Digest* (URSI, Boulder), p. 37.

Stark, A. A., 1984, private communication.

Stewart, W. C., 1968, Appl. Phys. Lett. **12**, 277.

Stewart, W. C., 1974, J. Appl. Phys. **45**, 452.

Sutton, E. C., 1983, IEEE Trans. Microwave Theory Tech. **MTT-31**, 589.

Tarutani, Y., and T. Van Duzer, 1983, IEEE Trans. Electron Devices **ED-30**, 34.

Taur, Y., J. H. Claassen, and P. L. Richards, 1974, Appl. Phys. Lett. **24**, 101.

Taur, Y., and A. R. Kerr, 1978, Appl. Phys. Lett. **32**, 775.

Thungren, T., E. L. Kollberg, and K. S. Yngvesson, 1982, *Proceedings of the 12th European Microwave Conference* (Microwave Exhibitions and Publishers, Kent), p. 361.

Tien, P. K., and J. P. Gordon, 1963, Phys. Rev. **129**, 647.

Tinkham, M., 1975, *Introduction to Superconductivity* (McGraw-Hill, New York).

Tiuri, M. E., 1966, in *Radio Astronomy*, by J. D. Kraus (McGraw-Hill, New York), Chap. 7.

Torrey, H. C., and C. A. Whitmer, 1948, *Crystal Rectifiers* (MTT Radiation Lab. Series, Vol. 15) (McGraw-Hill, New York).

Tucker, J. R., 1975, in *Proceedings of the 14th International Conference on Low Temperature Physics*, edited by M. Krusius and M. Vuorio (North-Holland, Amsterdam), Vol. 4, p. 180.

Tucker, J. R., 1979, IEEE J. Quantum Electron. **QE-15**, 1234.

Tucker, J. R., 1980, Appl. Phys. Lett. **36**, 477.

Tucker, J. R., 1983, in *Reviews of Infrared and Millimeter Waves*, edited by K. J. Button (Plenum, New York), Vol. 1, p. 1.

Tucker, J. R., and M. F. Millea, 1978, Appl. Phys. Lett. **33**, 611.

Tucker, J. R., and M. F. Millea, 1979, IEEE Trans. Magn. **MAG-15**, 288.

Uhlir, A., Jr., 1958, Bell Syst. Tech. J. **37**, 951.

van Kempen, H., W. R. McGrath, P. L. Richards, A. D. Smith, R. E. Harris, and F. L. Lloyd, 1981, in *Digest of the Sixth International Conference on Infrared and Millimeter Waves* (IEEE cat. no. 81CH1645-1 MTT), edited by K. J. Button (IEEE, New York), p. M-4-3.

Vernon, F. L., Jr., M. F. Millea, M. F. Bottjer, A. H. Silver, R. J. Pederson, and M. McColl, 1977, IEEE Trans. Microwave Theory Tech. **MTT-25**, 286.

Vystavkin, A. N., V. N. Gubankov, L. S. Kuzmin, K. K. Likharev, V. V. Migulin, and V. K. Semenov, 1977, IEEE Trans. Magn. **MAG-13**, 233.

Weinreb, S., D. L. Fenstermacher, and R. W. Harris, 1982, IEEE Trans. Microwave Theory Tech. **MTT-30**, 849.

Werthamer, N. R., 1966, Phys. Rev. **147**, 255.

Whiteley, S. R., 1982, Appl. Phys. Lett. **40**, 842.

Wilkins, J. W., 1969, in *Tunneling Phenomena in Solids*, edited by E. Burstein and S. Lundqvist (Plenum, New York), p. 333.

Wilson, W. J., 1983, IEEE Trans. Microwave Theory Tech. **MTT-31**, 873.

Winkler, D., 1984, Physica **126B**, 479.

Winkler, D., T. Claeson, and S. Rudner, 1985, IEEE Trans. Magn. **MAG-21**, 896.

Woody, D. P., R. E. Miller, and M. J. Wengler, 1985, IEEE Trans. Microwave Theory Tech. **MTT-33**, 90.

Yariv, A., 1976, *Introduction to Optical Electronics* (Holt, Rinehart, and Winston, New York).

Yu, K. W., 1984, Phys. Rev. B **29**, 181.

Yu, K. W., and O. Entin-Wohlman, 1981, Phys. Rev. B **24**, 1587.

Zorin, A. B., 1985, IEEE Trans. Magn. **MAG-21**, 939.

(a)

(b)

FIG. 7. Scanning electron microscope photographs of (a) a suspended photoresist bridge structure, and (b) a small-area SIS junction fabricated by angle evaporation past this photoresist bridge (Phillips *et al.*, 1981).